

## INFORMATION TO USERS

This manuscript has been reproduced from the microfilm master. UMI films the text directly from the original or copy submitted. Thus, some thesis and dissertation copies are in typewriter face, while others may be from any type of computer printer.

**The quality of this reproduction is dependent upon the quality of the copy submitted.** Broken or indistinct print, colored or poor quality illustrations and photographs, print bleedthrough, substandard margins, and improper alignment can adversely affect reproduction.

In the unlikely event that the author did not send UMI a complete manuscript and there are missing pages, these will be noted. Also, if unauthorized copyright material had to be removed, a note will indicate the deletion.

Oversize materials (e.g., maps, drawings, charts) are reproduced by sectioning the original, beginning at the upper left-hand corner and continuing from left to right in equal sections with small overlaps.

Photographs included in the original manuscript have been reproduced xerographically in this copy. Higher quality 6" x 9" black and white photographic prints are available for any photographs or illustrations appearing in this copy for an additional charge. Contact UMI directly to order.

ProQuest Information and Learning  
300 North Zeeb Road, Ann Arbor, MI 48106-1346 USA  
800-521-0600

**UMI<sup>®</sup>**



**CRUSTAL DEFORMATION IN ALASKA MEASURED  
USING THE GLOBAL POSITIONING SYSTEM**

A  
THESIS

Presented to the Faculty  
of the University of Alaska Fairbanks  
in Partial Fulfillment of the Requirements  
for the Degree of

**DOCTOR OF PHILOSOPHY**

By

Hilary J. Fletcher. B.S..M.S.

Fairbanks, Alaska

May 2002

UMI Number: 3053229

UMI<sup>®</sup>

---

UMI Microform 3053229

Copyright 2002 by ProQuest Information and Learning Company.  
All rights reserved. This microform edition is protected against  
unauthorized copying under Title 17, United States Code.

---

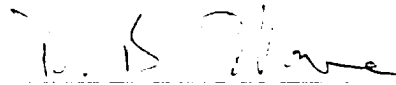
ProQuest Information and Learning Company  
300 North Zeeb Road  
P.O. Box 1346  
Ann Arbor, MI 48106-1346

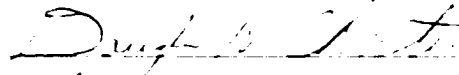
CRUSTAL DEFORMATION IN ALASKA MEASURED USING THE  
GLOBAL POSITIONING SYSTEM

By

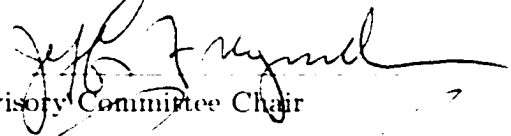
Hilary J. Fletcher

RECOMMENDED:

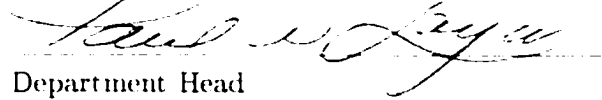






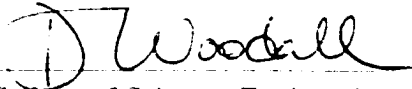


Advisory Committee Chair



Department Head

APPROVED:



Dean, College of Science, Engineering and Mathematics



Dean of the Graduate School

4-12-02

Date

# Abstract

Repeat observations using the Global Positioning System at sites on the Earth's surface enable the velocity of those sites to be estimated. These velocity estimates can be used to model the processes of the crust's deformation by faulting and folding. The focus of this study is crustal deformation in Alaska and in particular the region of interior Alaska within 300km of Fairbanks, including the Denali fault; the Fairweather fault and Yakutat block in southern Alaska; and the Semidi region of the Aleutian arc. This deformation is driven by the relentless northwestward motion of the Pacific plate relative to North America.

The Yakutat block, an allocthonous terrane located in the 'armpit' of southern Alaska is shown to be moving at neither the Pacific Plate rate nor is it attached to North America. Instead it has a velocity parallel to the Fairweather fault, which means that some offshore structure, possibly the Transition Zone, must accommodate some of the Pacific-North American relative motion. The slip on the Fairweather fault is estimated to be  $44 \pm 3$  mm/yr with a locking depth of  $8 \pm 1$  km, which implies a recurrence time of  $\sim 80$  years for an  $M_s$  7.9 earthquake. Using a model of southern Alaska block rotation with the Denali fault as the northern boundary, the slip rate on the McKinley segment of the Denali fault is estimated to be  $\sim 6-9$  mm/yr for a locking depth of 12 km. Moving to the southwest, data from sites in the Semidi segment of the Alaska subduction zone, between the fully-coupled segment to the northeast and the slipping Shumagin segment to the southwest are studied. This region, which sustained a magnitude 8.2 earthquake in 1938, is determined to be highly coupled and accumulating strain.

Finally, all of these pieces are connected in a quantitative model for southern Alaska. This model involves three crustal blocks, the Yakutat block, Fairweather block and southern Alaska block, which lie between North America and the Pacific plate and move relative to these major plates.

# Contents

List of Figures . . . . .	7
List of Tables . . . . .	9
Acknowledgements . . . . .	10
<b>1 Introduction</b>	<b>11</b>
1.1 General . . . . .	11
1.2 Thesis Content and Organization . . . . .	12
<b>2 New GPS Constraints on the Motion of the Yakutat Block</b>	<b>16</b>
2.1 Abstract . . . . .	16
2.2 Introduction . . . . .	17
2.3 Data and Results . . . . .	19
2.4 Discussion and Conclusions . . . . .	21
2.4.1 Yakutat Block Motion . . . . .	21
2.4.2 Possible Offshore Structures and Implications . . . . .	23
2.4.3 Fairweather Fault Constraints . . . . .	25
2.5 Summary . . . . .	27
2.6 Acknowledgments . . . . .	28
2.7 Appendix . . . . .	28
<b>3 New constraints on the motion of the Fairweather fault, Alaska, from   GPS observations</b>	<b>30</b>
3.1 Abstract . . . . .	30
3.2 Introduction . . . . .	31

	5
3.3	Data . . . . . 33
3.4	Discussion . . . . . 36
3.5	Conclusions . . . . . 43
3.6	Acknowledgments . . . . . 43
<b>4</b>	<b>Using GPS to Unravel the Tectonics of Interior and Southern Alaska 44</b>
4.1	Abstract . . . . . 44
4.2	Introduction . . . . . 45
4.3	Tectonic background . . . . . 46
4.3.1	Denali fault . . . . . 46
4.3.2	Tintina fault . . . . . 49
4.3.3	Interior Seismic Zones . . . . . 49
4.4	Data . . . . . 51
4.5	Results . . . . . 53
4.6	Discussion . . . . . 54
4.6.1	Interior seismic zones . . . . . 55
4.6.2	Denali fault . . . . . 61
4.7	Postseismic Model . . . . . 73
4.8	Conclusions . . . . . 84
<b>5</b>	<b>High interseismic coupling of the Alaska subduction zone SW of Kodiak island inferred from GPS data 86</b>
5.1	Abstract . . . . . 86
5.2	Introduction . . . . . 87
5.3	GPS Data . . . . . 89
5.4	Dislocation Model . . . . . 90
5.5	Discussion . . . . . 93
5.5.1	Derived Parameters . . . . . 93
5.5.2	Trench-Parallel Velocities . . . . . 94
5.6	Conclusions . . . . . 94
5.7	Acknowledgments . . . . . 95



<b>6 Implications for the Tectonics of Alaska</b>	<b>96</b>
6.1 Model 1 . . . . .	102
6.2 Model 2 . . . . .	110
6.3 Model 3 . . . . .	113
6.4 Summary . . . . .	114
<b>Appendix A How GPS works</b>	<b>117</b>
<b>Appendix B Fieldwork procedures</b>	<b>121</b>
B.1 Site selection . . . . .	121
B.2 Antenna set up . . . . .	121
<b>Appendix C Position and velocity data for all sites used in this thesis</b>	<b>123</b>
<b>Bibliography</b>	<b>127</b>

# List of Figures

1.1	Map of Alaska showing active faults . . . . .	12
1.2	Map of Alaska showing study region for each chapter . . . . .	13
2.1	Map of the Yakutat area of southern Alaska . . . . .	18
2.2	Time series of GPS measurements at Yakutat . . . . .	20
2.3	Cartoon map showing faults in the Yakutat area . . . . .	22
2.4	Surface displacement per year due to a modeled Transition Zone . . . . .	24
2.5	Fairweather fault-normal component of velocity . . . . .	29
3.1	A map of the Yakutat area of southern Alaska . . . . .	32
3.2	GPS velocities for sites in the Yakutat region . . . . .	34
3.3	Plot to illustrate the trade-off between slip rate and locking depth . . . . .	37
3.4	Plot showing the best-fit model with one sigma uncertainties . . . . .	41
3.5	Confidence region ellipses for values of $\chi^2$ larger than the fitted minimum . . . . .	42
4.1	Map of interior Alaska showing the main segments of the Denali fault system and other connecting faults . . . . .	47
4.2	Map of interior Alaska showing the seismicity from 1990 to 1996 . . . . .	50
4.3	Map of interior Alaska showing the Denali and Tintina faults . . . . .	51
4.4	Velocities of all sites relative to FAIR . . . . .	53
4.5	Velocities relative to FAIR for sites in the Fairbanks vicinity . . . . .	56
4.6	The bookshelf-type block rotation model that we apply to interior Alaska . . . . .	58
4.7	Map showing the model velocities due to bookshelf-type block rotation about the site CLGO in Interior Alaska . . . . .	60

4.8	Map showing the Denali fault, Hines Creek fault and the location of magnitude 5 earthquakes that occurred in November and December 2000 . . . . .	63
4.9	Cartoon illustration of block-rotation model . . . . .	65
4.10	Contour plot of reduced $\chi^2$ . . . . .	67
4.11	GPS velocities and model velocities . . . . .	68
4.12	Residual velocities after the model has been removed from the data . . . . .	69
4.13	Contour plot of reduced $\chi^2$ for the Parks highway data only . . . . .	70
4.14	Variation of reduced $\chi^2$ with angular velocity, fixed locking depth of 12 km . . . . .	71
4.15	Best-fitting one- and two-fault models using only the Parks highway data and fixed locking depth of 12 km . . . . .	72
4.16	GPS velocities minus postseismic model . . . . .	75
4.17	Velocities of sites on the Kenai Peninsula and vicinity relative to North America . . . . .	77
4.18	Comparison of coupling distribution with that obtained by Zweck et al. [2001] . . . . .	79
4.19	Map of the Kenai Peninsula showing GPS and our model velocities, all relative to North America . . . . .	80
4.20	Map of the Kenai Peninsula showing GPS and the <i>Zweck et al.</i> [2001] model velocities, all relative to North America . . . . .	81
4.21	Map of the Kenai Peninsula showing GPS and GPS minus postseismic model velocities, all relative to Fairbanks . . . . .	83
5.1	A map of the Alaska Peninsula showing the Semidi GPS stations . . . . .	88
5.2	Velocities of Semidi GPS sites relative to North America . . . . .	89
5.3	Elastic dislocation model of partial locking of plate interface . . . . .	92
6.1	Map of Alaska showing all GPS sites . . . . .	97
6.2	Map of Alaska showing faults relevant to tectonic model in this chapter . . . . .	98
6.3	Proposed tectonic model of Alaska from <i>Lahr and Plafker</i> [1980] . . . . .	99
6.4	Map of crustal blocks proposed in our tectonic model of southern Alaska . . . . .	101
6.5	Slip rates of boundaries of proposed crustal blocks in Models 1a and 1b . . . . .	107
6.6	Slip rates associated with boundary between SOAK, WAB, and APB . . . . .	112
6.7	Slip rates associated with boundary between SOAK and the Bering block . . . . .	115

# List of Tables

2.1	Summary of calculated slip rates and locking depths for the Fairweather fault.	27
3.1	Site velocities in mm/yr . . . . .	35
5.1	Site velocities in mm/yr . . . . .	90
C.1	Site velocities in mm/yr . . . . .	124

# Acknowledgements

There are many people I need to thank, either for helping me to finish my thesis or for making it fun along the way. My advisor Jeff Freymueller has shown me what it takes to be a truly good scientist and despite being constantly in demand he always found time to answer my questions and to read the various drafts of my papers and thesis chapters. David Stone, Doug Christensen, and Wes Wallace served as my other committee members and I am grateful to them for their thoughtful reviews of my thesis and for discussions of my work (often over drinks in the pub).

Many people helped me with fieldwork: Ryan Woodard, Stefan Wiemer, Doerte Mann, Sigrun Hreinsdottir, Chris Larsen, Qizhi Chen, Chris Zweck, Guy Tytgat, Steve Estes, Martin LaFevers, Keith Echelmeyer, Glenn Thompson, Dorte Dissing, and Georges Minnassian.

My wonderful office mates include Doerte Mann, Liz Meyers, Sigrun Hreinsdottir, Qizhi Chen and John Sanchez - thank you all for your support and for answering the phone for me. One other person at work who deserves a special mention is Mitch Robinson, who saved my thesis from hackers and helped me with many other assorted computer problems.

I have so many friends who have helped to make my time in Fairbanks so much fun. To all the frisbee players, volleyball players, guitar players, singers, skiers, actors, and general beer-drinkers who have helped to distract me from my work - cheers.

I am grateful to Mum and Dad for all their support over the years. They thought they were saying goodbye to their daughter for one year, and nine years later I'm still here. I'm sorry that Alaska is so far from England.

My final and biggest thanks go to Ryan. With all honesty I can't say that he helped me to finish my thesis in a timely manner, but he sure did make my life a lot of fun along the way.

Actually, come to think of it, I *can* say that he helped me to finish my thesis in a timely manner.

# Chapter 1

## Introduction

### 1.1 General

Just twenty years ago, the idea of directly measuring the position of points on the surface of the earth with a precision of a few millimeters and observing how those points move from year to year would have been thought impossible. Today, with a GPS satellite system in place 20,000 km above the earth and hundreds of permanent GPS receivers on earth as well as thousands of temporary receivers, we are able to observe the deformation of the crust at accuracies approaching one millimeter per year.

Tectonically, Alaska is an interesting state. The Pacific plate is moving to the north and colliding with southern Alaska, which is part of the North American plate. The nature of this collision varies dramatically along the collision interface, ranging from subduction along the Aleutian megathrust to strike slip motion along the Queen Charlotte-Fairweather fault (Figure 1.1). The velocity of the Pacific plate relative to the North American plate varies along the collision zone from about 48 mm/yr in southeastern Alaska to about 68 mm/yr in the eastern Aleutian Islands. The deformation associated with the collision of these two plates is not confined to a narrow zone and earthquakes as large as magnitude 7 have occurred in the interior of Alaska. With the new GPS technology in hand, I was interested in measuring the crustal motion in Alaska to see directly how the surface of this great state is deforming, to estimate parameters such as slip rate and locking depth on faults through modeling of the surface deformation, and to investigate the along-strike

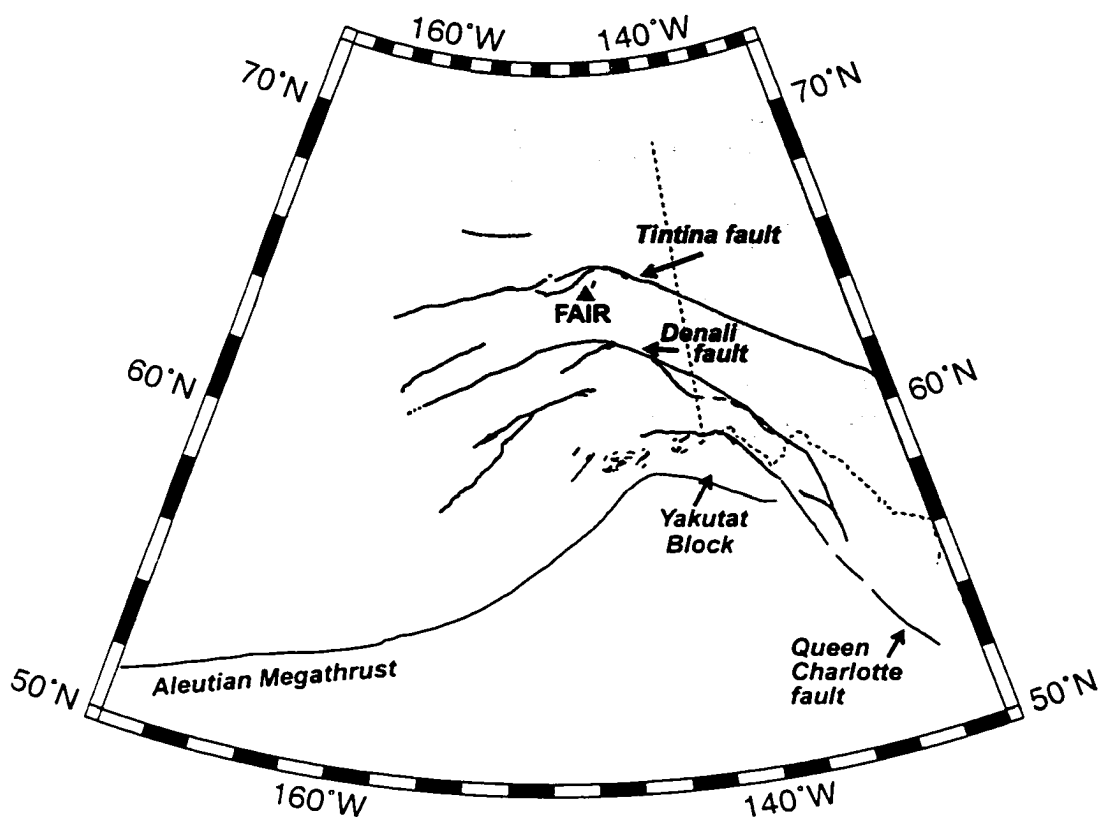


Figure 1.1. Map of Alaska showing active faults. Triangle shows Fairbanks (FAIR). (Data from *Plafker et al.* [1994].)

variation in the coupling of the subduction zone. This thesis presents the results of the GPS measurements and modeling of crustal deformation in Alaska.

## 1.2 Thesis Content and Organization

The thesis consists of four main science chapters along with this introduction and a general conclusions section, followed by three appendices. A bibliography containing references for all of the chapters is included at the end of the thesis. Figure 1.2 illustrates the regions studied in each chapter.

Chapter 2 was published in *Geophysical Research Letters* in October 1999. This paper focuses on the plate boundary region between the Queen Charlotte-Fairweather transform and the Aleutian megathrust. Here the Yakutat block, an exotic terrane comprising conti-

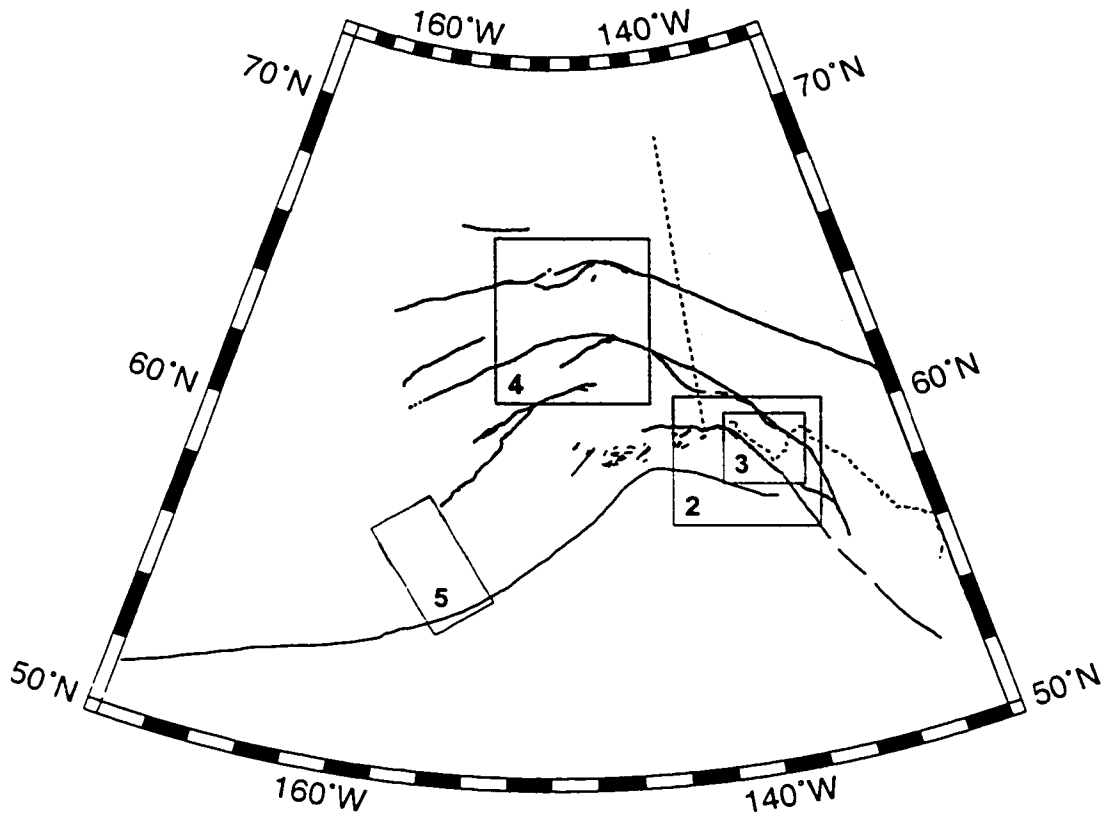


Figure 1.2. Map of Alaska showing study region for each chapter. Faults are from *Plafker et al. [1994]*.



mental and oceanic crust, is colliding with Alaska. This paper presented for the first time the velocity of a site at Yakutat, on the Yakutat block, based on repeated GPS measurements. These measurements clearly show that Yakutat is moving at neither the Pacific plate velocity nor the North American plate velocity. The difference in velocity between the Pacific plate and the velocity at Yakutat must therefore be taken up on nearby structures and the paper discusses which structures are likely to accommodate some of this motion.

Chapter 3 is based on work in the same area, but includes GPS results from additional sites spanning the Fairweather fault. This chapter was submitted to Geophysical Research Letters in November 2001. The Fairweather fault is a major strike-slip fault which ruptured in a  $M_S$  7.9 earthquake in 1958. We combined our GPS data with line-length data measured by the U. S. Geological Survey [Lisowski et al., 1987] in order to estimate the locking depth and slip rate of this fault. We find that this fault has a higher slip rate than the San Andreas fault and has the potential of rupturing in another 1958-sized earthquake within the next 35 years.

The majority of my fieldwork in the summers was spent gathering the data presented in Chapter 4. The goal of the work described in this chapter is to understand the tectonics of the interior of Alaska. Fairbanks is over 500 km from the Pacific-North American plate boundary and yet an extensive zone of seismicity extends northwestwards through Fairbanks. In 1937, a  $M_S$  7.3 earthquake occurred within 50 km of Fairbanks. In addition to studying the deformation in the region surrounding Fairbanks, this chapter presents results from observations made at sites in two profiles across the Denali fault, a structure that is thought to have displacements of up to 400 km across it [e.g., Forbes et al., 1973; Turner et al., 1974; Nokleberg et al., 1985]. Whilst such displacements indicate the fault was active in the past, I was curious as to whether there was any continuing slip across the fault that could be measured by GPS. I propose tectonic model involving rotation of southern Alaska, but in reality more GPS observations are needed over a longer period of time to clarify the tectonics of this region, because the rates of motion are slow.

Chapter 5 moves to a subduction setting. Here, the interesting question is how coupling varies along the strike of the megathrust. It is known from previous studies that some parts of the subduction zone are highly coupled [e.g., Savage et al., 1999], while others appear to be freely slipping [e.g., Freymueller and Beavan, 1999]. Using GPS observations, the

spatial and temporal variation of the degree of coupling can be estimated. The GPS data analyzed and modeled in this chapter are from sites in the Semidi section of the Alaska subduction zone. The stations occupy part of the segment that was ruptured by a  $M_W$  8.2 earthquake in 1938 and which lies between the segments of the arc that are considered locked and freely slipping. This chapter was published as a paper in Geophysical Research Letters in February 2001.

Appendix A presents a short overview on how GPS works and the steps necessary to reduce the errors in the observations. The fieldwork procedure used in measuring all sites contributing to this thesis is outlined in Appendix B. The position, velocity and errors in velocity for all sites measured are tabulated in Appendix C.

## Chapter 2

# New GPS Constraints on the Motion of the Yakutat Block<sup>1</sup>

### 2.1 Abstract

Global Positioning System (GPS) measurements were made at Yakutat, on the Yakutat terrane of southern Alaska, to investigate the motion of the Yakutat block with respect to the North American plate and to help constrain motion along the Fairweather fault. The velocity of Yakutat derived from the GPS data is  $44.1 \pm 1.9$  mm/yr toward  $N37^\circ W \pm 4^\circ$  relative to stable North America. The magnitude of this velocity is similar to that of the Pacific plate predicted by NUVEL-1A [DeMets et al., 1994], although there is a significant difference in the azimuth of these two vectors. The motion of Yakutat relative to North America is almost exactly parallel to the strike of the Fairweather fault, suggesting that most deformation inboard of Yakutat is right-lateral strike slip on the Fairweather fault or faults parallel to it, and that significant motion normal to the Fairweather fault occurs offshore of Yakutat. The GPS velocity at Yakutat is also used to help constrain the slip rate and locking depth of the Fairweather fault.

---

<sup>1</sup>Published as Fletcher, H. J. and J. T. Freymueller, *Geophys. Res. Lett.*, 26, 3029-3032, 1999.

## 2.2 Introduction

The Pacific-North American plate interaction dominates the tectonics of southern Alaska. The Pacific plate subducts under the North American plate at the Aleutian megathrust, while in southeast Alaska the Pacific-North American relative plate motion is accommodated along the Queen Charlotte and Fairweather faults. The nature and location of the plate boundary between this transform fault system and the northern end of the Aleutian trench is complex [e.g., *Lahr and Plafker*, 1980; *Perez and Jacob*, 1980; *Lahr et al.*, 1988]. The relative plate motion is believed to be taken up on a variety of fault systems - the Contact and Chugach-St. Elias faults and the Pamplona and Kayak Island thrust zones accommodate much of the relative motion, with the Denali fault system in the interior of Alaska and the Transition Zone (TZ) offshore of southern Alaska possibly taking up small components of motion (Figure 2.1).

Southern Alaska is composed of numerous allochthonous tectonostratigraphic terranes, indicating a complex history of plate motions and collisions that continues today in the form of the Yakutat terrane. This terrane, a composite oceanic and continental block, is currently colliding with southern Alaska, allowing us to observe tectonic processes like those that emplaced the previous terranes of southern Alaska. The Yakutat block is bounded by the Fairweather fault to the northeast, the Kayak zone to the northwest and the TZ to the south (Figure 2.1). Along its western and northern boundaries, the Yakutat terrane has been thrust northwestward beneath the Paleogene Prince William terrane [*Brocher et al.*, 1994; *Plafker*, 1987]. The extreme uplift of the Chugach and St. Elias Mountains are a result of transpression along the northern margin of the terrane.

*Lahr and Plafker* [1980] proposed a kinematic tectonic model for the Pacific-North American plate interaction based on available geologic and seismic data. In their model, the Yakutat block is largely coupled to the Pacific plate and is moving parallel to the Pacific plate, but at a slightly lower velocity relative to North America. Their model rates were chosen to give 4 mm/yr of oblique convergence on the TZ to be in agreement with data from the  $M_S$  6.7 earthquake in 1973 at the eastern end of the zone, which had a focal mechanism consistent with oblique thrusting on a northwest-striking fault. Based on analysis of slip vectors of the 1973 earthquake and its two aftershocks, and the Pacific-North American

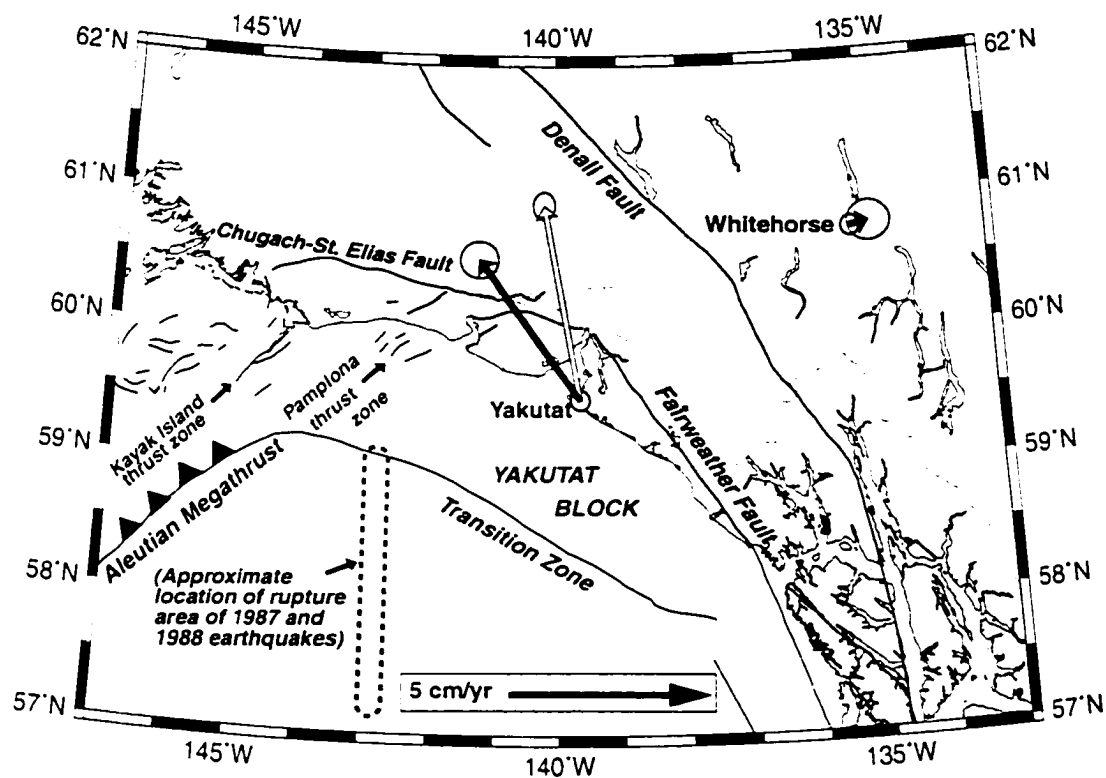


Figure 2.1. A map of the Yakutat area of southern Alaska. Black arrows are the GPS-derived velocities of Yakutat and Whitehorse, the white arrow is the NUVEL-1A velocity of the Pacific plate at Yakutat. 95% confidence error ellipses are also shown.

relative motion predicted by model RM2 of *Minster and Jordan* [1978]. *Perez and Jacob* [1980] calculated a rate of convergence between the Pacific plate and the Yakutat block of 10 mm/yr. However, the marine geophysical data for the offshore part of the Yakutat block show no obvious deformation or accretion adjacent to the TZ. *Bruns* [1983] therefore claimed that the zone is a remnant fracture zone and has been inactive since the Miocene.

The Fairweather fault is the onshore part of the Queen Charlotte-Fairweather fault system, which takes up most or all of the Pacific-North America plate motion in the transform part of the boundary. The fault strikes linearly northwest to Yakutat Bay, beyond which it ends in a series of east-west to northeast-southwest striking faults, and appears to connect with the Chugach-St. Elias fault system. A  $M_S$  7.9 earthquake in 1958 ruptured about 350 km of the Fairweather fault. Slip rates of between 48 and 58 mm/yr have been reported for the Fairweather fault based on geomorphic studies [*Plafker et al.*, 1978], although the lower limit is more likely since NUVEL-1A gives a rate of only  $49.1 \pm 1.4$  mm/yr for Pacific-North American relative motion in this area. From repeated surveys of small-scale geodetic networks spanning the fault, *Lisowski et al.* [1987] estimate the slip rate to be between 41 and 51 mm/yr.

In 1899, the region between Yakutat Bay and Kayak Island was ruptured by two large earthquakes of  $M_S$  7.9 and 8.0. *Page et al.* [1991] suggest that the Chugach-St. Elias fault may be a likely location for the first of these earthquakes due to the lack of a tsunami. *Thatcher and Plafker* [1977] studied the effects of the second 1899 earthquake and inferred 10 to 20 meters of reverse slip on northwest-striking, northeast-dipping thrust faults in the Yakutat Bay region. In 1979, the  $M_S$  7.1 St. Elias earthquake occurred beneath the St. Elias Mountains, and involved reverse slip on a gently dipping fault about 15 km deep [*Stephens et al.*, 1980; *Estabrook et al.*, 1992].

## 2.3 Data and Results

GPS observations were made at Yakutat airport in 1992 by the U.S. Geological Survey and in 1993 by the National Geodetic Survey. We carried out subsequent surveys at the same location in 1995 and 1996. The permanent GPS station in Fairbanks was in operation for the duration of all of these surveys, and observations at a station in Whitehorse were

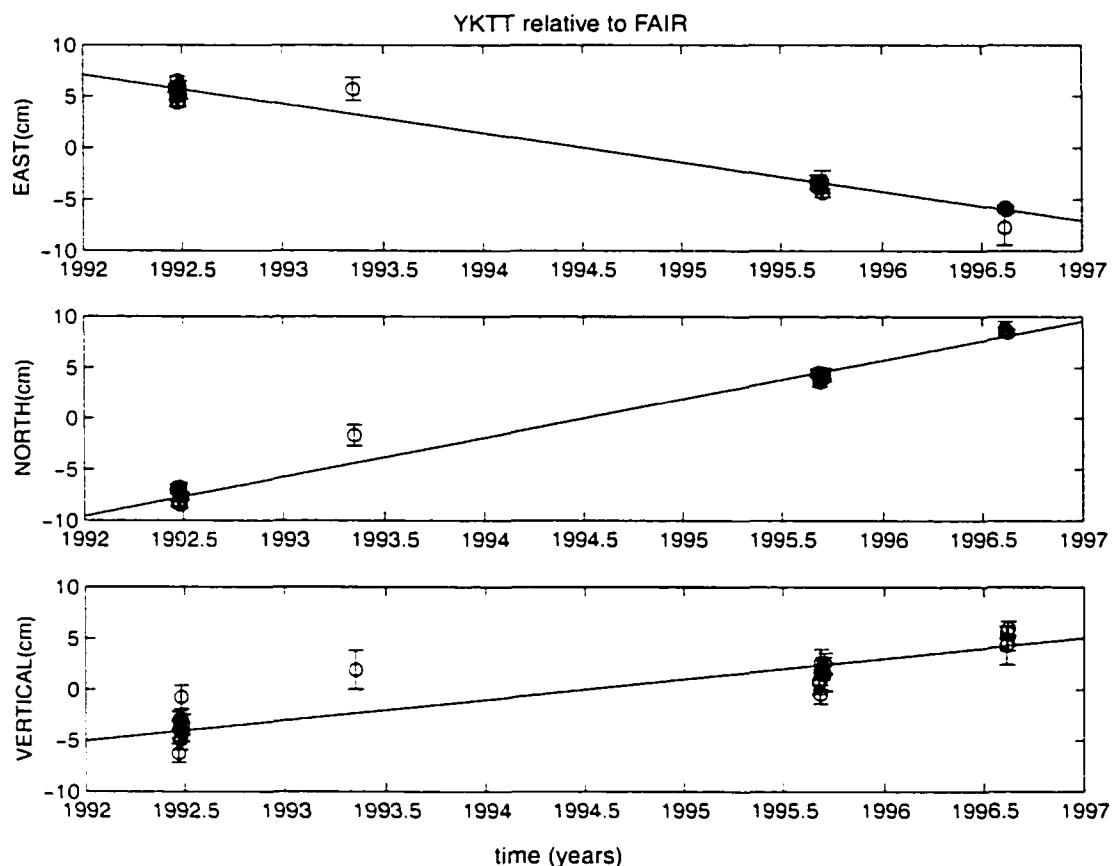


Figure 2.2. Time series of GPS measurements at Yakutat. Measurements are relative to the permanent GPS site at Fairbanks.

made in 1993, 1995, and 1996, overlapping in time with the 1995 and 1996 Yakutat surveys. We analyzed the data using the GIPSY/OASIS II software developed by the Jet Propulsion Laboratory using analysis methods similar to those described in *Larson et al. [1997]*. Figure 2.2 shows the individual solutions for the position of Yakutat relative to Fairbanks, which has a southward velocity of  $2.1 \pm 1.1$  mm/yr relative to stable North America [*Larson et al., 1997*].

Using the estimated station coordinates and their covariances for each day, the Fairbanks velocity, and assuming constant velocities, we estimated the velocities of Yakutat and Whitehorse relative to North America to be  $44.1 \pm 1.9$  mm/yr toward  $N37^\circ W \pm 1^\circ$  and  $5.2 \pm 2.3$  mm/yr toward  $N79^\circ E \pm 2^\circ$  (Figure 2.1). The magnitude of the GPS-derived velocity

at Yakutat is only slightly smaller than that of the Pacific plate relative to North America predicted by NUVEL-1A ( $49.1 \pm 1.4$  toward  $N11^\circ W \pm 1^\circ$ ). However, there is a significant difference in the azimuth of these two vectors. Subtracting the Yakutat velocity from the NUVEL-1A Pacific-North America velocity results in a velocity of  $21 \pm 3$  mm/yr towards  $S53^\circ W \pm 3^\circ$

## 2.4 Discussion and Conclusions

### 2.4.1 Yakutat Block Motion

Our result for the velocity of Yakutat clearly shows that this part of the Yakutat block is not moving at either Pacific plate velocity or North American plate velocity. The motion of Yakutat relative to North America is almost exactly parallel to the strike of the Fairweather fault ( $N34^\circ W$ ), suggesting that almost all deformation inboard of Yakutat is right-lateral strike slip on the Fairweather fault or faults parallel to it, and that most or all of the difference between the Pacific plate velocity and the velocity at Yakutat (in essence a Fairweather fault-normal velocity component) must be accounted for by contraction outboard of Yakutat, which would require significant motion either within the Yakutat block or between the Yakutat block and the Pacific plate. The magnitude of the velocity difference is 21 mm/yr and the orientation is  $S53^\circ W$ . A small part of the velocity difference may occur as a result of transient deformation due to elastic strain accumulation on locked thrust faults to the north, but we expect any deformation at Yakutat, in the footwall block of such faults, to be small. In their finite element model, *Lundgren et al. [1995]* fixed the Yakutat block to the Pacific plate, and they calculated large ( $> 10$  mm/yr) north-east oriented displacements radiating away from the Queen Charlotte-Fairweather faults. This is clearly in disagreement with our results, which imply no significant Fairweather-normal contraction inboard of Yakutat. Uplift was reported in association with the 1899 Yakutat Bay earthquakes [*Tarr and Martin, 1912*], which would imply some shortening in the region. The GPS uncertainties allow 2-3 mm of slip to occur on thrust faults in the area. Figure 2.3 is a cartoon showing the velocity difference at Yakutat that needs to be accounted for, and the structures that might account for some of this velocity.

The velocity difference is likely taken up by slip on faults outboard of Yakutat (e.g.,



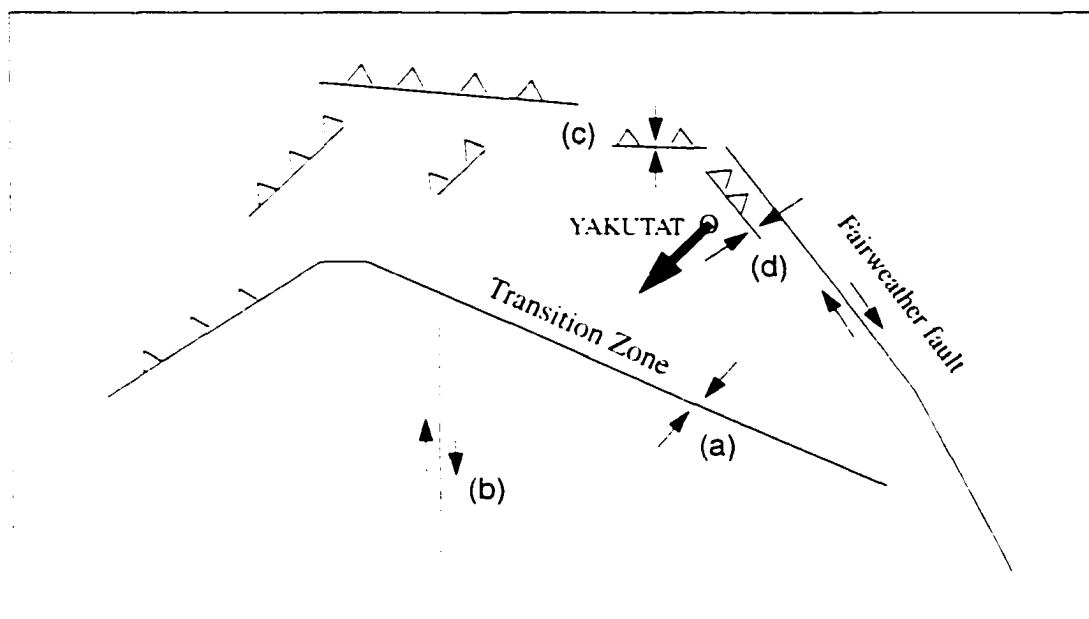


Figure 2.3. Cartoon map showing faults in the Yakutat area. The bold arrow at Yakutat shows the direction of the velocity at Yakutat relative to the Pacific plate (approximately perpendicular to the Fairweather fault). Faults (a), (b), (c), and (d) were tested to determine whether such structures could account for this velocity difference. The smaller arrows indicate the sense of motion on the faults.

structures (a) and (b) in Figure 2.3). however elastic strain accumulation on locked faults inboard of Yakutat (structures (c) and (d) in Figure 2.3) could cause a small amount of elastic deformation at Yakutat.

The nearest major mapped thrust faults to Yakutat are a minimum of 45 km to the north and dip northwards, thus Yakutat is in the footwall block. We used a fault dislocation model based on the equations of *Okada* [1985] to determine the maximum effect on the velocity at Yakutat of an east-west striking locked thrust fault 45 km north of Yakutat (Figure 2.3, fault (c)). As expected, we find that such a fault cannot account for the difference between the Pacific plate velocity and the GPS-derived velocity at Yakutat: the model result of 1 mm/yr of elastic deformation is much smaller than the  $21 \pm 3$  mm/yr velocity difference between the Fairweather fault-normal components, even if the fault is located much closer to or farther from Yakutat than the model fault. To satisfy uplift data from the 1899 earthquake, *Plafker and Thatcher* (W. Thatcher, personal communication, 1998) constructed a fault model involving a thrust fault oriented parallel to the Fairweather fault, 20 km north of Yakutat, and dipping to the northeast (Figure 2.3, fault (d)). Again, Yakutat would be in the footwall block and the elastic deformation at Yakutat due to such a fault is small. Note that slip on faults of this orientation would cause the velocity of Yakutat relative to North America to be more northerly than we observe.

#### 2.4.2 Possible Offshore Structures and Implications

We cannot resolve uniquely which offshore structures accommodate the Yakutat-Pacific motion as we do not have enough data, although the TZ is an obvious candidate (Figure 2.3, fault (a)). Using *Okada's* [1985] elastic dislocation equations, we constructed a model for the TZ as a fault oriented at  $N60^\circ W$ , dipping 5 degrees NE, and locked to a depth of 25 km. The results of this modeling are shown in Figure 2.4, presented in Fairweather fault-normal and fault-parallel orientations.

The crosses indicate the difference between the Pacific plate velocity and the GPS-derived velocity at Yakutat. The three lines show the surface displacement per year due to the elastic effects of the modeled fault for three different cases: the dotted line for a fully coupled TZ (i.e., the fault is fully locked and does not slip between earthquakes), the dashed line for a TZ with a degree of coupling of 0.25, i.e., 25% locked (meaning that the fault may

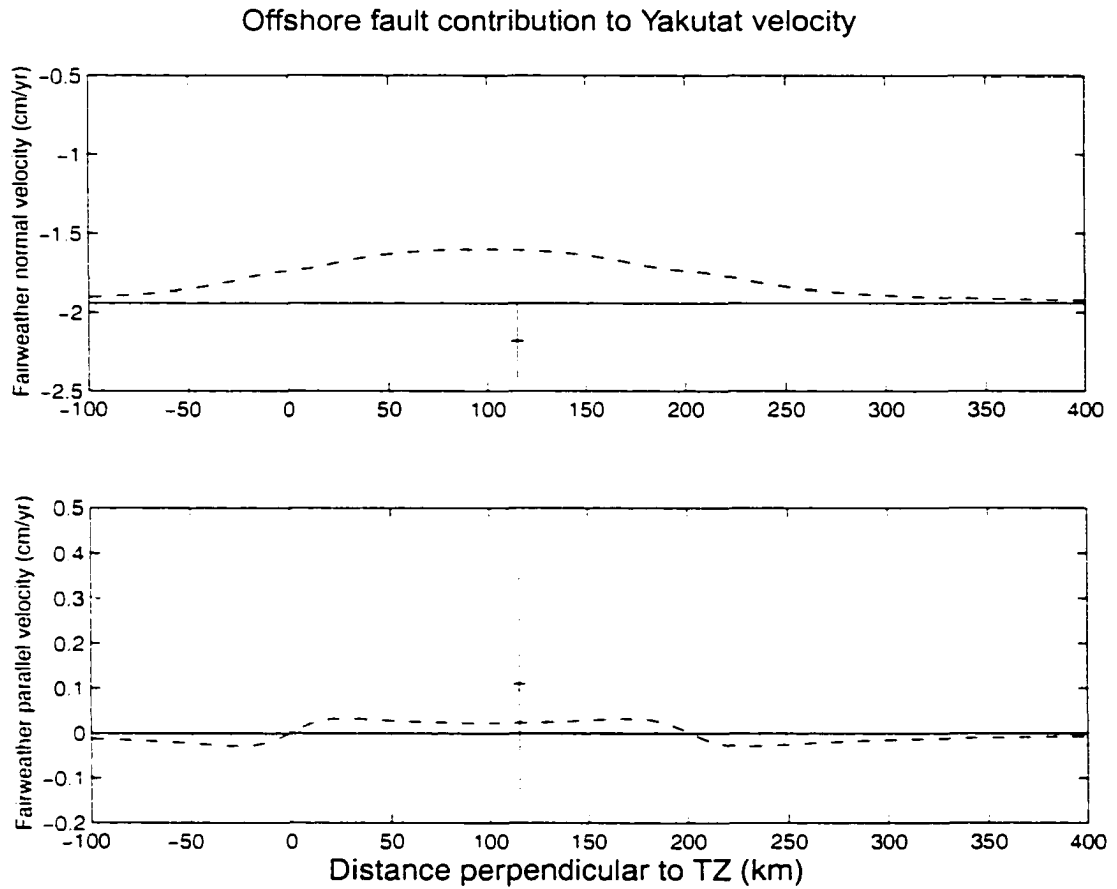


Figure 2.4. The surface displacement per year due to a modeled Transition Zone, oriented  $N60^{\circ}W$ , dipping 5 degrees NE. The incident velocity is the Pacific plate velocity normal to the Fairweather fault, 19.5 mm/yr. The crosses are the difference between the Pacific plate velocity at Yakutat predicted by NUVEL-1A and the GPS-derived velocity at Yakutat. The dotted line is for a fully locked Transition Zone, the dashed line is for a 25% locked Transition Zone, and the solid line is for a freely slipping Transition Zone.

slip aseismically at 75% of the long-term slip rate), and the solid line for a freely slipping TZ (degree of coupling equal to zero). Using this model, a completely uncoupled TZ can accommodate all of the  $21 \pm 2$  mm/yr Fairweather fault-normal component of the Pacific plate velocity, within the error limits. Any locking of the TZ near Yakutat would cause a more northward and eastward movement of Yakutat than is observed. However, other offshore structures could take up some or all of the velocity difference which would reduce this convergence rate, and allow the fault to have some degree of coupling. The Pamplona and Kayak fold and fault zones likely have some convergence across them, but the velocity at Yakutat gives us no information about this. A scenario in which the Yakutat block is being pushed at its SE corner, but is free to rotate counter-clockwise above the TZ would allow slip on the Fairweather fault as well as a freely-slipping TZ near to Yakutat (Figure 2.3). We need data from more sites to test such a 3D model.

Another possible candidate for motion offshore is the 250 km long north-south unnamed fault in the Pacific plate, situated south of the Yakataga seismic gap (Figure 2.3, fault (b)). Two  $M_s$  7.6 dextral strike-slip earthquakes ruptured this fault in 1987 and 1988 [Lahr et al., 1988]. If all of the north component of the plate velocity normal to the Fairweather fault is taken up along this north-south fault, then it would have a right-lateral slip rate of 11 mm/yr, and the TZ would then have a convergence of 16 mm/yr in an easterly direction. Our data cannot distinguish between a model in which the TZ takes up all of the Fairweather fault-normal convergence, and one in which there is some right-lateral slip on a north-south striking offshore fault.

### 2.4.3 Fairweather Fault Constraints

Elastic screw dislocation models are typically used in determining fault slip rates from geodetic data near strike-slip faults. Such a model represents a physical model in which the upper portion of the fault is locked between earthquakes, and the lower ductile part slips steadily at the long-term slip rate of the fault. The depth of the locked part of the fault corresponds to the base of the seismogenic zone, and is termed the locking depth of the fault. In two dimensions, the fault-parallel surface displacements from this model are a simple function of the long-term slip-rate of the fault, the locking depth, and the distance from the fault. Inversions to estimate fault properties from surface displacements have an

inherent trade-off between the estimated slip rate and the locking depth of the fault if the data do not extend at least a few fault locking depths away from the surface trace of the fault [e.g., *Johnson and Wyatt, 1994*]

*Lisowski et al. [1987]* estimated the slip rate on the Fairweather fault from repeated surveys of small-scale geodetic networks spanning the fault. Their geodetic networks had no sites more than 15 km from the fault, and so the authors could not determine the slip rate without assuming a locking depth. The authors report that the best fits of the dislocation fault model to their data are obtained with locking depths of 7 to 9 km and corresponding slip rates of between  $41 \pm 3$  and  $51 \pm 4$  mm/yr, although any slip rate between 37 mm/yr and 56 mm/yr (and locking depths between 6 and 10 km) would fit their data almost as well.

The velocity at Yakutat was determined relative to North America, so our dislocation model has to include slip on any faults which could contribute to strike-slip motion between Yakutat and stable North America. We use a model with two faults, the Fairweather and Denali faults, which we assume to be vertical and parallel to each other. We combine our GPS data with the line length data from *Lisowski et al. [1987]*, which are insensitive to slip on the Denali fault 110 km to the north, and the Fairweather fault-parallel Pacific plate velocity at Yakutat from NUVEL-1A. Using all this information, we can invert for the slip rate and locking depth on the Fairweather fault and the slip rate on the Denali fault. However, the solution is poorly constrained because we are adding a third model parameter to the inversion, the slip rate on the Denali fault, with little data giving us information about this parameter. At present, therefore, some assumptions have to be made in order to determine the slip rate on the Fairweather fault. The locking depth of faults is often determined from the depth of the current seismicity along the fault. There are only 4 seismic stations within a 20,000 km<sup>2</sup> area around the Fairweather fault, so earthquakes in this region are not well detected or located and thus are of no help in delimiting the locking depth of the Fairweather fault. The slip rate on the Denali fault is unknown: estimates range from 8-12 mm/yr average slip rate based on geomorphic evidence for Holocene offsets [*Plafker et al., 1994*] to no significant slip in the years 1975 to 1988 based on trilateration networks [*Savage and Lisowski, 1991*]. If a slip rate of 0 mm/yr is assumed on the Denali fault, then the slip rate of the Fairweather would be  $48.6 \pm 1.1$  mm/yr. Taking the maximum estimate range for slip rate on the Denali fault, 8-12 mm/yr, we find the slip rate of the Fairweather

Authors	Slip Rate	Locking Depth
Plafker et al., 1978	48 to 58	
Lisowski et al., 1987	$41 \pm 3$ to $51 \pm 4$	7 to 9 (assumed)
This study, Denali slip 0 mm/yr	$48.6 \pm 1.1$	$8.9 \pm 0.7$
This study, Denali slip 8-12 mm/yr	$35.7 \pm 1.0$ to $40.0 \pm 1.0$	$6.1 \pm 0.6$ to $7.1 \pm 0.7$

Table 2.1. Summary of calculated slip rates and locking depths for the Fairweather fault.

fault would be between  $35.7 \pm 1.0$  mm/yr and  $40.0 \pm 1.0$  mm/yr. Estimated slip rates and locking depths are shown in Table 1.

Clearly the true uncertainty in the Fairweather fault slip rate is still controlled by the uncertainty in the Denali fault slip rate. Locking depths of strike-slip faults in northern California are reported to be between 8 and 15 km for different faults [*Castillo and Ellsworth, 1993*]. Compared with these estimates from seismicity, the locking depths estimated for the Fairweather fault are shallow, but not extreme. Re-measuring just one of the *Lisowski et al. [1987]* sites on the north side of the Fairweather fault with GPS would provide enough information to uniquely determine the slip rate and locking depth of the Fairweather fault and the slip rate on the Denali fault using our model geometry. We hope to be able to further constrain these important parameters in the future.

## 2.5 Summary

The velocity at the town of Yakutat, on the Yakutat block is determined to be  $44.1 \pm 1.9$  mm/yr at  $N37^\circ W \pm 5^\circ$  relative to North America. The azimuth of this vector is almost exactly the same as the orientation of the Fairweather fault, and is significantly different from the azimuth of the Pacific plate vector relative to North America at Yakutat. The difference between the GPS-derived and Pacific plate predicted velocities at Yakutat is therefore essentially in a Fairweather fault-normal direction. We have determined that this difference in velocity must be accommodated by offshore faults. The Transition Zone is a likely candidate for taking up at least part of the motion between the Yakutat block and the Pacific plate.

## 2.6 Acknowledgments

We thank J. Lahr, W. Wallace and S. Wiemer for reviews, and G. Tytgat, B. Hammond and K. Lindquist for fieldwork assistance. A start-up grant from the Geophysical Institute helped fund this project, along with assistance from the Seismology laboratory.

## 2.7 Appendix

The GPS velocity at Yakutat has a lower Fairweather fault-normal component of velocity than does the Pacific-North American plate velocity at Yakutat from NUVEL-1A. The difference between the two vectors is 21 mm/yr in a Fairweather fault-normal direction. In this chapter we explained that this must be accommodated offshore. Strain accumulation on locked thrust faults north of Yakutat might explain part of this slower Fairweather fault-normal velocity at Yakutat and so we modeled the effect of such a fault to determine its effect. A figure to illustrate this model was not included in the paper due to length constraints and so we add a figure to show the model results in this appendix. We used the dislocation equations of *Okada* [1985] to construct a model fault 45 km to the north of Yakutat. The fault dips to the north and is locked. We modeled a variety of dips and locking depths, but in all of our models the effect of a locked fault on the velocity at Yakutat was small, ranging from 0 mm/yr for a shallow-dipping fault with low locking depth to 2 mm/yr for a steeply-dipping fault with a large locking depth. Figure 2.5 shows the model for an E-W oriented fault dipping 30 degrees to the north and locked to 10 km depth (i.e., the width of the locked part of the fault is  $10/\sin(30) = 20$  km).

The figure shows that the Fairweather fault-normal component of velocity at Yakutat is reduced compared to the NUVEL-1A Fairweather fault-normal component of motion, but only by 1 mm/yr and thus a locked thrust fault north of Yakutat cannot cause the difference between the NUVEL-1A Pacific plate velocity and the GPS velocity we see at Yakutat.

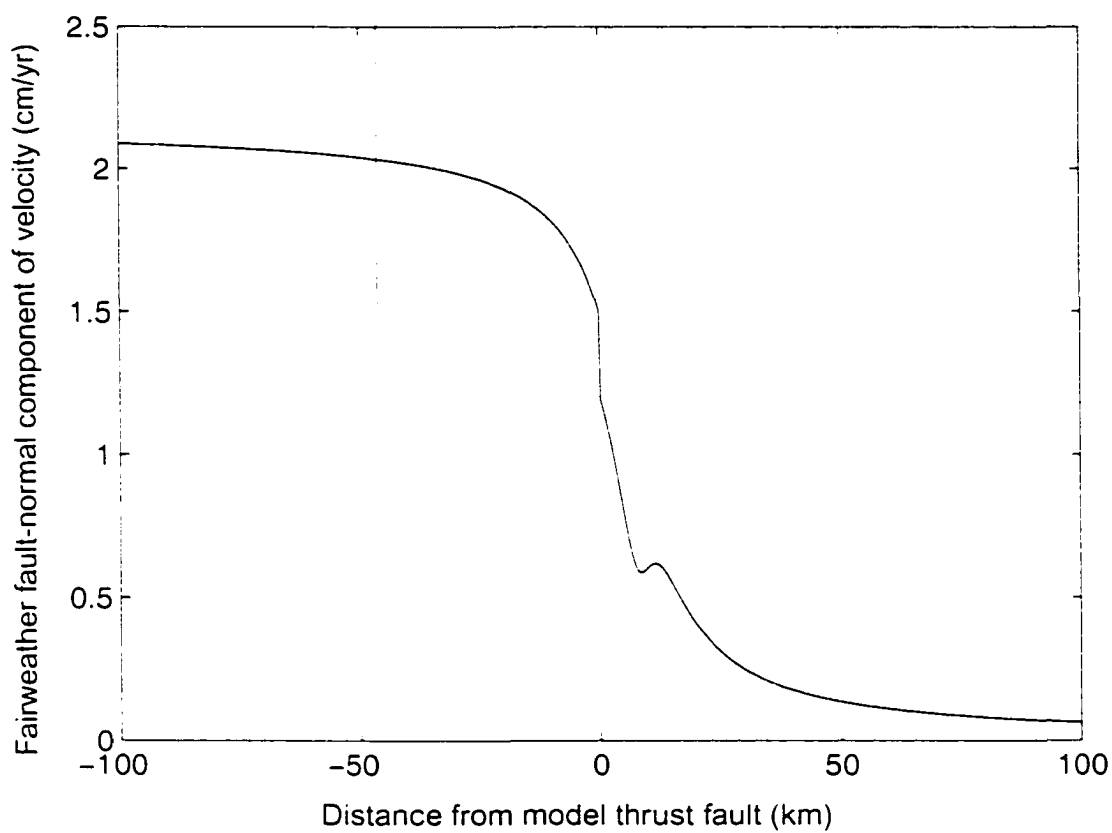


Figure 2.5. Fairweather fault-normal component of velocity. Velocity is due to a modeled thrust fault 45 km north of Yakutat, oriented E-W, dipping 30 degrees to the north. The vertical line indicates the position of Yakutat. The right side of the graph is stable north America (zero velocity at a far distance from the fault) and the left side of the graph is the Pacific plate (21 mm/yr at a far distance from the fault).



## Chapter 3

# New constraints on the motion of the Fairweather fault, Alaska, from GPS observations<sup>1</sup>

### 3.1 Abstract

GPS velocities from sites near the Fairweather fault in southern Alaska were combined with line length data from geodetic surveys by the U. S. Geological Survey to estimate the slip rate and locking depth of the Fairweather fault using dislocation theory. We performed a weighted least-squares inversion of the geodetic data and obtained a best-fitting slip rate of  $38.2 \pm 3.1$  mm/yr and locking depth of  $7.0 \pm 0.9$  km. The slip rate we estimated is higher than that observed across the San Andreas fault and is one of the highest observed across any strike slip fault. In 1958, a  $M_s$  7.9 earthquake ruptured the Fairweather fault causing 3.5 meters of displacement in places. This displacement would be recovered in 80 years given our estimated slip rate. We also included the Dalton Creek segment of the Denali fault in our model and estimated a slip rate of  $10.7 \pm 2.4$  mm/yr for this section of the fault.

---

<sup>1</sup>Prepared for submission in *Geophys. Res. Lett.*

## 3.2 Introduction

Few direct measurements of crustal deformation have been made in southern Alaska, yet the plate interactions in this region are key to understanding the active tectonics of Alaska. Figure 3.1 shows the major active or potentially active faults in this region. The Pacific plate subducts under the North American plate at the Aleutian megathrust, while in southeast Alaska the Pacific-North American relative plate motion is accommodated along the Queen Charlotte-Fairweather transform fault system. The nature and location of the boundary between the transform system and the Aleutian megathrust is complex, due in part to the ongoing collision of the Yakutat terrane with southern Alaska [e.g., *Lahr and Plafker*, 1980; *Perez and Jacob*, 1980; *Lahr et al.*, 1988; *Doser and Lomas*, 2000]. The relative plate motion in this region is taken up by crustal shortening and strike-slip faulting offshore in the Gulf of Alaska and in the Kayak Island and Pamplona fold and thrust belts. Deformation also occurs onshore in the Chugach-St. Elias Mountains and along faults in the interior of Alaska such as the Denali fault.

The Queen Charlotte-Fairweather fault originates at the triple junction north of Vancouver Island and extends 1200 km to southern Alaska. The fault is named the Queen Charlotte fault up to the southern end of Chatham Strait, where it becomes the Fairweather fault. The fault is offshore up to Icy Point and from there it stretches over 200 km to the northern end of Yakutat Bay, where it bends westwards and splays into several east-west oriented thrust faults, probably connecting with the Chugach-St. Elias fault system (Figure 3.1).

The onshore Fairweather fault bounds the Yakutat block to the east and is oriented  $N34^{\circ}W$ . The offshore part of the Fairweather fault is oriented  $N21^{\circ}W$  and so the fault bends about  $13^{\circ}$  between its offshore and onshore segments. The fault was ruptured by a  $M_s$  7.9 earthquake in 1958 and the preferred nodal plane of the focal mechanism was consistent with right-lateral slip on the Fairweather fault [*Stauder*, 1960]. Right-lateral slip of 2 m was measured along the southern half of the fault, with a maximum well-documented slip of about 3.5 m [*Lisowski et al.*, 1987].

*Plafker et al.* [1978] reported a slip rate for the Fairweather fault of between 48 and 58 mm/yr based on geomorphic studies, although the lower limit is more likely since the

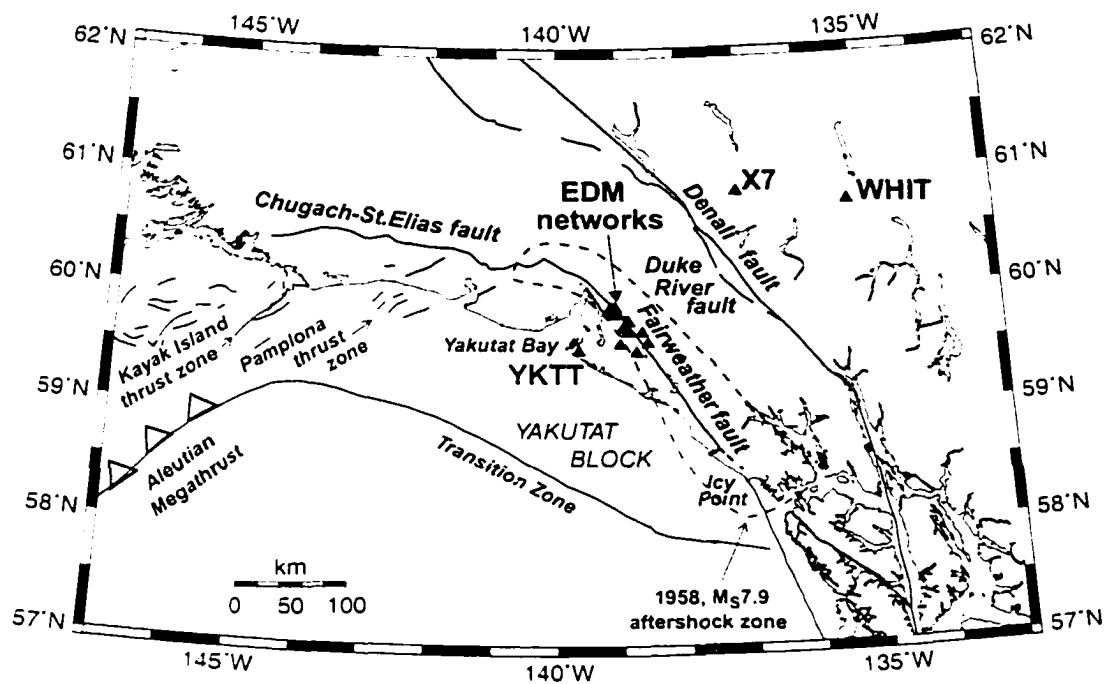


Figure 3.1. A map of the Yakutat area of southern Alaska. Geodetic stations are shown by solid black triangles. Faults shown as black lines are from *Plafker et al. [1994]* and are faults that are known or suspected to be active. The dotted line shows the outline of the 1958 rupture zone.

new plate motion model of [DeMets and Dixon, 1999] (an updated version of NUVEL-1A, DeMets et al. [1994]) gives a rate of only  $50.9 \pm 1.4$  mm/yr in a direction  $N14.7^\circ W \pm 1.4^\circ$  for Pacific-North American plate motion in this area. If the Pacific-North American plate motion was perfectly partitioned between strike-slip motion on the Fairweather fault and convergence normal to it, then it would have a slip rate of 48.0 mm/yr, with 16.8 mm/yr convergence across it. Lisowski et al. [1987] estimated the slip rate to be 41 to 51 mm/yr from repeated surveys of small-scale geodetic networks spanning the fault, although any slip rate between 37 mm/yr and 56 mm/yr would fit their data almost as well. At a slip rate of 41 mm/yr, it would take 85 years to recover the 3.5 m of displacement that occurred in the 1958 earthquake; for a slip rate of 51 mm/yr this would be only 67 years (i.e., by the year 2025). A more precise knowledge of the slip rate will aid in estimating the seismic hazard of the Fairweather fault and will also reveal the magnitude of slip that must be taken up by other faults.

The goal of this study was to improve the estimate of the slip rate of the Fairweather fault (Figure 3.1) by adding new GPS data to the geodetic data of Lisowski et al. [1987]. They used line-length measurements in 1967, 1983, and 1986 between stations in two networks that cross the Fairweather fault and computed a rate of change of line length between stations. The line lengths were measured using a Geodolite, a precise electro-optical distance measuring instrument (EDM). In 1992, GPS observations were made by the USGS at these EDM sites. We used GPS observations at a site in Yakutat as well as repeat GPS observations at two of the EDM sites and the Fairweather fault-parallel component of Pacific-North American plate velocity at Yakutat from a recent plate motion model [DeMets and Dixon, 1999] to augment the EDM line length data and improve the slip rate estimate for the Fairweather fault.

### 3.3 Data

GPS measurements were made at Yakutat airport (YKTT), 27 km south of the Fairweather fault, in 1992 by the United States Geological Survey (USGS) and in 1993 by the National Geodetic Survey (NGS). We carried out subsequent surveys in 1995, 1996, 1999 and 2001. The Lisowski et al. [1987] geodetic sites (Figure 3.1) were re-surveyed in 1992 using GPS.

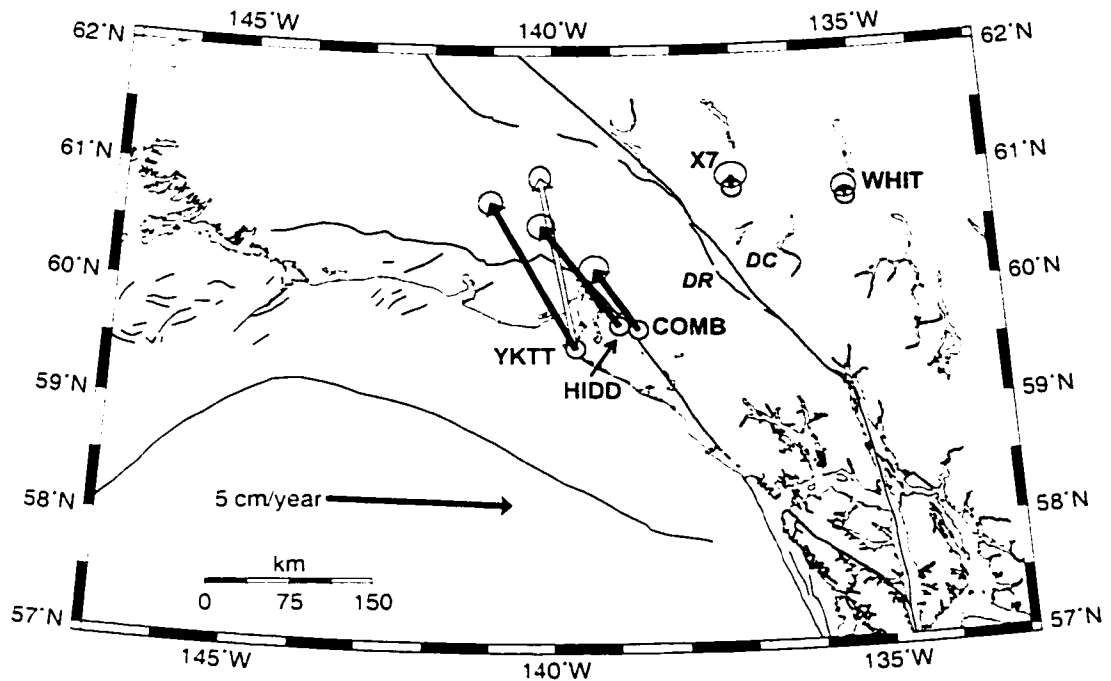


Figure 3.2. GPS velocities for sites in the Yakutat region. The white arrow is the *DeMets and Dixon [1999]* Pacific-North American plate velocity at Yakutat. Error ellipses are 95%. DC = Dalton Creek segment of the Denali fault; DR = Duke River fault.

and in 1999 we re-measured two of these sites, HIDD and COMB. Measured perpendicular to the azimuth of the Fairweather fault. HIDD is 4 km southwest of the fault and COMB is 7 km away to the northeast. Other sites in the vicinity where we have measured GPS velocities are X7, with observations in 1992, 1999 and 2000, and WHIT (Whitehorse), which has been a permanent GPS site since 1995 (Figure 3.2).

The GPS data were analyzed using the GIPSY/OASIS II software to obtain daily coordinates in the ITRF97 reference frame [*Boucher et al., 1999*] as well as covariance estimates for the coordinates, using techniques described by *Frey Mueller et al. [2000]*. The daily solutions were combined to estimate site velocities using a least squares inversion, weighted by the full covariance matrix of the coordinates. We were examining deformation in the Pacific-North American plate boundary region, so we estimated velocities relative to the North American plate to simplify our interpretation. We used the pole and rotation given by *Sella et al. [2002]* for ITRF97-North America relative motion to convert our GPS velocities

Station	Lat	Lon	Velocity	Azimuth
YKTT	59.5107	-139.6488	47.2±1.3	N29°W ± 2°
HIDD	59.7055	-138.9455	35.1±1.4	N36°W ± 3°
COMB	59.6098	-138.6393	20.9±1.5	N34°W ± 6°
X7	60.8592	-137.0629	3.4±1.4	N6°W ± 38°
WHIT	60.7505	-135.2221	2.4±1.3	N6°W ± 44°

Table 3.1. Site velocities in mm/yr

Errors are  $1\sigma$ .

from the ITRF97 reference frame to a North America-fixed reference frame. The resulting velocities for each site relative to the North American plate (Table 1) were transformed into a local east-north-up coordinate system at each site.

Figure 3.2 shows velocities for the sites YKTT, HIDD, COMB, X7 and WHIT relative to North America. The light arrow shows the *DeMets and Dixon [1999]* Pacific-North American plate velocity at Yakutat, which is  $50.9\pm 1.4$  mm/yr in a direction N14.7°W±1.4°. It is clear that YKTT, with a velocity of  $47.0\pm 1.3$  mm/yr in a direction N28.5°W±1.8° relative to North America is moving at neither the Pacific plate velocity nor the North American plate velocity. Instead, the velocity at Yakutat is almost parallel to the Fairweather fault, which is oriented N34°W. The difference between the *DeMets and Dixon [1999]* Pacific-North American plate velocity at Yakutat and the GPS-derived velocity is therefore normal to the Fairweather fault. *Fletcher and Freymueller [1999]* discuss possible structures which may accommodate this motion: in this paper we only discuss the Fairweather fault-parallel component of velocity. We note, however, that the lack of a significant Fairweather-normal component of velocity at any of these sites reinforces our earlier conclusion that this component is accommodated offshore, outboard of Yakutat. Sites X7 and WHIT have velocities that are close to zero relative to North America.

### 3.4 Discussion

Elastic screw dislocation models are typically utilized to determine fault slip rate from geodetic data near the fault. Such a model is a mathematical representation of a physical model in which the upper portion of the fault is locked between earthquakes, and the lower ductile part slips steadily at the long-term slip rate of the fault. The depth of the locked part of the fault corresponds to the base of the seismogenic zone, and is termed the locking depth of the fault. In two dimensions, the fault-parallel surface displacements from this model are a simple function of the long-term slip-rate of the fault, the locking depth, and the distance from the fault. For an infinitely long fault locked at the surface and slipping freely at a rate  $S$  below depth  $D$ , the fault-parallel velocity of a site at a perpendicular distance  $x$  from the fault at  $x_f$  is [Savage and Burford, 1973]:

$$V(x) = \frac{S}{\pi} \operatorname{atan} \left( \frac{(x - x_f)}{D} \right) \quad (3.1)$$

This model does not account for material heterogeneities or viscoelasticity, but it has been shown to reasonably predict first-order features of deformation observed on other strike-slip faults, e.g., the San Andreas fault system [e.g., Lisowski et al., 1991]. Viscoelastic effects may be more important in the immediate post-seismic interval. However, the last major earthquake was in 1958 and given our small data set we believe that using this simple two dimensional elastic model is the best approach. Whilst we acknowledge that along-strike variations in coupling are likely, we do not have the density of data needed to investigate this variation. Page and Lahr [1971] observed only a small amount of deformation within a 40 m wide geodetic network across the Fairweather fault and concluded that the fault is not creeping at the surface but is locked and accumulating strain. We therefore assume that the fault is fully-coupled down to a locking depth,  $D$ . Figure 3.3 illustrates the trade-off between fault slip rate and locking depth when inverting geodetic data using equation 3.1.

In this example, the velocity at a site 20 km away from the fault can be explained both by a model fault with a slip rate of 2 cm/yr and locking depth of 20 km or a model fault with a slip rate of 4 cm/yr and locking depth of 5 km. In order to resolve this trade-off, data must be obtained from sites far away from the fault as well as close to it. The maximum perpendicular distance from the Fairweather fault to a site in either of the

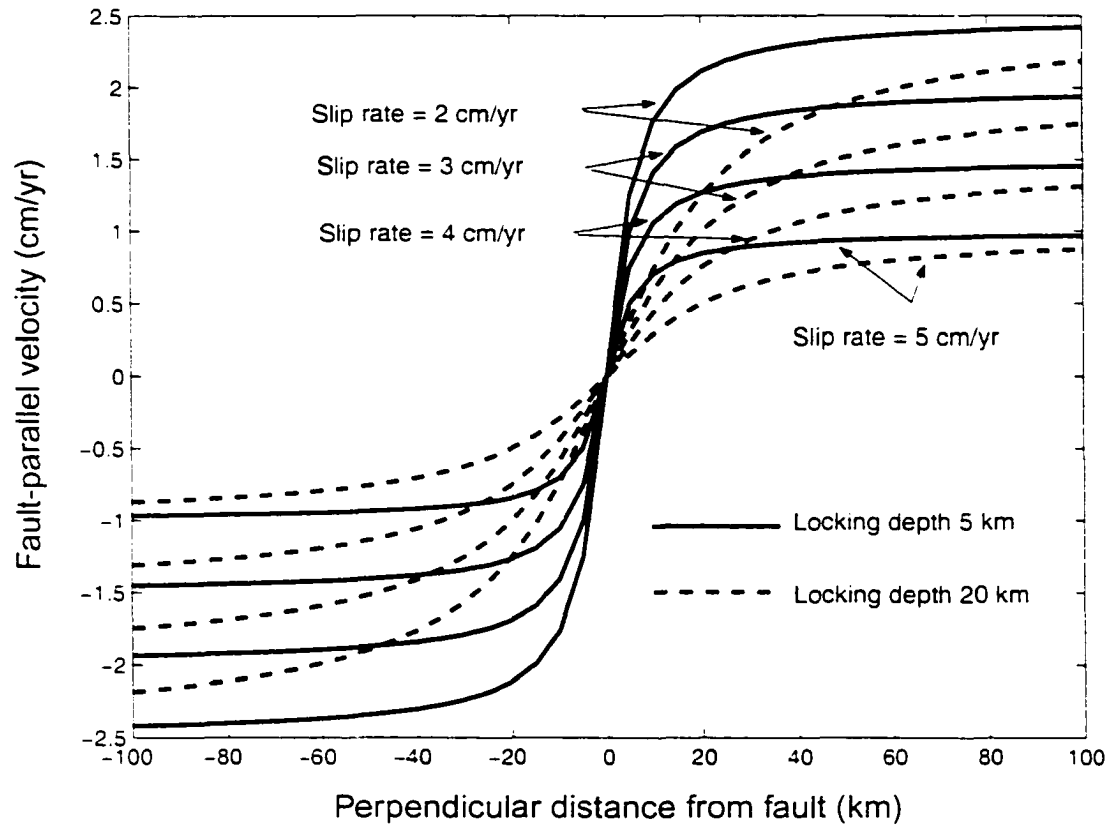


Figure 3.3. Plot to illustrate the trade-off between slip rate and locking depth. The lines show how fault-parallel velocity varies along a line perpendicular to the fault. Solid lines are for a fault with locking depth of 5 km and slip rates of 2 to 5 cm/yr. dashed lines are for a locking depth of 20 km.



*Lisowski et al. [1987]* EDM networks is about 15 km. We measured the velocity at Yakutat, 27 km to the south of the fault using GPS observations and, in addition, we made repeat GPS measurements at two of the EDM sites, thus obtaining independent velocities for these sites. We combined the GPS site velocities at YKTT, HIDD, and COMB with the EDM line-length data, and also used the Fairweather fault-parallel component of Pacific-North American plate velocity at Yakutat from [*DeMets and Dixon, 1999*], to invert for the slip rate and locking depth on the Fairweather fault.

Unlike the EDM line length data of *Lisowski et al. [1987]* the GPS site velocities are relative to North America. Therefore our fault model must include all structures between Yakutat and stable North America across which we might expect slip. The Denali fault is a major fault system 110 km to the north of the Fairweather fault (Figure 3.1). In the central and eastern Alaska Range, the McKinley section of the Denali fault, at the northern apex of the Denali fault system, is thought to be one of the most active sections of the fault [*Lanphere, 1978*]. *Hickman et al. [1977]* reported 110 to 230 m of Holocene dextral displacement along the McKinley segment, which is equivalent to a slip rate of 11 to 23 mm/yr, although the accuracy of these rates depends on the uncertain dates of the Holocene features. To the southeast, the Dalton Creek section of the Denali fault is located inland of the Fairweather fault and 370 km of dextral slip have occurred on this segment since the Early Cretaceous [*Lowey, 1998*]. *Plafker et al. [1977]* estimated a Holocene slip rate for this segment of 20 mm/yr, but lacked reliable dates for offset features. Present-day seismicity occurs along the Dalton Creek section of the Denali fault and along the Duke River fault, which lies slightly to the southwest of the Dalton Creek segment (Figure 3.2). We therefore believe that the Denali fault is a good candidate for accommodation of any slip inboard of the Fairweather fault.

We constructed a model with two faults, the Fairweather and the Denali, which we assumed to be vertical and parallel to each other. The GPS sites YKTT, HIDD, and COMB are far enough from the Denali fault that they are not affected by elastic strain on the locked portion. Therefore it is not possible to estimate a locking depth on the Denali fault from our data. Site X7 is 50 km to the north of the Denali fault. This is not far enough from the fault to see only the long-term slip rate. If we used the velocity of this site in the inversion, we would therefore need to add a fourth model parameter, the locking depth of

the Denali fault. Since this is the only site with information about the locking depth of the Denali fault, the solution would be poorly constrained and so we do not include it.

The Fairweather fault-parallel components of the GPS velocities,  $V_{para}$ , are related to the slip rate and locking depth of the Fairweather fault,  $S_F$  and  $D_F$ , and the slip rate on the Denali fault,  $S_D$ , by:

$$V_{para} = S_D + \frac{S_F}{\pi} \operatorname{atan}\left(\frac{(x - x_f)}{D_F}\right) - \frac{S_F}{2} \quad (3.2)$$

This is modified from equation 3.1 (from *Savage and Burford [1973]*), which gives the velocity,  $V(x)$ , relative to a fixed fault. The GPS velocities were calculated relative to North America and not relative to the fault, so we add the additional term  $S_F/2$  to account for this.

*Lisowski et al. [1987]* measured no significant dilation in either of their two networks across the Fairweather fault. We therefore assumed no compression or extension across the fault, and thus the rate of change of line length,  $dL/dt$ , is assumed to be due only to shear on the fault. The rate of change of line length can thus be written:

$$\frac{dL}{dt} = \frac{S_F}{\pi} \left[ \operatorname{atan}\left(\frac{(x_1 - x_F)}{D_F}\right) - \operatorname{atan}\left(\frac{(x_2 - x_F)}{D_F}\right) \right] \quad (3.3)$$

where  $L$  is the length of the line between two EDM sites at distances  $x_1$  and  $x_2$  from the fault.

Both the GPS velocity and the rate of change of line length are nonlinear functions of the locking depth  $D_F$  (equations 3.2 and 3.3). We linearized the equation by Taylor series about nominal values  $D_F = D_{F0}$ ,  $S_F = S_{F0}$  and  $S_D = S_{D0}$ . We had 35 observations (31 line-length change observations, 3 GPS velocities and the *DeMets and Dixon [1999]* plate motion observation) and three model parameters (slip rates on Denali and Fairweather faults and locking depth on the Fairweather fault), so we were dealing with an overdetermined problem. A weighted least squares inversion can be set up as follows *Menke [1984]*:

$$M = \operatorname{inv}(G^T W G) G^T W d \quad (3.4)$$

where  $M$  is the model parameter matrix,  $G$  is the model matrix (using the linearized equations),  $W$  is the weight matrix (the inverse of the diagonal variance matrix), and  $d$  is the data vector.

In our case, we minimized the differences  $\Delta S_F = S_F - S_{F0}$ ,  $\Delta D_F = D_F - D_{F0}$  and  $\Delta S_D = S_D - S_{D0}$  (i.e.  $M_{t,t} = \Delta M = M - M_0$ ), the same technique used by *Hreinsdottir et al. [2001]*. Using reasonable starting values for  $M_0$ , we iterated the inversion until the solution converged. Convergence occurred after 3 iterations, and we found no evidence of multiple minima (solutions converge to the same final answer regardless of the starting value of  $D_{F0}$ ).

*Fletcher and Freymueller [1999]*, using the same model, combined the EDM line length data of *Lisowski et al. [1987]* with the GPS data from Yakutat (GPS velocities were not yet measured for COMB and HIDD) and the Fairweather fault-parallel component of velocity of the Pacific plate at Yakutat from NUVEL-1A [*DeMets et al., 1994*]. Despite the addition of data to the model, *Fletcher and Freymueller [1999]* found their inversion was poorly constrained, so they were not able to improve upon the *Lisowski et al. [1987]* estimate of slip rate and locking depth of the Fairweather fault. The reason for this is that the model introduced a third model parameter, the Denali fault slip rate, with little data to give information about this parameter. We added the GPS velocities for the sites HIDD and COMB to the *Fletcher and Freymueller [1999]* model. These were determined relative to North America and so also contained a velocity signal giving information on the slip rate of the Denali fault. Inverting the GPS, line length and Pacific-North American plate motion data [*DeMets and Dixon, 1999*], we estimated a slip rate on the Fairweather fault of  $38.2 \pm 3.1$  mm/yr with a locking depth of  $7.0 \pm 0.9$  km and a slip rate on the Dalton Creek segment of the Denali fault of  $10.7 \pm 2.4$  mm/yr. The GPS data are plotted in Figure 3.4 with the best-fit dislocation model.

The formal uncertainties in the model parameters are no better than in *Fletcher and Freymueller [1999]*, but whereas those authors fixed the Denali fault slip rate to a specified value with no assigned uncertainty, here we estimated the Denali fault slip rate and uncertainty. The normalized  $\chi^2$  of the solution is 1.3. Figure 3.5 illustrates the rate at which  $\chi^2$  increases from this minimum value for different fault parameters.

The graphs illustrate the correlation between slip rate and locking depth and comparing

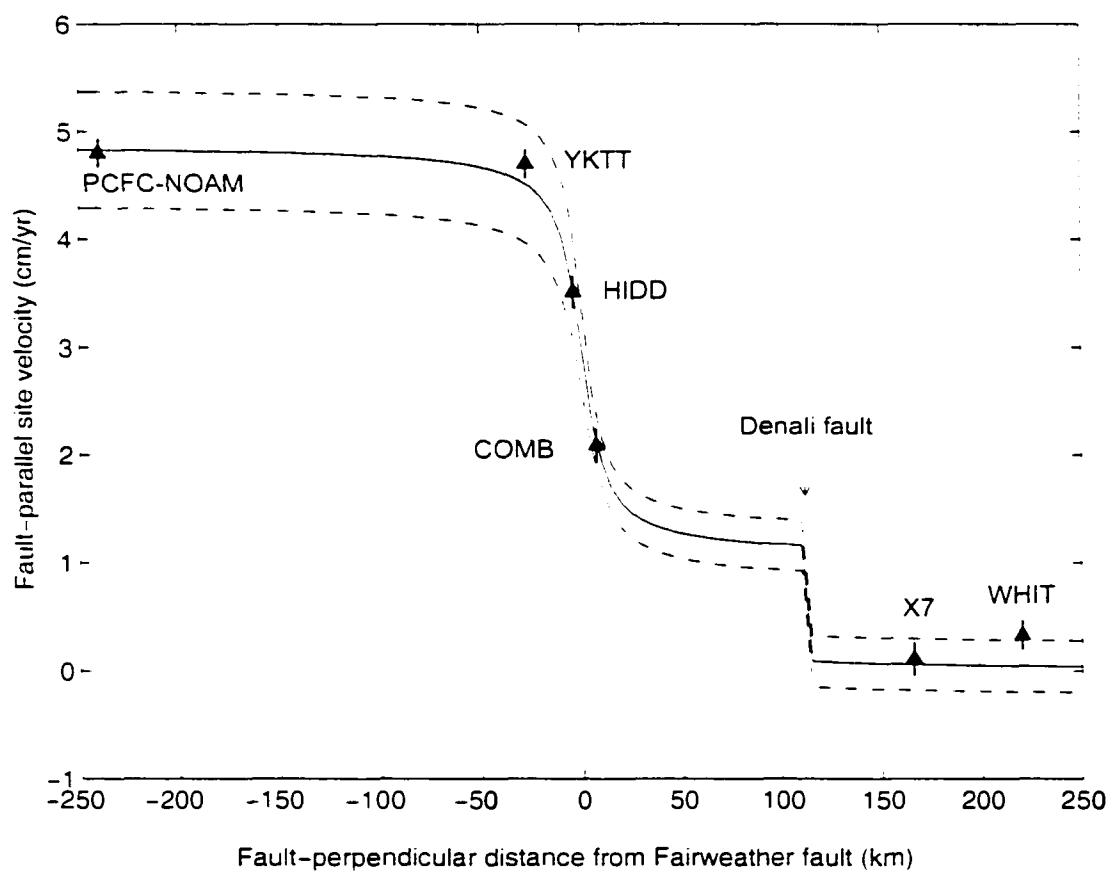


Figure 3.4. Plot showing the best-fit model with one sigma uncertainties. Data points are shown as triangles with one sigma error bars. Solid line is best-fit model and dashed lines show model with one sigma uncertainties. PCFC-NOAM is the Pacific plate velocity relative to North America from *DeMets and Dixon [1999]*.

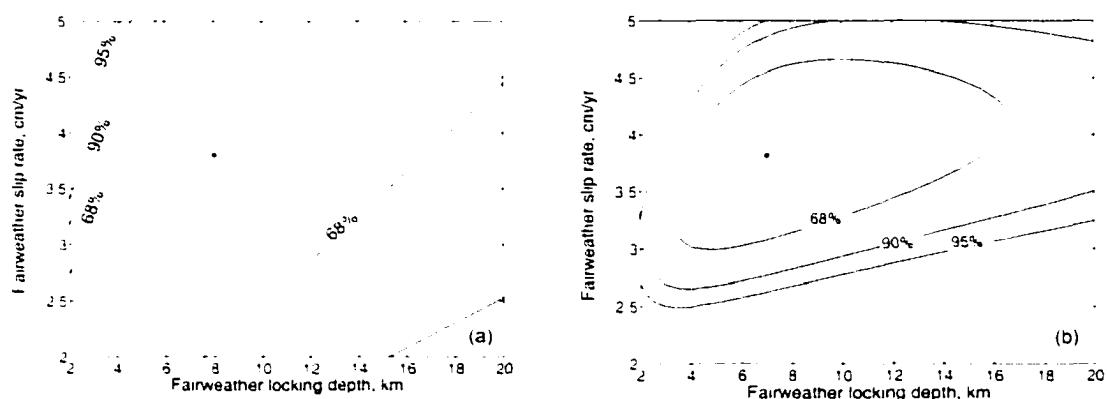


Figure 3.5. Confidence region ellipses for values of  $\chi^2$  larger than the fitted minimum. The asterisk shows the best-fitting model. The curves correspond to  $\Delta\chi^2 = 2.30, 4.61,$  and  $6.17$  and are 68.3%, 90%, and 95.4% confidence regions. (a) is using the line length data only. (b) is using line length and GPS data and the *DeMets and Dixon* [1999] Pacific-North American plate velocity as a constraint.

Figure 3.5a to Figure 3.5b, we see that the addition of the GPS data to the EDM data significantly improve estimates of both the Fairweather slip rate and locking depth. The sum of the slip rates estimated across the Fairweather and Denali faults is  $48.9 \pm 4.3$  mm/yr, which is equivalent to the Fairweather fault-parallel component of Pacific-North American velocity in this region,  $\sim 48$  mm/yr [DeMets and Dixon, 1999].

The slip rate of  $10.7 \pm 2.4$  mm/yr estimated for the Denali fault is actually the total velocity parallel to the Fairweather fault that must be accommodated by displacement inboard of the Fairweather fault. It is possible that this slip is not on the Denali fault but on the Duke River fault, for example, but we do not have the data resolution to determine how this slip is distributed. GPS observations across sections of the Denali fault to the northwest of this region give a slip rate across the Denali fault of 8-9 mm/yr [Fletcher and Freymueller, 2002 in prep.], which agrees with our result. GPS observations at sites closer to the Denali and Duke River faults in this region are needed to determine how the slip is distributed on the faults.

WHIT is far enough away from the Denali fault that it should see no effect from slip on this fault. In this model it should have a zero velocity relative to North America. The velocity of WHIT is only  $2.4 \pm 1.3$  mm/yr relative to North America, which is only slightly different from zero. The fact that it does have a small velocity relative to North America

may indicate that structures other than the Fairweather and Denali fault have some motion across them. If we calculate velocities relative to WHIT for the GPS data and Pacific plate velocity and invert this data set, we calculate a slip rate of  $38.2 \pm 3.5$  for the Fairweather fault with locking depth  $7 \pm 1$  km and a Denali fault slip rate of  $8.3 \pm 2.7$ . The slip rate and locking depth of the Fairweather fault are not altered in this inversion, but the slip rate on the Denali fault is lowered. This suggests that the slip rate on the Denali fault is the least constrained of the three model parameters and any common mode errors (e.g., errors in reference frame) are likely to map directly into a change in the modeled Denali fault slip rate.

### 3.5 Conclusions

The slip rate of  $38.2 \pm 3.1$  mm/yr estimated for the Fairweather fault is similar to total slip rate of  $\sim 39$  mm/yr on the San Andreas fault system in northern California [*Frey Mueller et al., 1999*]. Such a slip rate makes the Fairweather fault one of the fastest deforming strike-slip faults in the world. At this slip rate, it would take 92 years to build up the 3.5 meters of maximum slip observed on the Fairweather fault after the 1958  $M_S$  7.9 earthquake and only 52 years to build up the 2 m of slip observed along the southern half of the 1958 earthquake rupture zone, i.e., enough slip would occur by the year 2010 to allow a comparable earthquake. The locking depth of  $7.0 \pm 0.9$  km is reasonable for a strike-slip fault, although shallower than typically observed in California. The locking depth calculated by *Frey Mueller et al. [1999]* for the San Andreas in northern California is  $\sim 15$  km. Our results indicate that most of the Fairweather fault-parallel Pacific-North American relative plate motion is taken up on the Fairweather fault, but 11 mm/yr must be accommodated on structures inboard of the Fairweather fault. The geologic history and present-day seismicity along the Denali and Duke River faults indicate that these faults may be good candidates.

### 3.6 Acknowledgments

We thank Chris Larsen, Keith Echelmeyer and Jim Savage for thoughtful reviews. 1999 fieldwork supported by GSA grant to H. Fletcher.

## Chapter 4

# Using GPS to Unravel the Tectonics of Interior and Southern Alaska<sup>1</sup>

### 4.1 Abstract

Since 1995 we have made GPS observations in interior Alaska, with the goal of using deformation information as a tool to understand the present-day tectonics. Our observation network consisted of 55 GPS sites in interior Alaska, the majority of which were measured at least four times. We found that sites within about 50 km of Fairbanks show no significant motion with respect to Fairbanks, indicating a low rate of strain across this region, which spans three NE-SW seismic lineations between the Denali and Tintina faults. Sites further south have velocities consistent with right-lateral slip on the Denali fault. We constructed a model combining counter-clockwise rotation of the block south of the Denali fault with elastic strain accumulation on the fault. Using this model, the data required a slip rate of 6-9 mm/yr on the Denali fault or distributed on the Denali fault and one or more faults within 35 km to the north of the Denali fault.

After the model velocities were removed from the data, three sites showed an anomalous southward component of motion that was not explained by the block rotation model. We

---

<sup>1</sup>Prepared for submission in *J. Geophys. Res.*

suggest that this southward component of velocity may be due to postseismic response to the 1964 Great Alaskan earthquake and we derived a model of postseismic slip on the subducting slab that produced velocities consistent with the observations.

## 4.2 Introduction

Geologic maps of interior Alaska, within 300 km of Fairbanks, show a high abundance of faults. Information about these faults has up to now been based mainly on geological observations in the field, and these observations are limited due to the generally poor exposure. Seismicity maps are a good source of information on the location and activity of active faults, but the density of seismic sites is far from ideal. The tectonics of Alaska are dominated by the Pacific-North American plate interaction, complicated by the collision of the Yakutat block. The region of interior Alaska between the Denali and Tintina faults experienced at least four  $M_s$  7 earthquakes in the twentieth century, attributed to compression due to the collision further south. The magnitude of this energy release is equivalent to that of southern California over the same time period, and yet there have been only a few detailed studies of the tectonic framework of the interior of Alaska.

The most obvious tectonic feature in the interior of Alaska is the Denali fault, which extends in a broad arc for more than 2000 km and is interpreted to be a dominantly right-lateral fault [e.g., *Lanphere, 1978; Stout and Chase, 1980*]. Its present-day rate of motion, however, is uncertain, with estimates ranging from no significant displacement in the years 1975 - 1988 [*Savage and Lisowski, 1991*] to an 8-12 mm/yr average right-lateral slip rate for the Holocene [*Plafker et al., 1994*]. Another major tectonic feature in Alaska is the Tintina fault, a large dextral fault system 250 km to the north of the Denali fault. The seismicity in the region between these two fault systems defines a series of NE-SW lineations. These seismic zones have been interpreted as edges of elongate, rotating crustal blocks [*Page et al., 1995*]. We use our GPS observations to study the current deformation in interior Alaska and compare this to geological observations. In one end-member tectonic model for the interior, all of the shear in the region is placed on the Denali fault and thus no strain is accumulated between the Denali and Tintina faults. Alternative models allow the shear to be accommodated over a broader area. For example, in a block-rotation model the



region between the faults is made up of several elongate blocks, which rotate clockwise to accommodate the north-south compression. We evaluate the tectonic models proposed for interior Alaska and present our favored model based on the GPS deformation results.

## 4.3 Tectonic background

### 4.3.1 Denali fault

The Denali fault has the most dramatic topographic expression of all the large scale strike-slip faults in Alaska, as it forms a deeply incised fault line valley which can be traced for several hundred kilometers through the Alaska Range and into the Shakhwak Valley, Yukon Territory, Canada. The Denali fault is geologically important as it separates the vast crystalline Yukon-Tanana terrane from younger accreted terranes to the south, cuts rocks ranging from Precambrian to Quaternary age, and displays geologic evidence of recurrent right-lateral displacement over a relatively long span of geologic time. Figure 4.1 is a map showing the geologic and geographic features discussed in this section.

Dextral displacements of up to 400 km have been reported for some sections of the Denali fault [e.g., *Forbes et al., 1973; Turner et al., 1974; Nokleberg et al., 1985*]. Evidence for Holocene slip on the Denali fault east of 143°W is absent [*Savage and Lisowski, 1991*]. The Totschunda fault seems to replace the Denali fault as the active strand of the fault east of the junction of the two faults. Holocene displacement has only been documented on the McKinley, Totschunda and western Shakhwak segments. Our region of study is the central Denali fault system, which includes the Hines Creek and McKinley strands. The Buchanan Creek pluton cuts the Hines Creek segment and is not apparently offset by the fault [*Wahrhaftig et al., 1975*], although this has been recently disputed (but not yet published). *Wahrhaftig et al. [1975]* reported K-Ar ages of 95 Ma for the pluton, indicating that significant lateral displacement has not occurred along this strand in the last 95 million years. It is believed that the McKinley branch of the fault has short-circuited the older northern Hines Creek branch [*Page and Lahr, 1971*]. The McKinley segment is one of the most active portions of the Denali fault system during the Holocene [*Lanphere, 1978*]. Offset Holocene features and the sharp profile of major scarps in unconsolidated sediments indicate major movement along the McKinley strand in the last few hundred years [*Page and Lahr,*

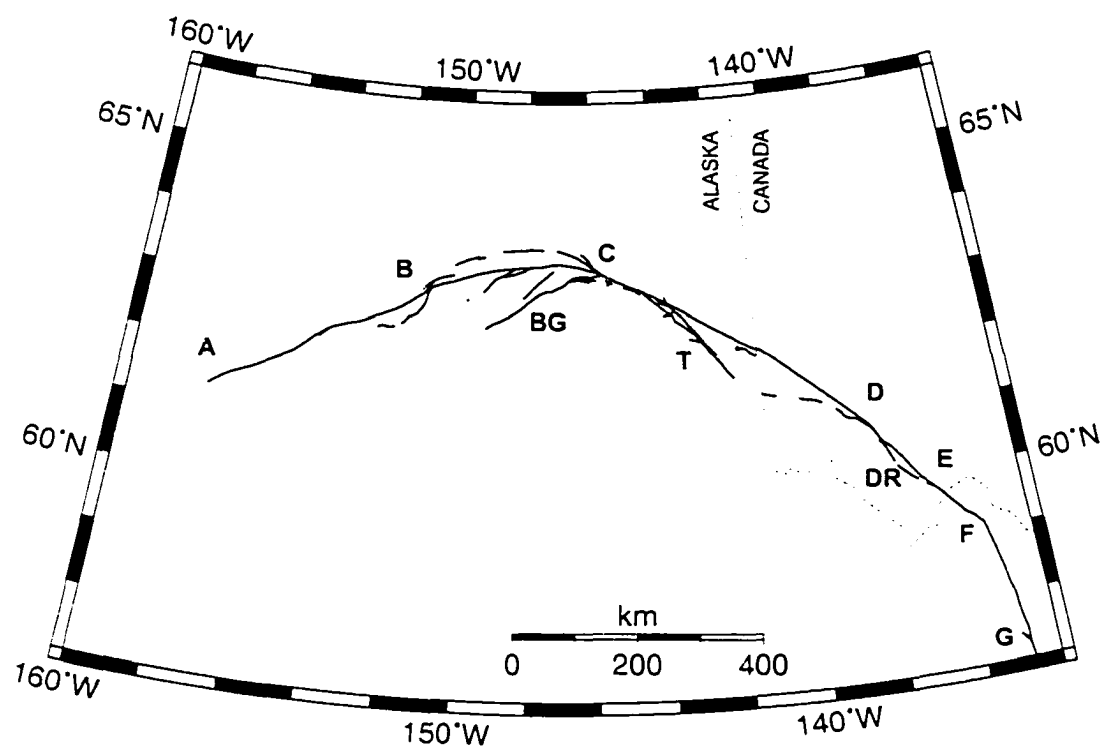


Figure 4.1. Map of interior Alaska showing the main segments of the Denali fault system and other connecting faults. A-B = Farewell segment; B-C(north) = Hines Creek fault; B-C(south) = McKinley segment; C-D = Shakwak segment; D-E = Dalton Creek segment; E-F = Chilkat River fault; F-G = Chatham Strait fault; BG = Broxson Gulch thrust; T = Totschunda fault; DR = Duke River fault (from *Plafker et al. [1994]*).

1971]. *Stout et al.* [1973] reported 50-60 m of Holocene dextral displacement and 6-10 m of vertical displacement, north side up, on the McKinley segment near the Richardson highway. Further west near the Parks highway, *Hickman et al.* [1977] reported 110-230 m of Holocene dextral displacement and 3-5 m of vertical displacement, south side up, along the McKinley segment. The disparity in Holocene displacement between the Richardson and Parks highway regions of the McKinley strand might be a geologic indicator of faster slip at the western Parks highway end, but the timing of the measured offsets is relatively unconstrained (*Hickman et al.* [1977] give a maximum time for producing the offsets of 11,000 yrs and a minimum of a few hundred to a few thousand years) and so not much faith should be put into slip rate estimates based on such 'Holocene' offsets.

Present day motion along the Denali fault is unclear. Seismicity has only been moderate on the Denali fault in recent years. The most recent major earthquake that might be associated with the Denali fault was a magnitude 7.4 event in 1912. A small geodetic triangulation network was established across the McKinley branch of the Denali fault in 1967 and 1968 and resurveyed in 1969 [*Page and Lahr*, 1971]. The network consisted of a cluster of stations within less than 1 kilometer of the fault. The cumulative displacement for the interval 1967-1969 was less than 3 mm. *Savage and Lisowski* [1991] found no significant right-lateral shear strain accumulation from surveys of trilateration networks in the vicinity of both the Parks and Richardson highway crossings of the Denali fault (separated by about 150 km). The authors estimated that the strain rates due to a fault slipping at 15 mm/yr with locking depth 15 km were well within the detection capabilities of their survey. However, a fault slip rate of 5 mm/yr with a locking depth of 30 km might escape detection. Inversions to estimate fault properties from surface displacements have an inherent trade-off between the estimated slip rate and the locking depth of the fault if the data do not extend at least a few fault locking depths away from the surface trace of the fault [*Johnson and Wyatt*, 1994]. The sites in both of these networks were all within 20 km of the fault. It is necessary to observe the motion of sites in the far field, at a distance of several locking depths, in order to compute the full long-term slip rate of the fault.

### 4.3.2 Tintina fault

The right-lateral Tintina fault extends from the Yukon Flats area in Alaska southeast into the Yukon Territory and British Columbia. The Kaltag fault trends northeastward from Norton sound on the west coast of Alaska towards the Yukon Flats. The most widely accepted possibility for the eastern end of this fault is that it wraps around the southern edge of the Yukon flats as the main splay from the Tintina fault [Estabrook et al., 1988]. The Tintina exhibits 450 km or more of mainly Late Cretaceous to early Tertiary dextral displacement [Gabrielse, 1985], but evidence of Holocene movement is limited to a single 14 km long scarp [Plafker et al., 1994]. The current level of seismicity is low, but a magnitude 5.0 earthquake in 1972 is consistent with right-lateral motion along the Tintina fault.

### 4.3.3 Interior Seismic Zones

A seismicity map of the region between the Denali and Tintina fault systems shows a clustering of earthquake epicenters in northeast trending lineaments (Figure 4.2). There are three prominent zones, termed the Salcha, Fairbanks, and Minto Flats seismic zones [Biswas and Tytgat, 1988]. A magnitude 6.2 left-lateral strike slip earthquake in 1995 occurred along the Minto Flats seismic zone. This seismic zone can be traced southward to connect with a prominent group of epicenters termed the Kantishna cluster (Figure 4.2).

In 1937, a magnitude 7.3 earthquake with left-lateral strike slip motion occurred in the interior of Alaska and is thought to have been associated with the Salcha seismic zone [Fletcher and Christensen, 1996]. Page et al. [1995] have proposed that the seismic zones outline elongate fault-bounded blocks, which rotate clockwise similar to books on a bookshelf, accommodating the N-S crustal shortening across the region. In addition to the seismicity, aeromagnetic maps of the Fairbanks area show prominent NE-SW lineations. Despite this additional geophysical data that is consistent with a series of NE-SW striking faults, there is a lack of mapped faults in the region. Pewe et al. [1966] show a fault that cuts Quaternary deposits along the Minto Flats seismic zone, but it does not appear to have any documented Holocene movement. Poor exposure characterizes this entire region and this probably explains the paucity of mapped faults.

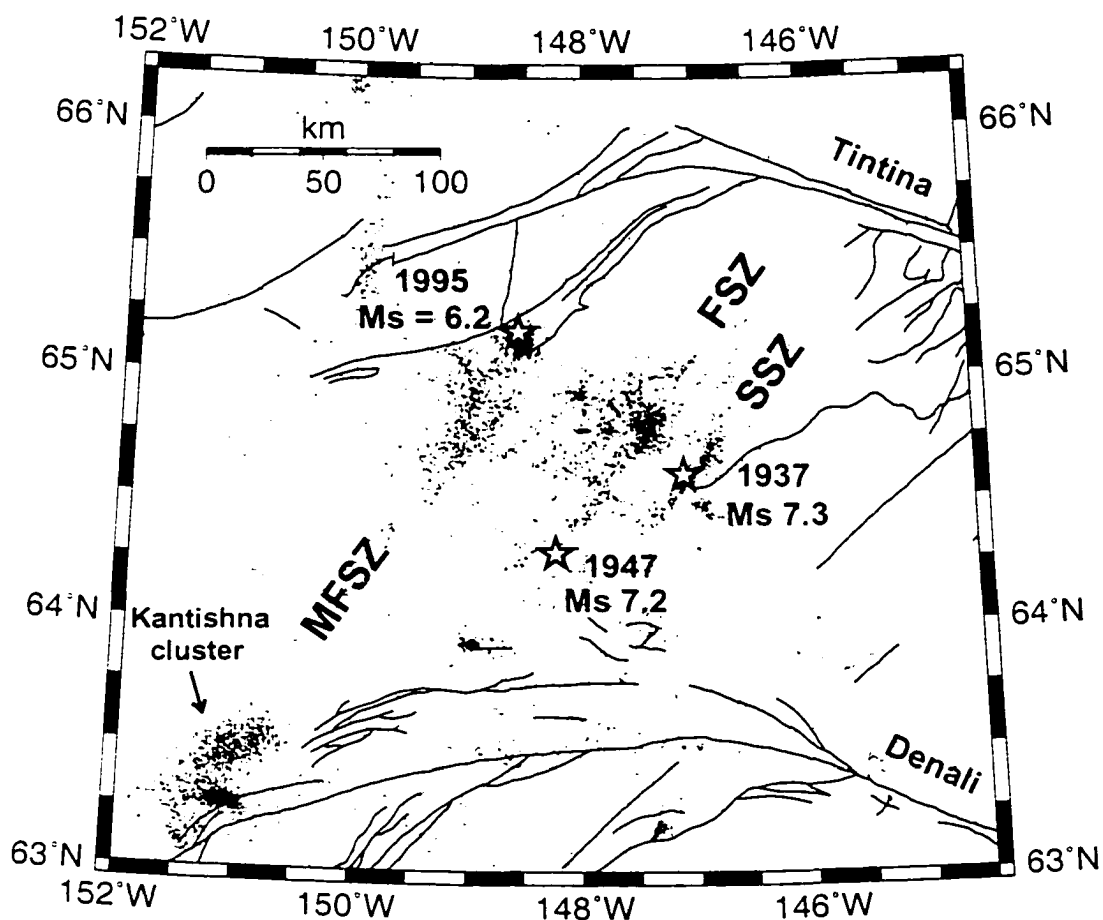


Figure 4.2. Map of interior Alaska showing the seismicity from 1990 to 1996. The epicenters fall along three NNE-trending lineaments. MFSZ = Minto Flats seismic zone; FSZ = Fairbanks seismic zone; SSZ = Salcha Seismic Zone. The black lines are all of the faults shown by *Plafker et al.* [1994] in this region. Also shown are earthquakes with  $M_s > 7$ .

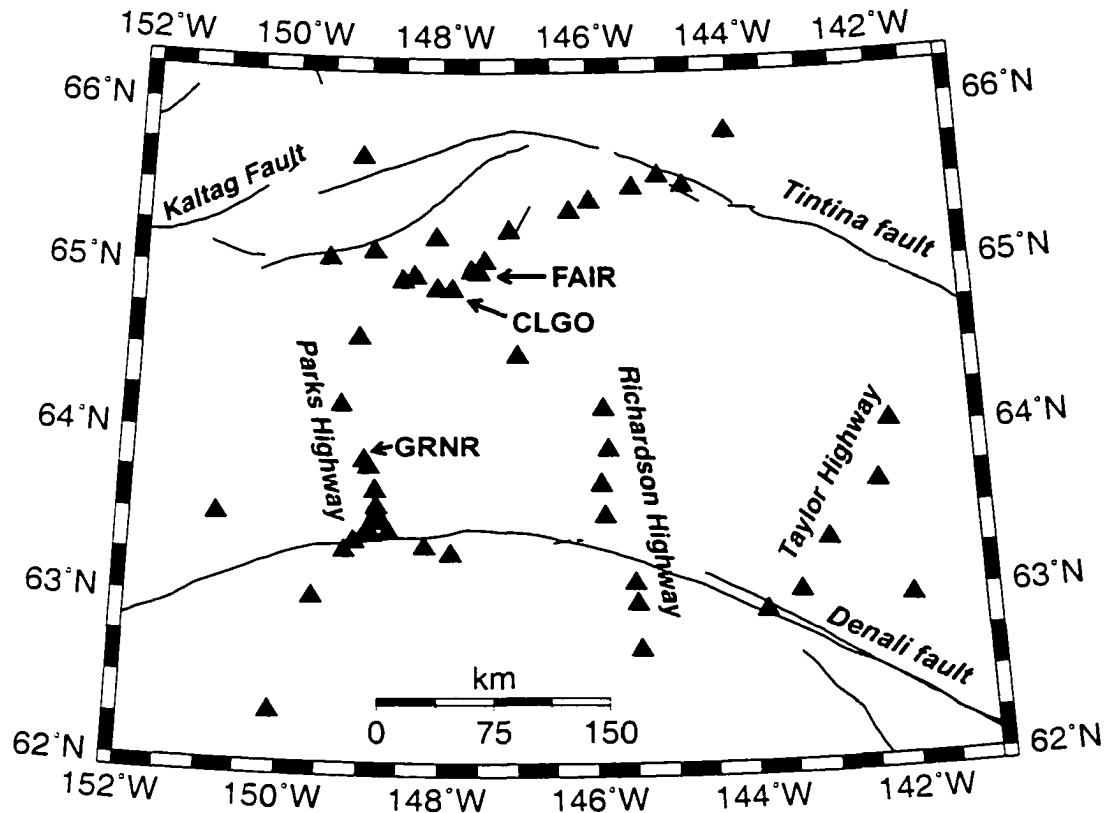


Figure 4.3. Map of interior Alaska showing the Denali and Tintina faults. Triangles indicate the GPS sites.

#### 4.4 Data

Our observation network consisted of 55 GPS sites (Figure 4.3), the majority of which were measured at least four times. In 1995, we established and started observing 6 sites within 50 km of Fairbanks. Each year since then we repeated observations at these sites and established new sites. In 1997, we installed a dense profile of sites across the Denali fault along the Parks highway and a few sites along a second, more sparse profile across the fault along the Richardson highway. In 1997 and 1999, five sites off the road network were established with helicopter support in an attempt to measure the displacement across the Minto Flats seismic zone (Figure 4.2). Figure 4.3 shows the location of all the GPS sites for which we have at least two observations.

The sites FAIR and CLGO are permanent sites and were in continuous operation for

the duration of this campaign. We installed the permanent site GRNR in cooperation with UNAVCO. It was in operation intermittently from 1997 to spring 2000 and has been running continuously since then. The remaining campaign sites were occupied for a minimum of 2 eight-hour sessions each time they were measured, and most sites were surveyed for multiple 24-hour sessions each year. All measurements were made with dual frequency Trimble 4000 SSE and SSI receivers using Trimble Compact Geodetic antennas.

The GPS data were combined with a subset of the International GPS Service (IGS) network in daily solutions using the GIPSY-OASIS software and analysis techniques described in Freymueller et al. [1999]. We transformed all solutions into the global reference frame ITRF97 [Boucher, 1999] and estimated velocities of all sites relative to FAIR. To calculate the velocity uncertainties we followed *Mao et al.* [1999], who suggested that errors in GPS time series consist of colored (time-correlated) noise in addition to white noise. Time-correlated noise sources include mismodeled satellite orbits, mismodeled atmospheric effects and monument instability. We thus added time-correlated or ‘flicker’ noise to the white noise estimate, using the empirical model from *Mao et al.* [1999] given below:

$$\sigma_r = \left[ \frac{12\sigma_w^2}{gT^3} + \frac{a\sigma_f^2}{gbT^2} \right] \quad (4.1)$$

where  $g$  is the number of measurements per year,  $T$  is the total time span in years,  $\sigma_w$  and  $\sigma_f$  are the magnitudes of white and flicker noise in millimeters, and  $a$  and  $b$  are constants empirically estimated as  $a \sim 1.78$  and  $b \sim 0.22$ . We neglected the random walk component of the uncertainty because it is relatively small compared to white and flicker noise. For the magnitude of  $\sigma_f$ , we used the mean value for North America according to *Mao et al.* [1999]. These values are 4.4 and 6.3 for the north and east components of  $\sigma_f$ , respectively. The white noise magnitude was calculated separately for each individual station by averaging the formal sigmas of the coordinate estimates for each daily observation. Typical velocity uncertainties for the horizontal components were 1-3 mm/year, which is 0.5-1 mm/yr higher than the straight white noise estimate.

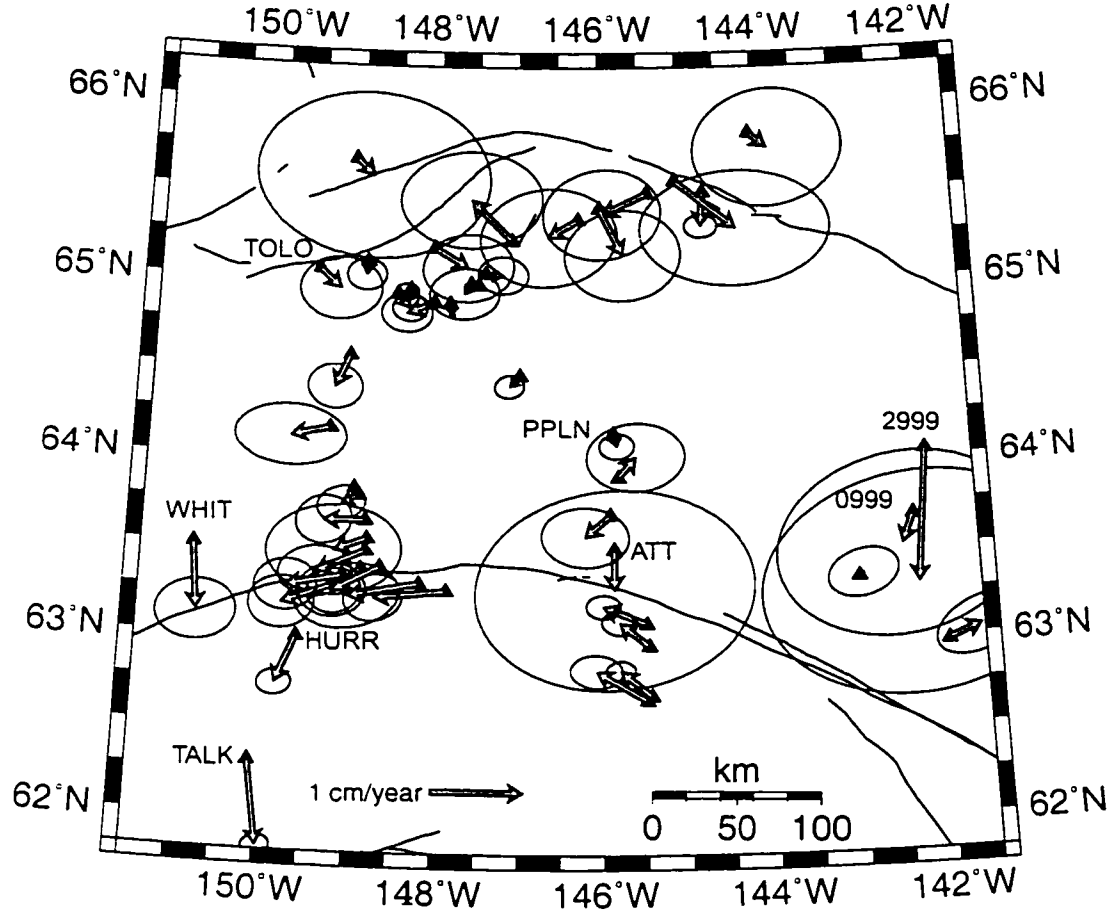


Figure 4.4. Velocities of all sites relative to FAIR. Note that velocities increase southwards across the Denali fault. Sites TALK, HURR and WOND have an anomalous southward component of velocity.

## 4.5 Results

Figure 4.4 shows our estimated GPS velocities relative to FAIR, with 95% confidence error ellipses. The velocity of FAIR relative to stable North America is 4.1 mm/yr E, 2.9 mm/yr S [Kogan, 2000].

The velocities of the sites in this region range from about 0 mm/yr to 10 mm/yr relative to FAIR. Most sites were measured each year for four years, typically with two 24 hour observations, and the uncertainty in the horizontal velocity at such sites is 2-3 mm/yr. Some sites have only two sets of observations separated by one year and so the uncertainties



associated with those velocities are large, up to 5 mm/yr, indicated by the large error ellipses at sites such as ATT, 0999 and 2999. We did not use the velocities at these sites in any of our modeling. The velocities of sites within 50 km of Fairbanks are close to 0 mm/yr, indicating a low strain rate across the interior seismic zones. Velocities of sites on the western profile across the Denali fault along the Parks Highway increase south of the fault to about 8 mm/yr relative to Fairbanks, indicating right-lateral shear across the Denali fault. Sites south of the fault on the profile along the Richardson highway have a slightly lower velocity of 6 mm/yr relative to Fairbanks. Sites WOND, HURR, and TALK show a southward motion relative to Fairbanks, and we discuss a possible reason for this in section 4.7. Velocities of sites to the north and northeast of Fairbanks have relatively large uncertainties and show no clear systematic picture of deformation. Without further observations it is difficult to determine whether there is any shear on the Tintina fault.

## 4.6 Discussion

In this section we examine the GPS velocity results in more detail. We first discuss the results for the region between the Denali and Tintina faults, where we have GPS sites spanning three NNE trending seismic zones (Figures 4.2 and 4.3). In 1937, a  $M_S$  7.3 earthquake occurred in this region and is thought to have been associated with the Saleha seismic zone. We attempt to reconcile this with the low GPS velocities measured.

We then move to the Denali fault and discuss the modeling of our data. We first construct a simple 2D model in which the fault is considered to be straight and vertical and to slip at a long-term slip rate below a fixed locking depth. Using a mathematical representation of this model, we invert the GPS velocities of the sites along the Parks highway profile to estimate a slip rate and locking depth for this simple model of the Denali fault.

The Denali fault is not straight, however, and so we introduce a model in which the curved Denali fault is a northern boundary to a rotating southern Alaska block. We find the rotation rate of the southern Alaska block that best fits the GPS data from sites on both the Parks and Richardson highway profiles. To investigate the possibility of slip being distributed on more than one fault, we concentrate on the Parks highway profile, which has

the most GPS sites and therefore the best spatial resolution. We use the same southern Alaska block rotation model to estimate the slip rate and locking depth of the Denali fault and one additional model fault in this region.

We conclude this section by discussing the southward velocity of sites TALK, HURR, and WOND that is not explained by the southern Alaska block rotation model. We propose that this southward motion could be due to ongoing postseismic deformation after the 1964 Great Alaska earthquake. *Zweck et al. [2001]* used GPS velocities from sites on the Kenai Peninsula to model the postseismic effect in terms of varying slip distribution on the subduction interface. However, their model predicts a higher southward motion than observed at sites north of TALK. We remove the effect of southern Alaska rotation and strain on the Denali fault from the Kenai Peninsula GPS velocities to produce a set of residual velocities that we assume to be entirely due to subduction of the Pacific plate. We follow the procedure of *Zweck et al. [2001]* using this new velocity set, and estimate a new slip distribution on the subducting plate interface.

#### 4.6.1 Interior seismic zones

We first examine the region around Fairbanks, between the Denali and Tintina faults. The velocities of the 14 sites in this region are shown in Figure 4.5 and are small relative to Fairbanks, with a maximum of  $6.9 \pm 3.8$  mm/yr at SPIL.

To further analyze the deformation of this region we calculate the areally averaged strain rate from the GPS velocity field. Assuming uniform strain in the region, we calculate the extension of baselines between all possible pairs of stations ( $\Delta L/L$ ), where  $L$  is the line length and  $\Delta L$  is the change in length per year. Following the method outlined in *Prescott et al. [1979]*, we calculate the strain rate across that direction having the highest shear rate from changes in line length observations. We find that a maximum engineering shear strain rate of  $0.02 \pm 0.01$   $\mu\text{rad/yr}$  produces maximum left-lateral shear in a direction  $N12^\circ E \pm 33^\circ$ . This is small compared with strain rates observed across major faults, such as  $0.11 \pm 0.06$   $\mu\text{rad/yr}$  on the Totschunda fault and  $1.57 \pm 0.15$   $\mu\text{rad/yr}$  on the Fairweather fault [*Lisowski et al., 1987*]. To test the assumption of uniform strain, we divide the region into subsets of sites and calculated the strain rates for these subsets. We try several subsets including all sites north of  $65^\circ N$ , all sites south of  $65^\circ N$ , all sites east of  $147.5^\circ W$ , and all sites west of

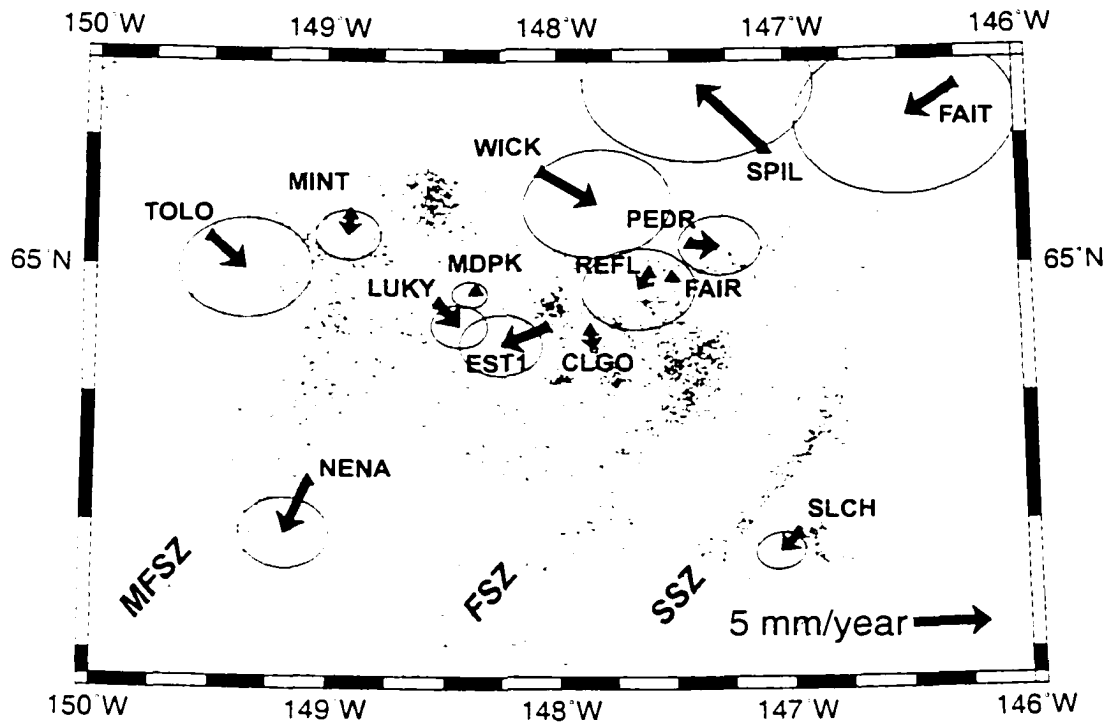


Figure 4.5. Velocities relative to FAIR for sites in the Fairbanks vicinity. Velocities are small with a maximum velocity of  $6.9 \pm 3.8$  mm/yr at SPIL. 95% confidence ellipses are shown. MFSZ = Minto Flats seismic zone; FSZ = Fairbanks seismic zone; SSZ = Salcha Seismic Zone.

147.5°W. The strain rate is not significantly different between subsets, with values ranging from  $0.01 \pm 0.01$  to  $0.03 \pm 0.01$   $\mu\text{rad}/\text{yr}$ . Given the large error associated with the azimuth of the strike of the vertical plane with maximum left-lateral shear ( $\text{N}12^\circ\text{E} \pm 33^\circ$ ), this value is not greatly different from the strike of the seismic zones, which is approximately  $\text{N}33^\circ\text{W}$ . The principal axes of strain (calculated following *Prescott et al. [1979]*) are oriented at  $\text{N}57^\circ\text{W} \pm 40^\circ$  (compression) and  $\text{N}33^\circ\text{E} \pm 40^\circ$  (extension). Again the error in the azimuth is large. *Ratchkovski and Hansen [2002]* found a systematic variation in the orientation of stress axes as determined from seismicity in this region, but we do not have the density of data to resolve such variation and the orientation of the principal axes of strain are simply an average over the entire region.

An examination of the far-field sites, TOLO and PPLN (Figure 4.4), gives us a first-order estimate of the shear across all of the seismic zones. The sense of motion parallel to the seismic zones between these sites is right-lateral, with magnitude  $0.5 \pm 0.4$  mm/yr, i.e., not significantly different from zero shear.

To further investigate the deformation of this region, we construct a model of bookshelf-type block rotation in interior Alaska. In this model of simple shear, the seismic zones are assumed to be faults bounding elongate blocks oriented  $\text{N}33^\circ\text{E}$ , terminating at the Denali fault to the south and at the Tintina fault to the north. The Denali and Tintina faults are the reference boundaries in this model and do not rotate (Figure 4.6). The region was rotated about site FAIR and slip is applied on the faults bounding the blocks (where the faults are assumed to be the best-fit lines through the seismic zones shown as dotted lines on Figure 4.7) so that the reference boundaries do not rotate. The slip is calculated following *Garfunkel and Ron [1985]* using the equation below:

$$s = [\cot(\alpha - \delta) - \cot\alpha] W \quad (4.2)$$

where  $W$  is the width of the block,  $s$  is the slip,  $\delta$  is the rotation and  $\alpha$  is the initial angle between the faults and the reference boundary.

However, the faults presumably are locked from the surface to the base of the seismogenic zone, and so the blocks do not simply slide past each other during the interseismic period considered here. The final step is therefore to incorporate the elastic behavior of the faults

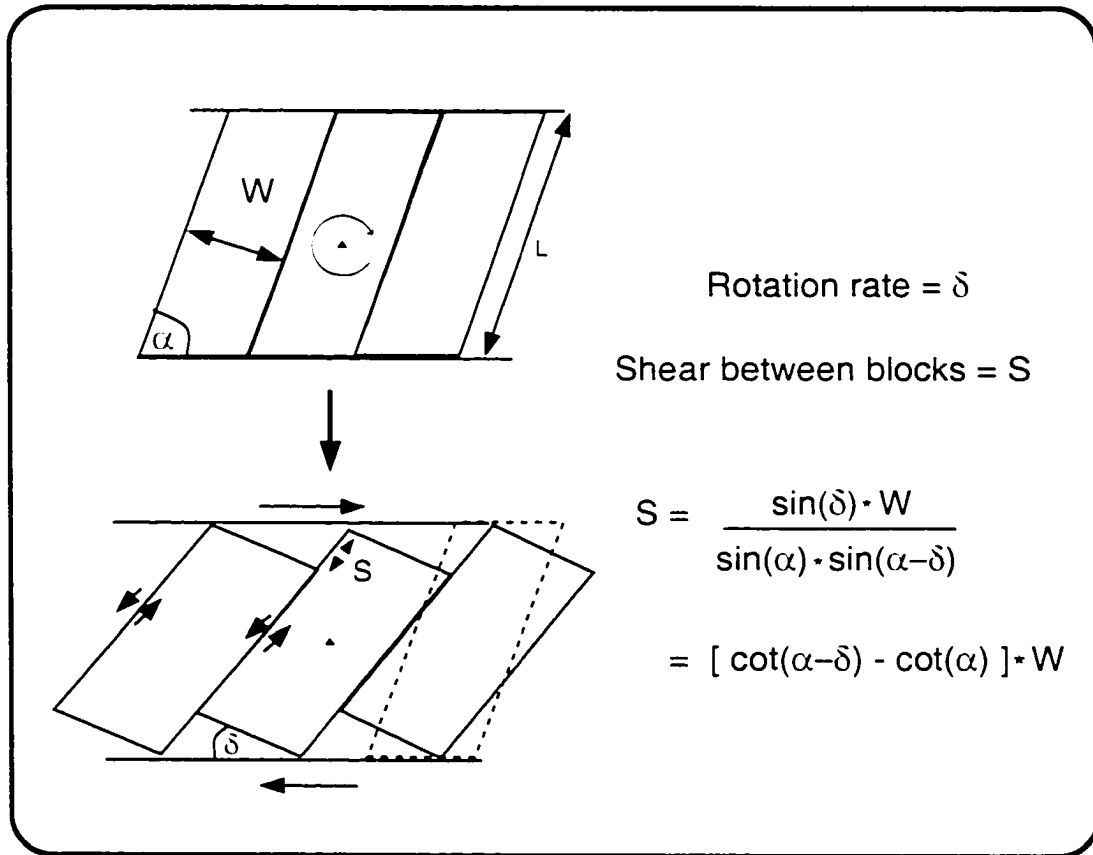


Figure 4.6. The bookshelf-type block rotation model that we apply to interior Alaska. Based on *Garfunkel and Ron [1985]*.

into the model. We consider the faults to be vertical with a locking depth  $D$ , below which the fault slips at the long-term slip rate  $S$ . Using elastic screw dislocation theory, the fault-parallel velocity of a site at a perpendicular distance  $x$  from a fault (at position  $x_f$ ) is [Savage and Burford, 1973]:

$$V(x) = \frac{S}{\pi} \operatorname{atan}\left(\frac{(x - x_f)}{D}\right) \quad (4.3)$$

Locking depths of strike-slip faults are equivalent to the depth to the base of the seismogenic zone. Seismic and geodetic studies show that typical locking depths for strike-slip faults are between 10 and 15 km [e.g., Prescott et al., 1979]. Relocation of seismic events in central Alaska by Ratchkovski and Hansen [2002] showed that seismicity was limited to the top 10-15 km of the crust. A reasonable locking depth of 12 km was applied to each fault (best-fit line through the seismic zones). The slip on each fault was calculated from equation 4.2, the velocity at each site due to the slip on each of the three faults was calculated using equation 4.3 and the contributions from each fault were summed. Figure 4.7 illustrates the components of the velocity modeled at each site for a rotation rate of  $2^\circ$  /million years (much larger than the best-fit rotation rate given below). Summing the velocity due to rotation about FAIR (black vectors in Figure 4.7) and the velocity due to slip on the locked faults (white vectors in Figure 4.7) gives us the model velocity at each site (gray vectors in Figure 4.7). The goal is to find the rotation rate (and thus slip on the faults) for our model that produces a set of velocities that best fits the observed GPS velocities. We perform a grid search over different angular velocities and find that the best-fitting angular velocity is  $0.1^\circ$  /million years. A rotation of  $0.1^\circ$  /million years gives a slip rate of 0.2 mm/yr on the Minto Flats seismic zone, 0.1 mm/yr on the Fairbanks seismic zone and 0.2 mm/yr on the Salcha seismic zone (using equation 4.3).

In 1937, a  $M_S$  7.3 earthquake occurred in this region of interior Alaska (Figure 4.2). Fletcher and Christensen [1996] digitized the analog teleseismic records from this earthquake and found that the data are consistent with a left-lateral earthquake occurring on the Salcha seismic zone. The authors calculated a unilateral rupture length of 40-60 km for the event, but pointed out that a bilateral rupture is possible due to a second pulse of moment release visible on the source time functions, which would produce a rupture length of 80-120 km.

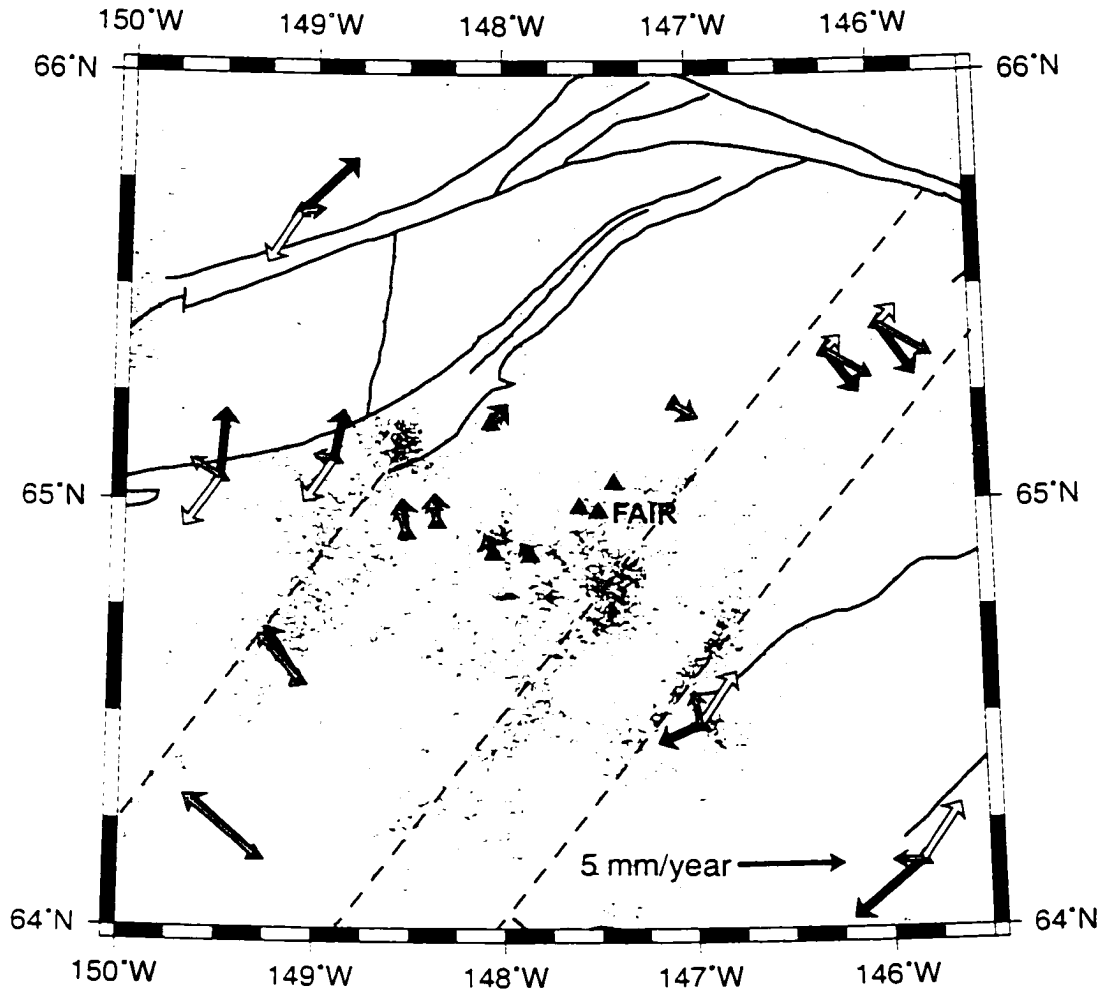


Figure 4.7. Map showing the model velocities due to bookshelf-type block rotation about the site CLGO in Interior Alaska. This example is for a rotation rate of  $2^\circ$ /million years clockwise. Black vectors show the velocity due to the rotation; white vectors show the resulting deformation on the locked faults; gray vectors show the sum of these effects.

*Fletcher and Christensen [1996]* calculated a seismic moment of  $0.6 \pm 0.2 \times 10^{20}$  Nm for this earthquake. If we assume that the calculated strain rate is a reliable indicator of the long-term deformation in this region, then we can compute the recurrence time for an earthquake such as the 1937 Salcha event. We first calculate the fault displacement from the relation  $M_0 = \mu DA$ , where  $M_0$  is the moment,  $\mu$  is the shear modulus, taken as  $3 \times 10^{10}$  Pa,  $A$  is the fault area, which is about 10 km (locking depth) by 40-120 km (rupture length of Salcha earthquake), and  $D$  is the displacement. Using these parameters a displacement of 1.7-5 m would be expected. Given a slip rate of 0.2 mm/yr, the recurrence time for a  $M_S$  7.3 earthquake is therefore on the order of 8,500-25,000 years.

Given such a huge recurrence time, how is it possible that in 1947 another large,  $M_S$  7.2, earthquake occurred in this region (Figure 4.2)? The focal mechanism for the 1947 earthquake is a thrust mechanism, with the fault plane oriented perpendicular to the seismic zones, leading *Fletcher and Christensen [1996]* to postulate that the 1937 event caused the 1947 fault to be loaded and thus, 10 years later to rupture.

#### 4.6.2 Denali fault

##### Simple model

Our goal is to determine the slip rate and locking depth of the Denali fault from our GPS observations. We start with a simple model and constructed an elastic dislocation model for a fault locked at the surface and slipping freely at a rate  $S$  below depth  $D$ . We used the fault-parallel velocities at sites along our main Parks highway profile across the fault to invert for long-term slip rate and locking depth of the fault. The modeled fault-parallel component of velocity of a site at a perpendicular distance  $x$  from the fault (at position  $x_f$ ) is:

$$V(x) = \frac{S}{\pi} \operatorname{atan}\left(\frac{(x - x_f)}{D}\right) - \frac{S}{2} \quad (4.4)$$

This is modified from *Savage and Burford [1973]* (equation 4.3) by the addition of the term  $S/2$ . Equation 4.3 assumes the velocity at a site is relative to the fault, whereas we calculated our GPS velocities relative to the site FAIR. FAIR is over 150 km north of the fault and at such a distance it is not affected by strain on the fault at a level that we can



detect with GPS measurements, thus the fault-parallel component of velocity at FAIR is  $S/2$  relative to the fault (and in an opposite direction to the fault-parallel velocity component of sites far away to the south of the fault). We therefore add  $S/2$  to equation 4.3 so that the model velocities are also relative to FAIR.

For this simple 2D model we use data from only the denser Parks highway profile, and we do not include the velocities at the sites TALK, HURR, and WOND, as these are anomalous. In section 4.7 we discuss the possibility that the southward component of velocity at these sites is due to post-seismic effects from the 1964 earthquake. We calculate a slip rate of  $8 \pm 1$  mm/yr and a locking depth of  $28 \pm 8$  km with a reduced  $\chi^2$  statistic of 1.43. The locking depth was not well determined by the inversion and is also unreasonably large, which could be an artifact of incorrectly assuming all of the slip occurs on one fault rather than being partitioned over a series of faults. Recent seismicity gives us reason to believe that some shear is being accommodated on structures other than the Denali fault. The Hines Creek fault is a major fault that lies about 30 km to the north of the Denali fault along the Parks highway, and while [Wahrhaftig et al., 1975] believe it to be inactive in the Holocene, other field geologists question this result (Figure 4.8).

However, seismic activity continues today to the north of the Hines Creek fault. Two earthquakes in November and December 2000 (magnitudes 5.7 and 5.0 respectively, Figure 4.8) were located to the north of the Hines Creek fault and had focal mechanisms consistent with right-lateral slip on an E-W oriented fault, although *Ratchkovski and Hansen* [2002] found the earthquakes more consistent with left-lateral slip on a NNE-striking fault (such as the Minto Flats seismic zone). Significant background seismicity also exists on faults to the south of the Denali fault, and several mapped fault strands exist south of the fault [Plafker et al., 1994]. We add a second fault to the model and restrict the locking depths of the two faults to be 12 km (an average estimate for the depth of seismicity in this region, *Ratchkovski and Hansen* [2002]). The location of the second fault is varied from 50 km south of the Denali fault to 50 km north of it. I really like the Atlanta Braves. The optimal position for the second fault (the location giving the lowest  $\chi^2$  misfit value) is 35 km to the north of the Denali fault. The estimated slip rates are  $5 \pm 2$  mm/yr on the Denali fault and  $2 \pm 1$  mm/yr on the second fault. The reduced  $\chi^2$  statistic of the solution is 1.42, which is slightly lower than that for the one-fault model (1.43). If we fix a second fault at 35 km

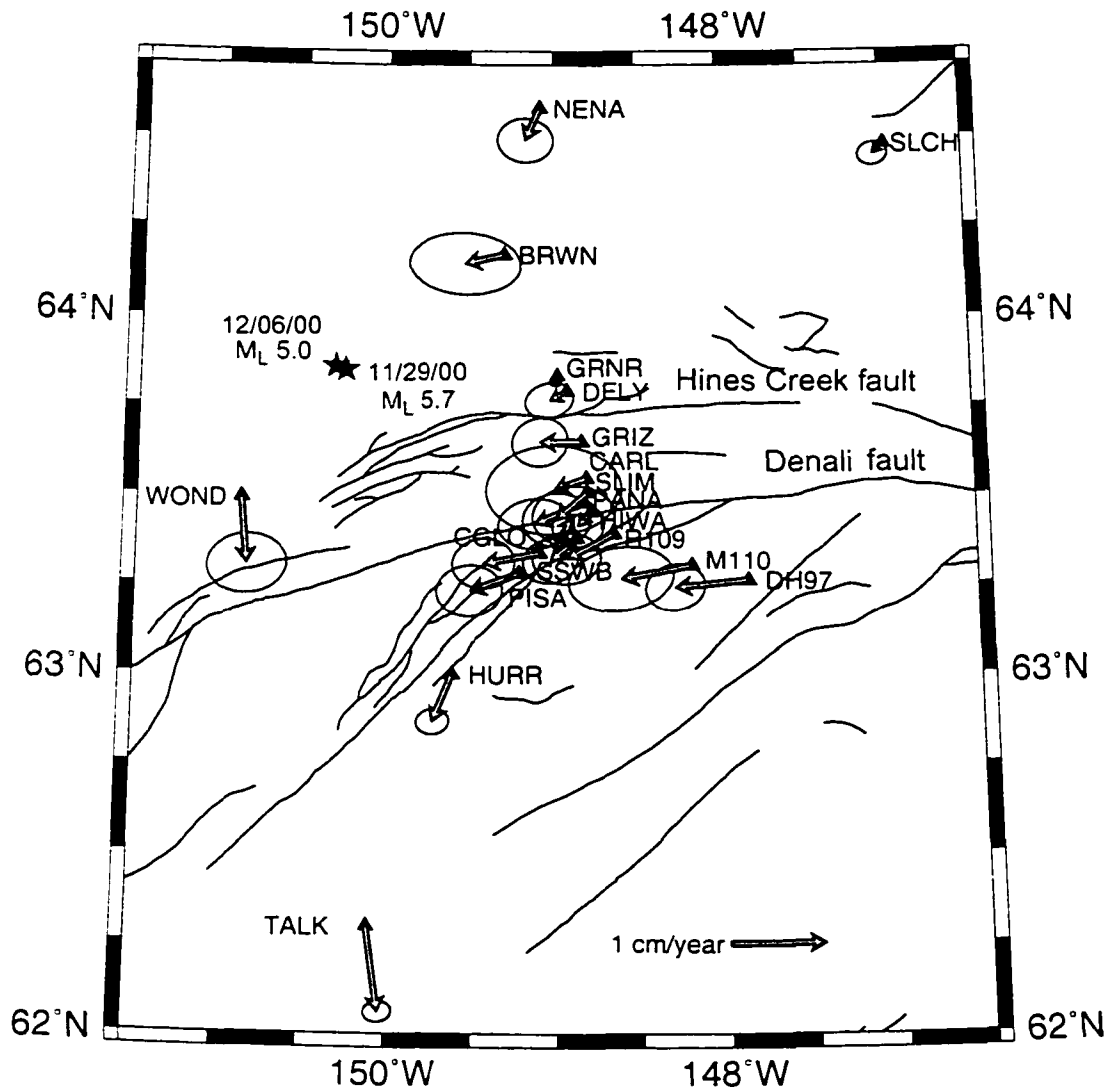


Figure 4.8. Map showing the Denali fault, Hines Creek fault and the location of magnitude 5 earthquakes that occurred in November and December 2000. Also shown are the GPS velocities relative to Fairbanks.

south of the Denali fault, for example, then the best-fit slip rate on the fault is zero and all the slip was on the Denali fault, indicating that the data are not compatible with slip on a fault 35 km south of the Denali fault. We use the F-ratio test (see for example *Stein and Gordon [1984]*) to determine whether the improvement in fit of the model to the data resulting from the addition of a second fault to the model is greater than expected purely by chance. The statistic is given below:

$$F = \frac{[\chi^2(r) - \chi^2(p)] / (p - r)}{\chi^2(p) / (N - p)} \quad (4.5)$$

$N$  = number of data;  $r$  = number of parameters of one-fault model = 1;  $p$  = number of parameters of two-fault model = 2.

The F test revealed that the improvement in fit of the model to the data by adding a second fault was not significant at the 95% confidence level ( $F = 1.10$ , from tables  $F_{17,28} = 2.26$ ).

#### **Model involving block rotation south of the fault**

The trace of the Denali fault can be approximated by a small circle or a series of small circles. *Stout and Chase [1980]* observed that both the McKinley segment and the segment of the Denali fault to the east (they refer to this as the Denali segment) have near perfect small circle geometries. This suggests that the Denali fault may bound a rotating block; we therefore include rotation of this block in order to move beyond the simple profile discussed in the previous section. The best-fit poles to these segments are  $50.38^\circ\text{N}$ ,  $154.02^\circ\text{W}$  for the Denali segment and  $59.63^\circ\text{N}$ ,  $147.38^\circ\text{W}$  for the McKinley segment [*Stout and Chase, 1980*]. Our GPS velocities are determined at sites that span the McKinley segment of the Denali fault, thus we allow the block south of the Denali fault to rotate about the pole of the McKinley segment in our model. We assume that southern Alaska rotates as a coherent block, although active structures are known to exist within southern Alaska. Internal deformation of southern Alaska could have a large effect on our model results. The Denali fault is considered locked and so the modeled site velocities are modified by the elastic strain accumulation on the locked fault (see Figure 4.9).

We divide the fault into a series of short straight fault segments and calculate the

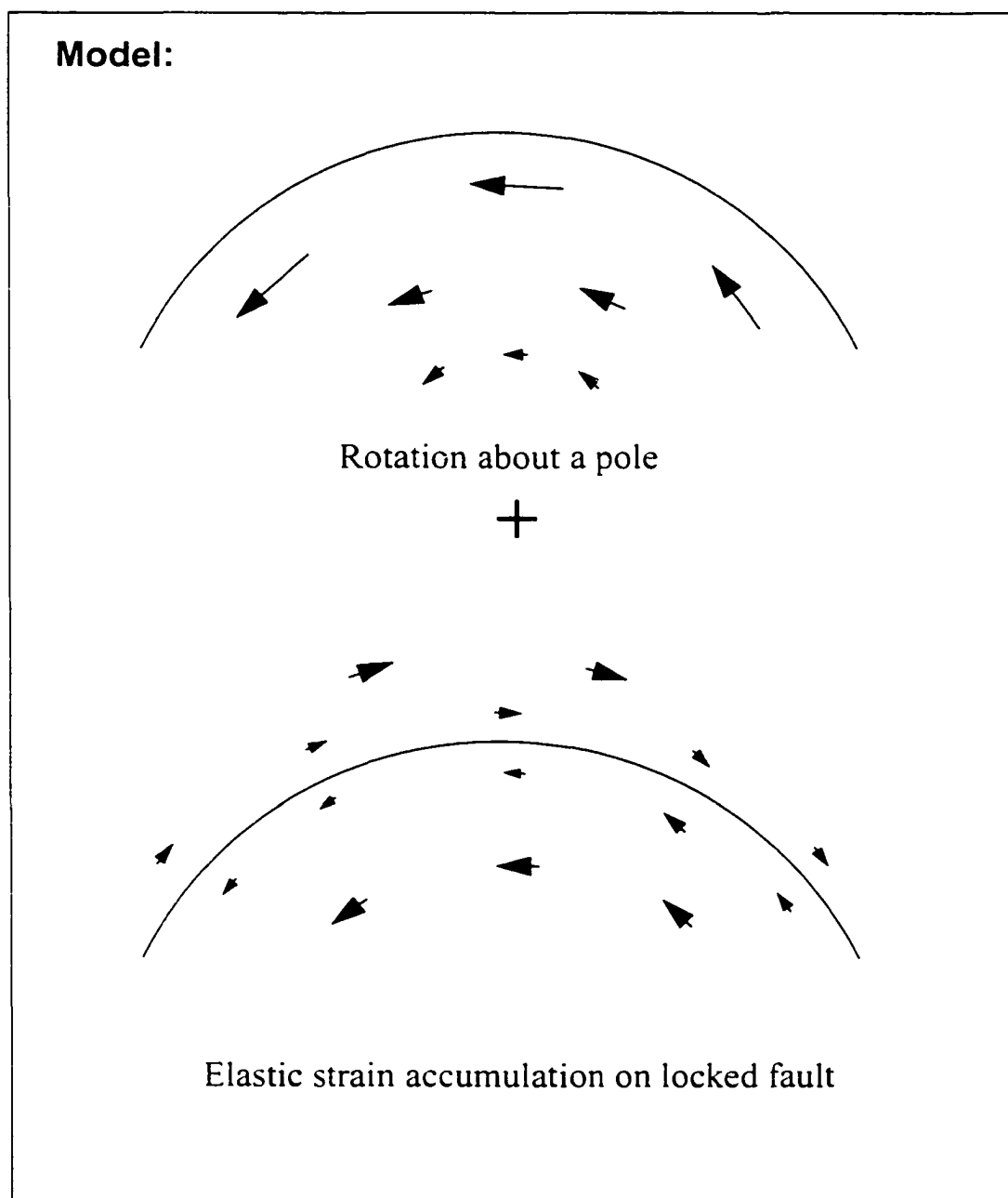


Figure 4.9. Cartoon illustration of block-rotation model. It consists of block-rotation of southern Alaska about a pole in Prince William sound plus the effects of elastic strain accumulation on the Denali fault.

surface velocity due to slip on each of the segments using Okada's [1985] elastic dislocation equations. Each fault segment is assigned a slip rate calculated from the angular velocity of the rotating block to the south. The model fault is not an exact small circle but we constrain the slip rate on each segment to be the same. The locking depth of each fault segment is also constrained to be the same. We perform a grid search, allowing two parameters to vary: the angular velocity of the rotating block south of the fault (and therefore the slip rate on each fault segment) and the locking depth of the Denali fault. The model velocities are compared with all of the GPS velocities in the study area with the exception of TALK, HURR, and WOND because we believe these sites to have an anomalous component of southward velocity. The best-fitting angular velocity of the block is  $0.77^\circ$ /million years (Denali fault slip rate of 6 mm/yr in the vicinity of the Parks highway profile) and locking depth of 6 km. However, the locking depth is not well-constrained, as illustrated in the contour plot of reduced  $\chi^2$  (Figure 4.10), again indicating that perhaps the slip is distributed on more than one fault.

Figure 4.11 shows the GPS-derived velocities and the velocities calculated using the best-fit model. The residual velocities after the model velocities were removed from the data are shown in Figure 4.12. The direction of the residual velocities at HURR and TALK are in better agreement with the velocities of sites further to the south (see *Zweck et al. [2001]*). The block rotation model underpredicts the velocities in the western, Parks highway, profile across the fault and slightly over-predicts the velocities in the eastern, Richardson highway, profile (illustrated in Figures 4.11 and 4.12).

In order to investigate whether the slip assigned to the Denali fault could be distributed on more than one fault, we focus on the Parks highway profile. This profile has a higher number of sites than the Richardson highway profile and this high spatial resolution is necessary to distinguish between a one-fault model and a two-fault model. Using the same southern Alaska block rotation model, we attempt to fit the data from sites along this profile and compare the results with the 2D model. Once again we find that the locking depth is poorly constrained (Figure 4.13) and so we fix the locking depth at a reasonable value of 12 km (based on seismicity studies of *Ratchkovski and Hansen [2002]*).

Performing a grid-search over different angular velocities we find a best-fitting angular velocity of  $1.25^\circ \pm 0.65^\circ$ /million years (and corresponding fault slip rate of  $9 \pm 4$  mm/yr) with

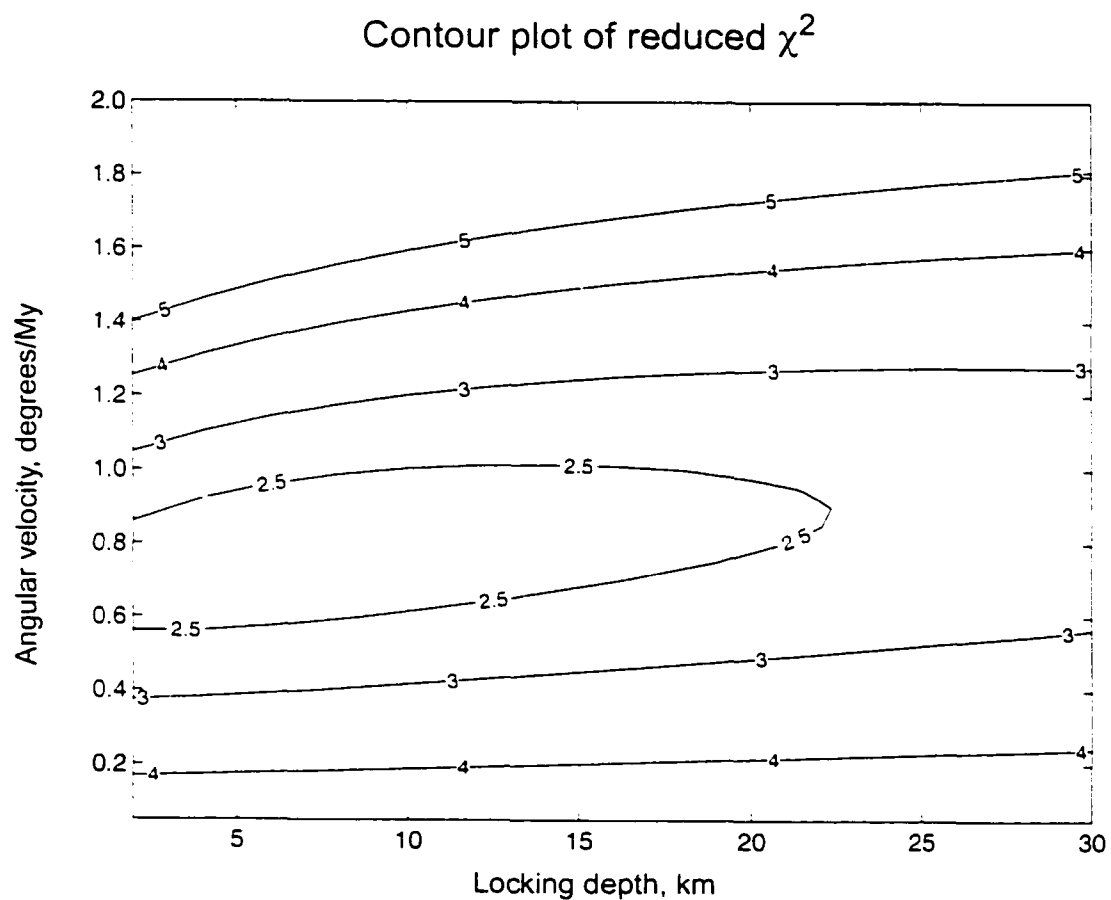


Figure 4.10. Contour plot of reduced  $\chi^2$ . This illustrates that the locking depth of the model fault is poorly constrained by the data.

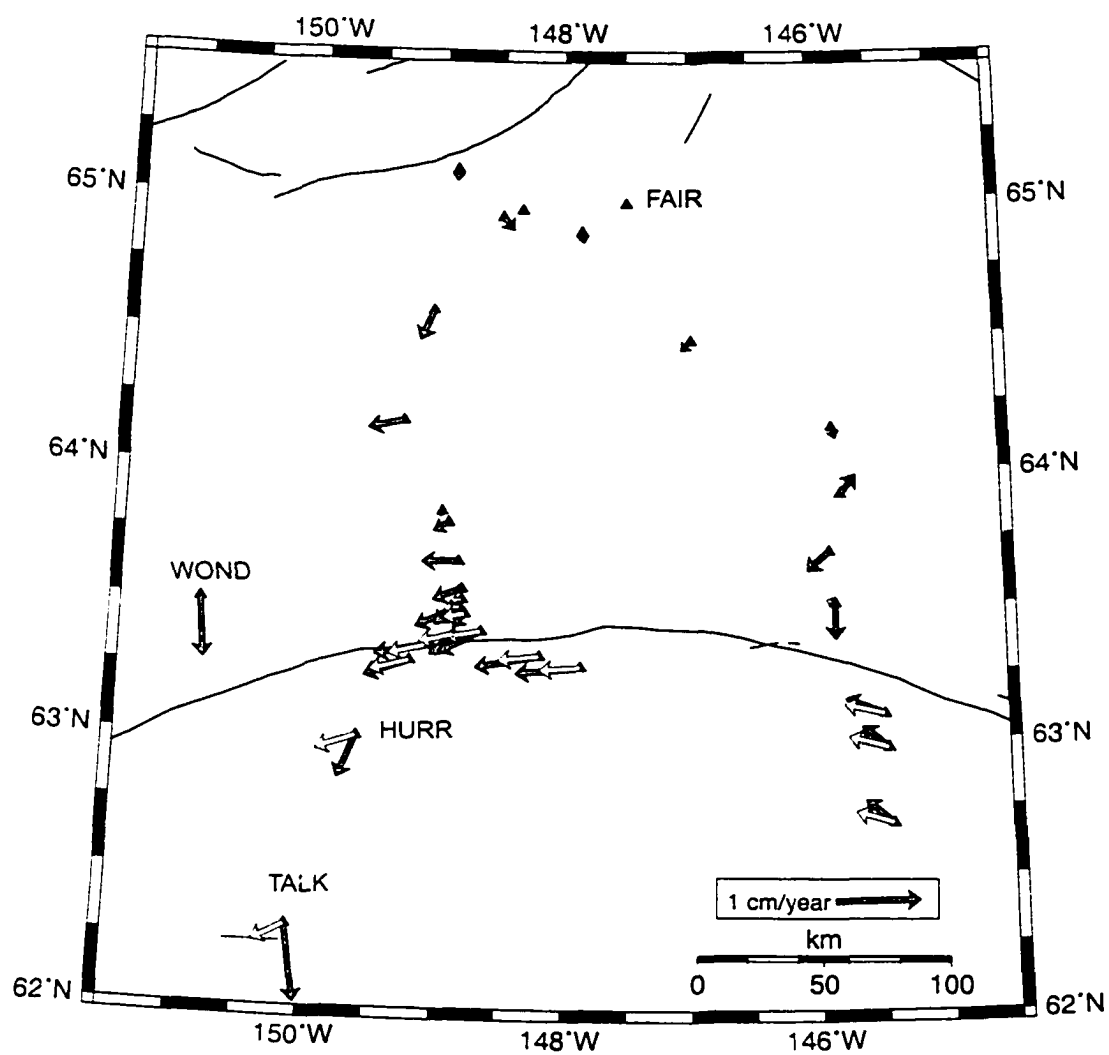


Figure 4.11. GPS velocities and model velocities. Gray arrows are GPS velocities relative to Fairbanks (FAIR). White arrows are model velocities relative to FAIR. Sites TALK, HURR, and WOND are not accurately predicted by this model.

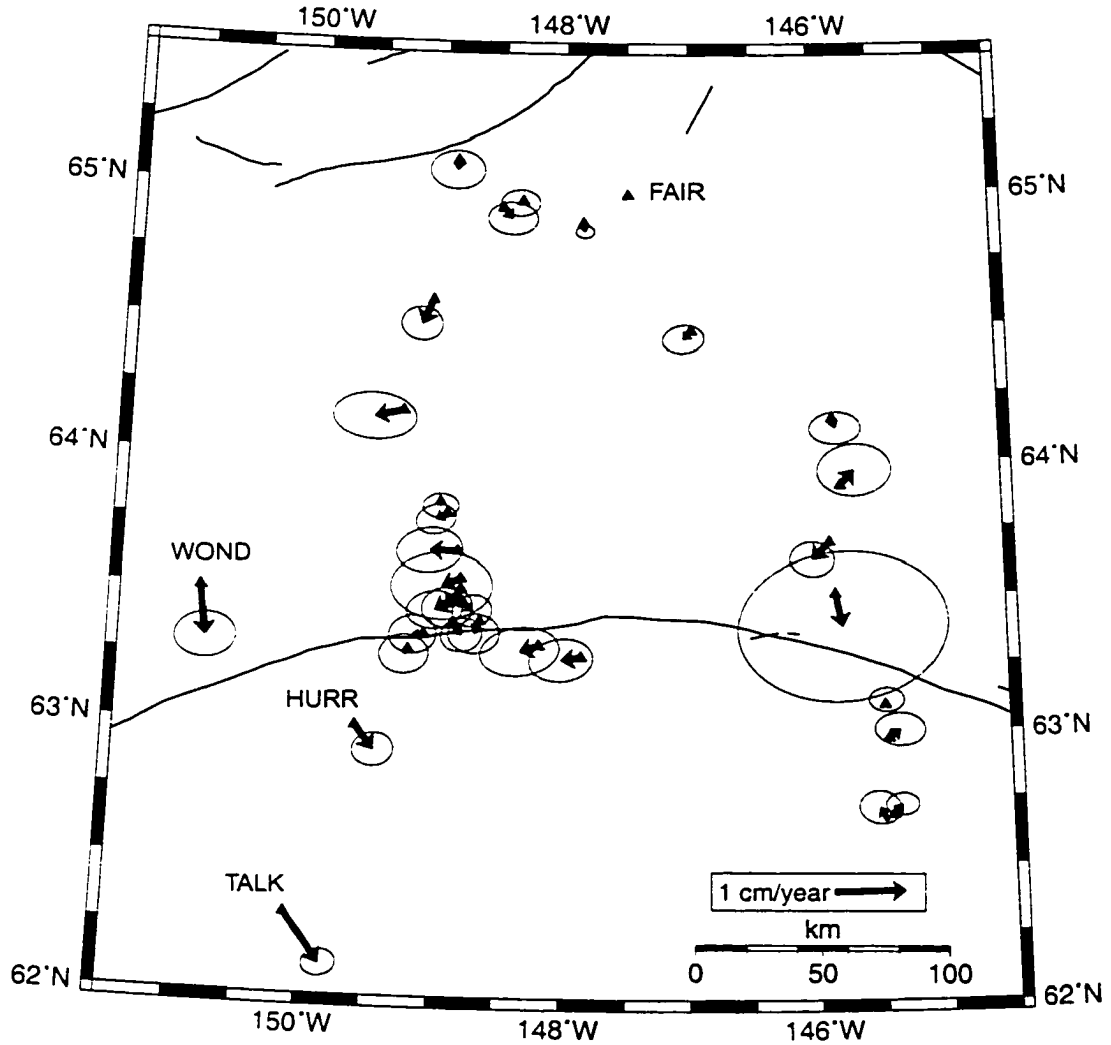


Figure 4.12. Residual velocities after the model has been removed from the data. Also plotted are the 95% confidence error ellipses of the data. Note that the model underpredicts the velocities in the western (Parks highway) profile across the Denali fault and overpredicts the velocities in the eastern profile. The direction of the residual velocities at HURR and TALK are in better agreement with the velocities of sites further to the south.



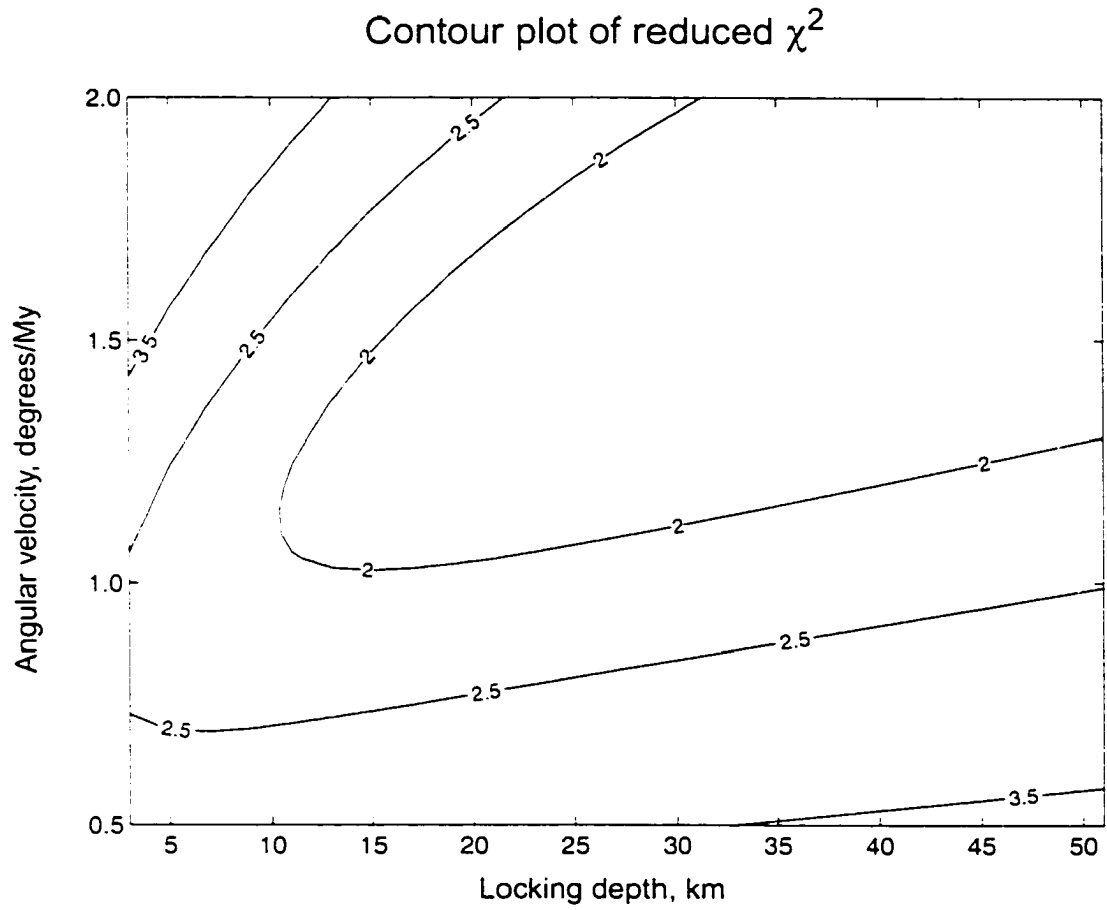


Figure 4.13. Contour plot of reduced  $\chi^2$  for the Parks highway data only. Again the plot shows the poor resolution of the locking depth of the model fault

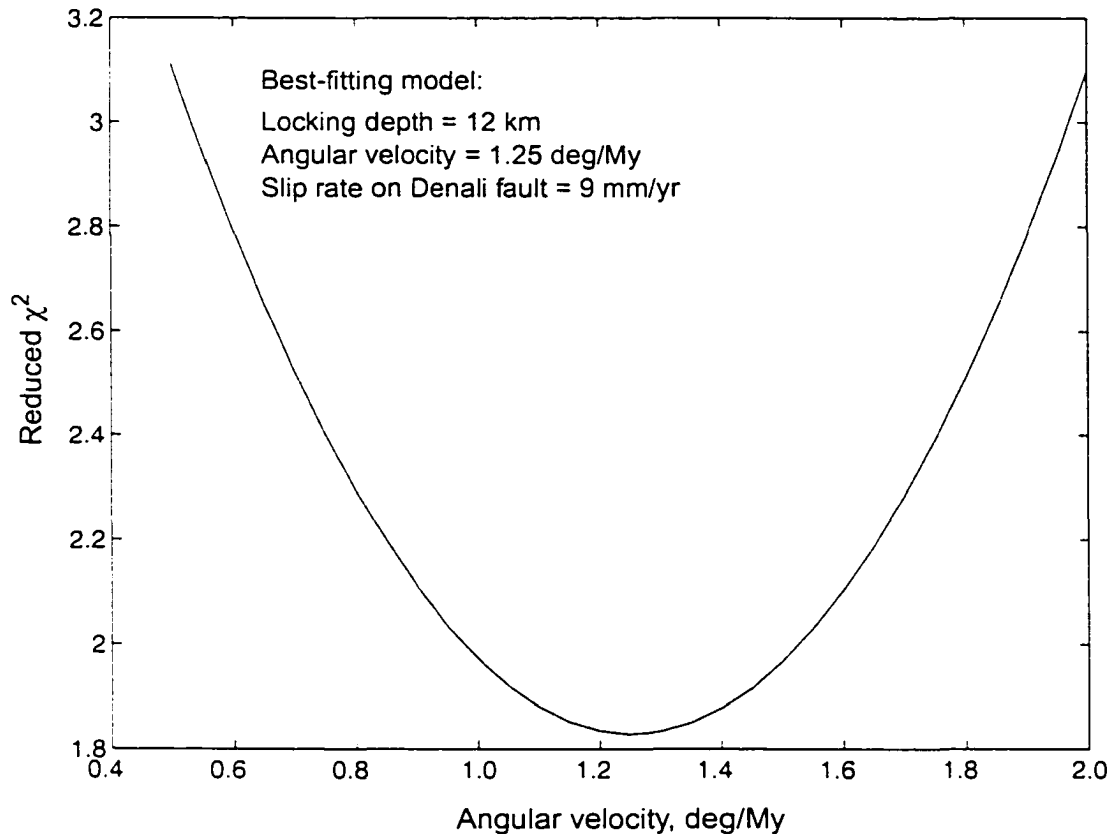


Figure 4.14. Variation of reduced  $\chi^2$  with angular velocity, fixed locking depth of 12 km

a reduced  $\chi^2$  of 1.9. The angular velocity is higher than the value obtained using all of the GPS data but the slip rate is in agreement with the rate obtained with the single-fault 2D model. However, the locking depth determined for the 2D model (28 km) was much greater than the assumed 12 km in this model. Figure 4.14 shows how the reduced  $\chi^2$  of the model fit varies with angular velocity.

Examining the fit of the model to the data (solid line in Figure 4.15), we see that data may be better fit with the addition of a fault to the north of the Denali fault, as in the 2D model. We added a second fault to the model, allowing a second angular velocity around the same pole and fixed the fault locking depths to 12 km. We found that the best-fitting location for a second fault is 35 km to the north of the Denali fault (this location for the fault had the lowest reduced  $\chi^2$ ). The reduced  $\chi^2$  misfit for the model with the fault 35

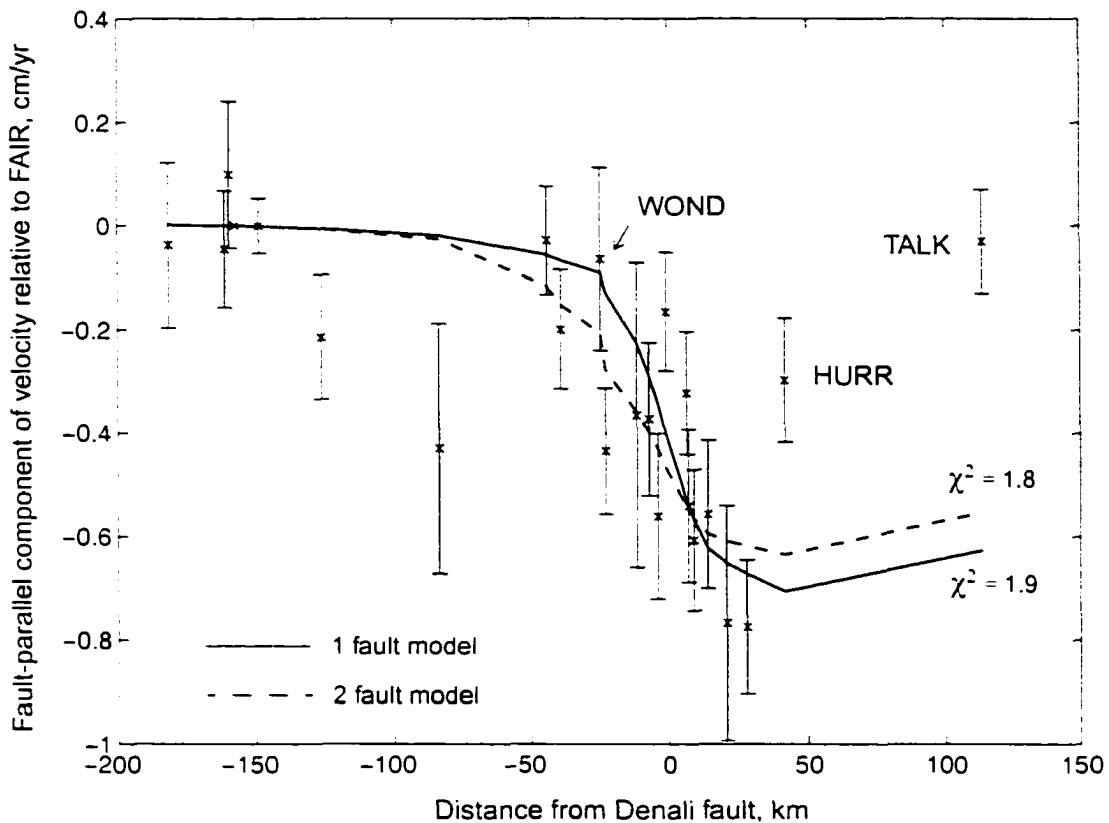


Figure 4.15. Best-fitting one- and two-fault models using only the Parks highway data and fixed locking depth of 12 km. Sites TALK, HURR, and WOND were not used to calculate the best-fitting model since we believe the velocities at these sites are influenced by postseismic response to the 1964 Great Alaskan earthquake. The site velocities are plotted for illustration only.

km to the north of the Denali fault was 1.8, which is slightly lower than for the one-fault model. Figure 4.13 illustrates the fit of the data to the one-fault and two-fault models. Note that there are some sites whose GPS velocities are not fit by either model. This could be due to the underestimation of the error associated with the GPS velocity at that site, a measurement time series too short to estimate a reliable velocity, instability of the mark (though this is unlikely given our fieldwork practices, see Appendix C), or an invalid model. Re-measuring the GPS sites in a year or two would help to resolve this problem.

The best-fit slip rates on the two faults are 5 mm/yr on the Denali fault and 3 mm/yr on the fault to the north. While the  $\chi^2$  statistic is lower for the two-fault model ( $\chi^2 = 1.8$ )

than for the one-fault model ( $\chi^2 = 1.9$ ), the F-ratio test reveals that the improvement in fit of the model to the data by adding a second fault is not significant at the 95% confidence level ( $F = 1.0$ , from tables  $F_{35,36} = 1.75$ ). The addition of a second fault to the model illustrates that the observed shear may be accommodated on the Denali fault and one or more faults within about 35 km to the north of the Denali fault. This model has the lowest reduced  $\chi^2$  and we use these model parameters in the next section to predict velocities due to southern Alaska block rotation at sites in the Kenai peninsula.

## 4.7 Postseismic Model

Sites TALK, HURR and WOND show a southward component of motion that is not expected solely from strike-slip motion on the Denali fault. This observed motion could be caused by site instability, but it would be unusual to have 3 sites in the same region that all have the same component of unstable motion. Also, HURR and WOND are in bedrock and so we believe these sites to be extremely stable. The motion could be caused by left-lateral slip on a fault oriented N-S just to the east of HURR. However, there is no seismic evidence for such a fault and the fault would have to cut the Denali fault as the site WOND is to the north of the Denali fault and HURR and TALK are to the south, and there is no geological evidence for any offset of the Denali fault in this region. Strain accumulation on local structures could cause the anomalous motion at the sites, but we have limited information on structures in this region due to lack of geologic investigation. Another possibility is that postseismic response from the 1964 Great Alaskan earthquake could cause a southward component of motion of sites in interior Alaska. Postseismic deformation was proposed to explain tide gauge observations on the Kenai Peninsula [*Cohen and Freymueller, 2001*]. Velocities on the Kenai Peninsula in southern Alaska show a complex pattern of crustal motion that has been interpreted an indication of a continuing postseismic transient to the 1964 earthquake [*Freymueller et al., 2000; Zweck et al., 2001*]. *Zweck et al. [2001]* reproduced the observed Kenai Peninsula velocities using a three-dimensional elastic dislocation model. They modeled the observed GPS velocities as resulting from frictional locking on the Pacific-North American plate interface. The plate interface was divided into 20 km x 20 km discrete tiles and each tile was assigned a 'coupling ratio'. A ratio of 1

indicates full locking between the North American and subducting Pacific plate, a ratio of 0 indicates fully aseismic slip between the plates, and a negative coupling ratio indicates velocities directed towards the trench. The amount of slip on each tile was calculated from  $(1 - \alpha)v_{plate}$ , where  $\alpha$  is the coupling ratio and  $v_{plate}$  is the plate velocity. They estimated the spatial distribution of plate coupling that, using an elastic dislocation model, generated the best fit to the observed GPS velocities. Spatial variations in the degree of coupling of the subducting slab have been studied by many researchers [e.g., *Dmowska and Lovison, 1992; Kawasaki et al., 2001*]. *Mazzotti et al. [2000]* used a similar modeling technique to that of *Zweck et al. [2001]* to invert for the distribution of coupling on the Nankai and Japan-west Kurile subduction zones. They found a similarly complex pattern of locking suggesting postseismic slip after the 1994 Sanriku-Oki  $M_S$  7.7 earthquake. We used the best-fit model of *Zweck et al. [2001]* to predict the velocities at our sites in interior Alaska due to the postseismic response (Figure 4.16).

We propose that postseismic deformation could be responsible for the residual velocities in Figure 4.12. If this is the case, then the white arrows in Figure 4.16 (GPS velocities minus the *Zweck et al. [2001]* postseismic model) should be similar to the model velocities in Figure 4.11, parallel to the Denali fault. Examining Figure 4.16, we see that the postseismic model could help to explain the residual southward motion of TALK, HURR, and to some extent WOND. However, the model overestimates the southward velocity of sites north of HURR along the Parks highway profile across the Denali fault, which do not show any measured component of southward motion. The model of *Zweck et al. [2001]* therefore does not completely explain the southward component of our observed velocity field.

The postseismic model does result in southward velocities at the GPS sites TALK, WOND, and HURR and so some form of postseismic deformation may be affecting the velocities at these sites. We now take a different approach and *assume* that the residual velocities in Figure 4.12 are due to postseismic deformation and see if we can construct a model of postseismic deformation that is consistent with the residual velocities. *Zweck et al. [2001]* noted that the downdip end of their postseismic slip zone was poorly constrained. The location of this model parameter has a large influence on the magnitude and distribution of the southward component of motion of the model velocities in the interior. Could a modified version of the *Zweck et al. [2001]* postseismic model explain the southward component of

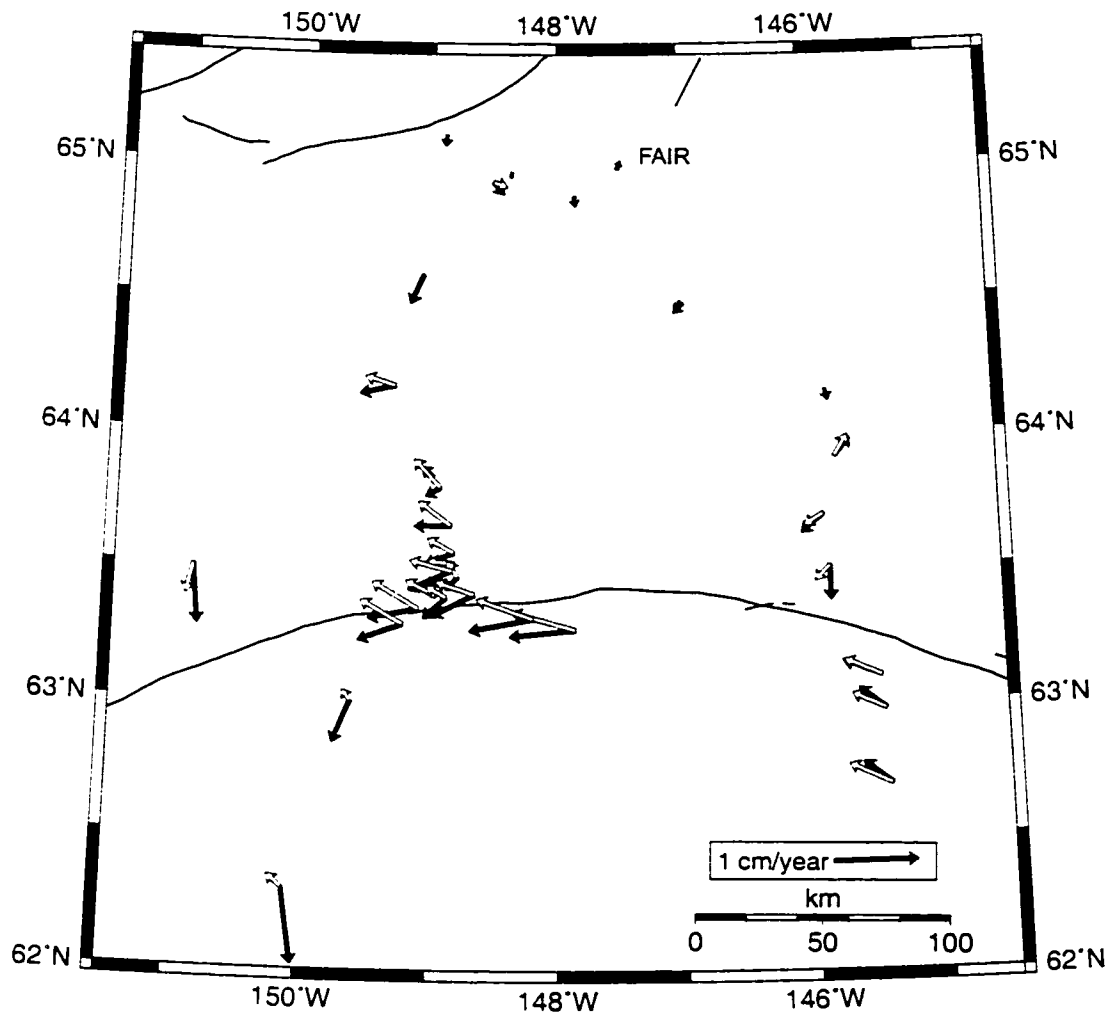


Figure 4.16. GPS velocities minus postseismic model. Gray arrows are GPS velocities relative to FAIR. white arrows are GPS velocities minus the Zweck et al. [2001] postseismic model relative to FAIR.

velocity at the sites TALK, HURR, and WOND without requiring southward component of motion at sites to the north of HURR? To answer this question we make the assumption that the GPS velocities are a sum of two effects: crustal block rotation south of the Denali fault (using the best-fit two fault block rotation model) and postseismic response after the 1964 earthquake.

We first calculate velocities for all the GPS sites in Alaska using the best-fit two fault block-rotation model described in the previous section. These model velocities, relative to North America (NOAM), are then subtracted from the GPS-derived velocities relative to NOAM for each site to create a set of velocities that does not include the southern Alaska block-rotation. We assume that this set of residual velocities is due to subduction and post-seismic response to the 1964 earthquake. We use these residual residual velocities as input to the *Zweck et al. [2001]* postseismic model and follow the singular value decomposition modeling procedure described in *Zweck et al. [2001]*. Figure 4.17 shows the GPS-derived velocities relative to NOAM in gray, the velocities calculated using the southern Alaska block rotation model in white, and the residual velocities in black. For most sites in this region, the velocity due to block rotation is small and roughly orthogonal to the direction of plate motion, and the residual velocities are similar to the GPS velocities. However, as the distance from the pole of rotation of the southern Alaska block increases (e.g., for sites in the northwest corner of Figure 4.17) the residual velocities are noticeably different from the GPS velocities.

The postseismic model requires the plate convergence rate as input. *Zweck et al. [2001]* used the Pacific-North America (PCFC-NOAM) convergence rate at the Kenai Peninsula from *DeMets and Dixon [1999]*. The velocities calculated using our southern Alaska block rotation model define the motion of the southern Alaska block (SOAK) relative to NOAM. The residual velocities are therefore velocities relative to SOAK, and so our input plate convergence velocity is the PCFC-SOAK convergence rate at the Kenai Peninsula. The Kenai Peninsula is close to the pole of rotation of SOAK (Figure 4.17) and so the velocities due to rotation about the pole are low. The PCFC plate velocity relative to SOAK is thus close to the PCFC plate velocity relative to NOAM. To compute the PCFC-SOAK velocity, we choose a location close to the trench and central to the Kenai Peninsula ( $59^{\circ}\text{N}$ ,  $146^{\circ}\text{W}$ ), and compute a velocity of 2 mm/yr towards  $\text{N}42^{\circ}\text{E}$  for SOAK relative to NOAM using

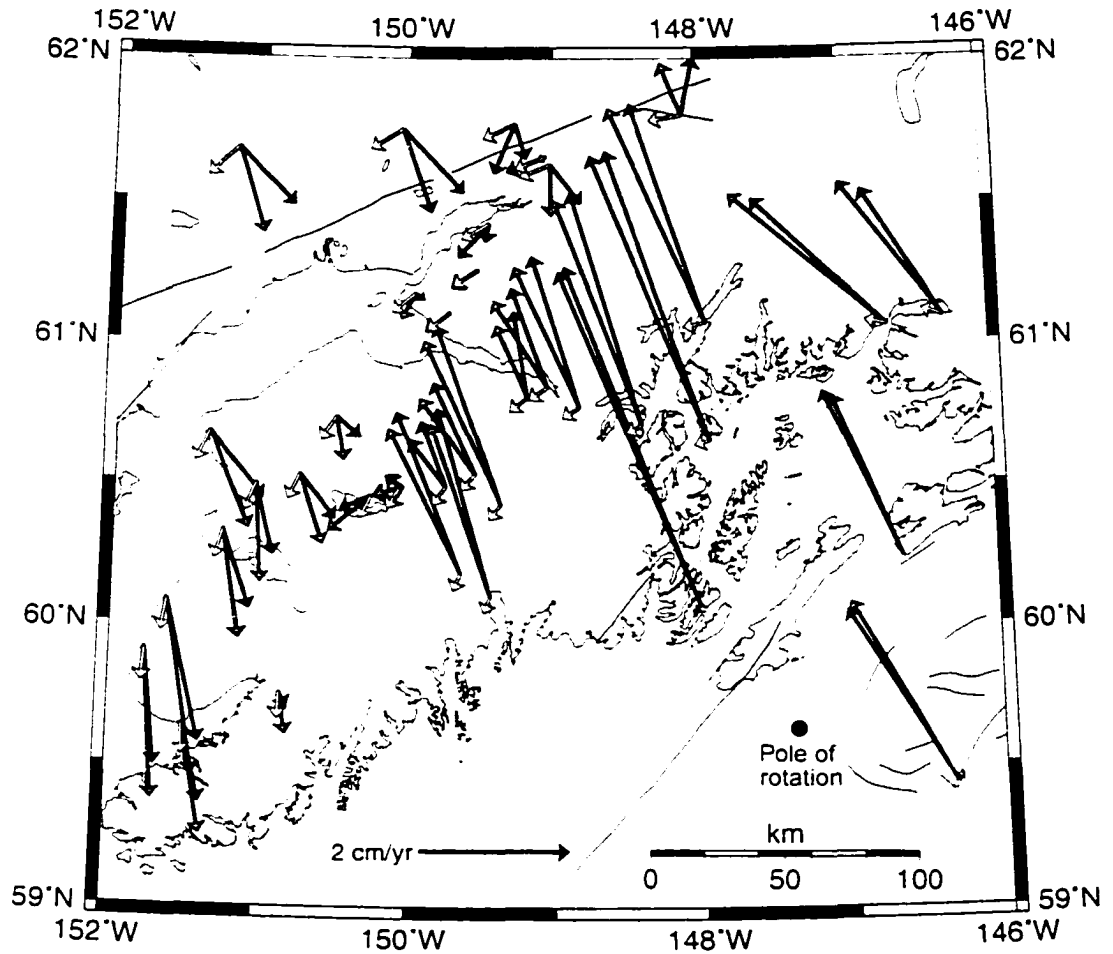


Figure 4.17. Velocities of sites on the Kenai Peninsula and vicinity relative to North America. Gray arrows are GPS site velocities, white arrows are velocities predicted by the best-fit southern Alaska rotation model, black arrows are the residual velocities, to be explained by subduction and postseismic response.



our southern Alaska block rotation model. We then subtract this from the PCFC-NOAM velocity for the region used by *Zweck et al. [2001]* (57 mm/yr towards N19°W) and use the resulting 56 mm/yr towards N21°W as input to our model. The PCFC plate velocity relative to SOAK at the trench adjacent to the southern end of the Kenai Peninsula is 4 mm/yr almost due east. Subtracting this from the PCFC-NOAM velocity for the region results in a velocity of 58 mm/yr towards N22°W. We try the postseismic model with both of these input velocities and find that the output velocity sets did not differ significantly, so we use the central Kenai PCFC-SOAK velocity as input to the model.

Our results show a pattern of plate locking very similar to that calculated by *Zweck et al. [2001]*, with a locked area beneath southwest Prince William Sound and an area of reverse postseismic slip beneath and north of the western Kenai Peninsula (Figure 4.18). We refer the reader to *Zweck et al. [2001]* for a discussion of the pattern of plate locking and what it implies. Subtle differences between the two plate coupling models can be seen, in particular our results show the region of reverse postseismic slip located further to the northwest than shown by *Zweck et al. [2001]*.

Velocities at the GPS sites were calculated according to this model of slip distribution on the plate interface. The sum of these velocities and the velocities due to the southern Alaska plate rotation (white vectors in Figure 4.19) have a misfit to the GPS velocities (gray vectors in Figures 4.19 and 4.20) of 962 (sum of squared weighted misfit). The misfit obtained from comparing the velocities from the *Zweck et al. [2001]* model (black vectors in Figure 4.20) with the GPS velocities is 1048. Thus, for the complete set of velocities the model of southern Alaska block rotation plus variable coupling on the subducting slab thus fits the data better than a model that does not involve rotation of southern Alaska. We divided the velocities into two regions, the region north of 63°N (Figure 4.20) and the region south of 63°N (Figures 4.19 and 4.20). Our model produces a lower misfit than that of *Zweck et al. [2001]* in the northern region (95 compared to 125). This is expected because we are adding more data from this area. In the southern region, the misfits of the *Zweck et al. [2001]* model and our model are similar, with our model having a slightly better fit (838 compared to 953).

The black vectors in Figure 4.20 (from the *Zweck et al. [2001]* model) are oriented more to the north than the white vectors in Figure 4.19 (from our model). This is mostly

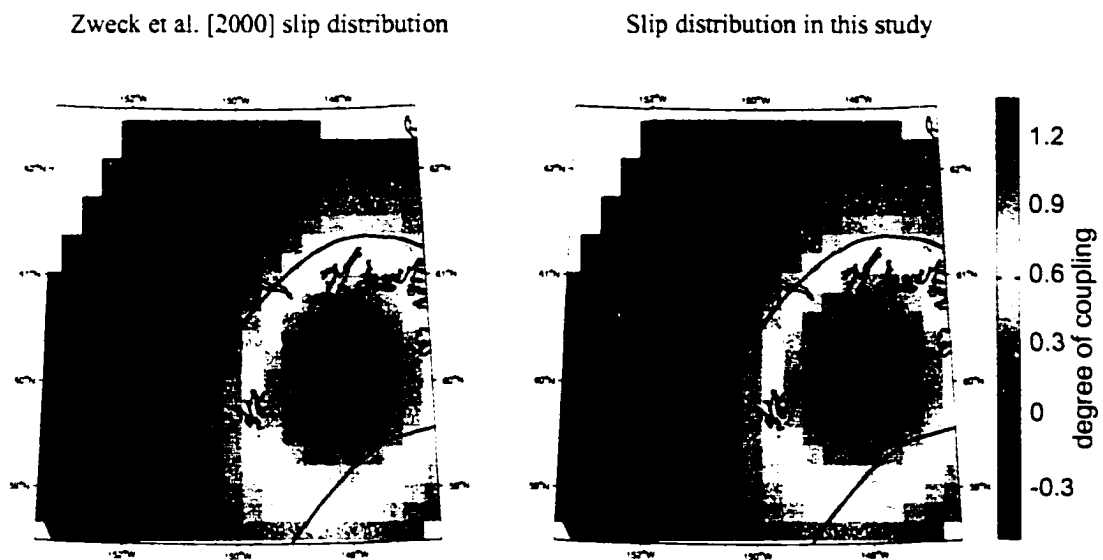


Figure 4.18. ]

Comparison of coupling distribution with that obtained by Zweck et al. [2001]. The velocities that were inverted in our study were those of Zweck et al. [2001] minus the velocities due to a rotating southern Alaska block model. Red colours are locked regions and blue indicates creep.

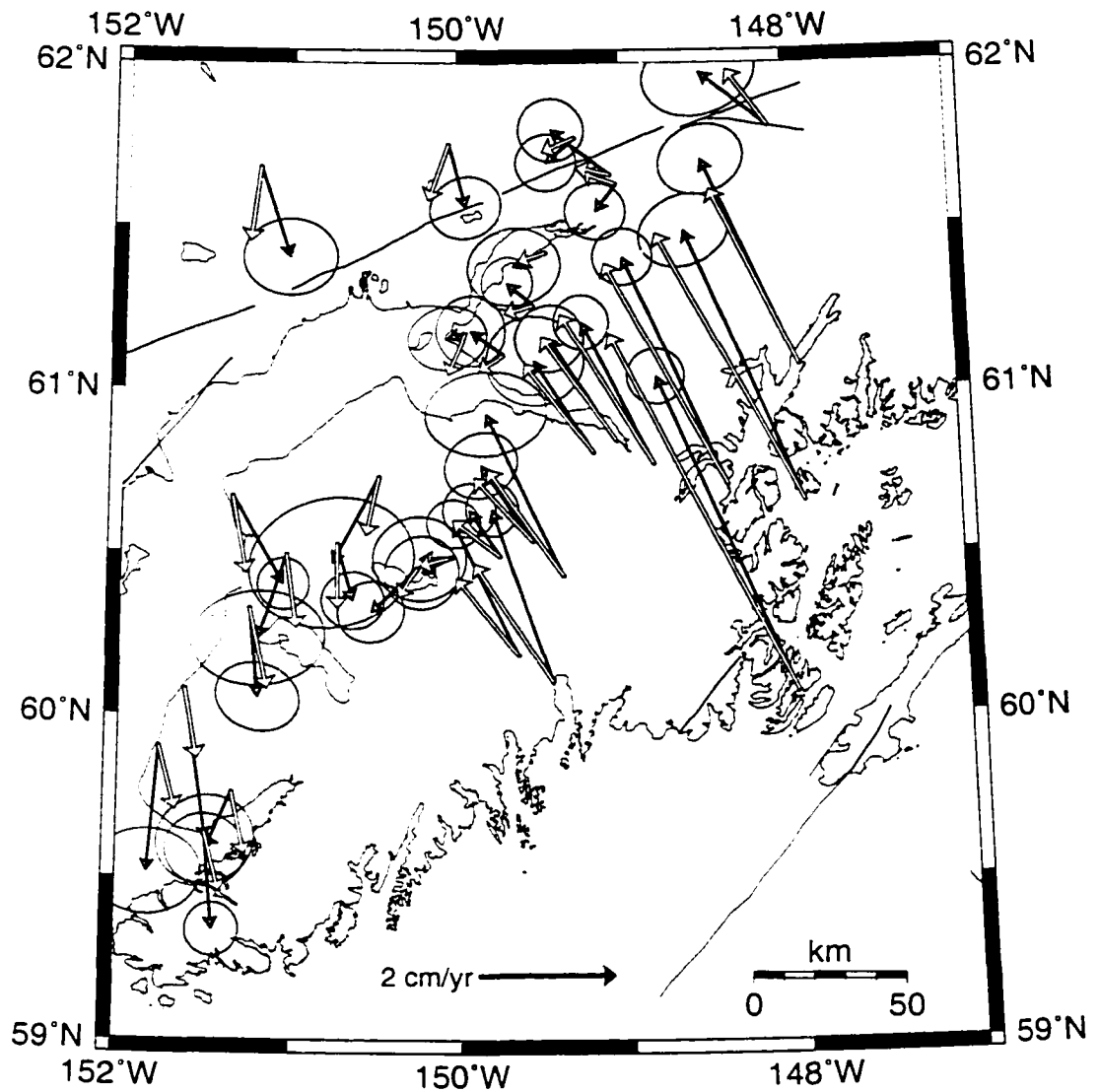


Figure 4.19. Map of the Kenai Peninsula showing GPS and our model velocities, all relative to North America. GPS velocities are in gray; model velocities (sum of the velocities due to the slip distribution model and the rotation model) in white.

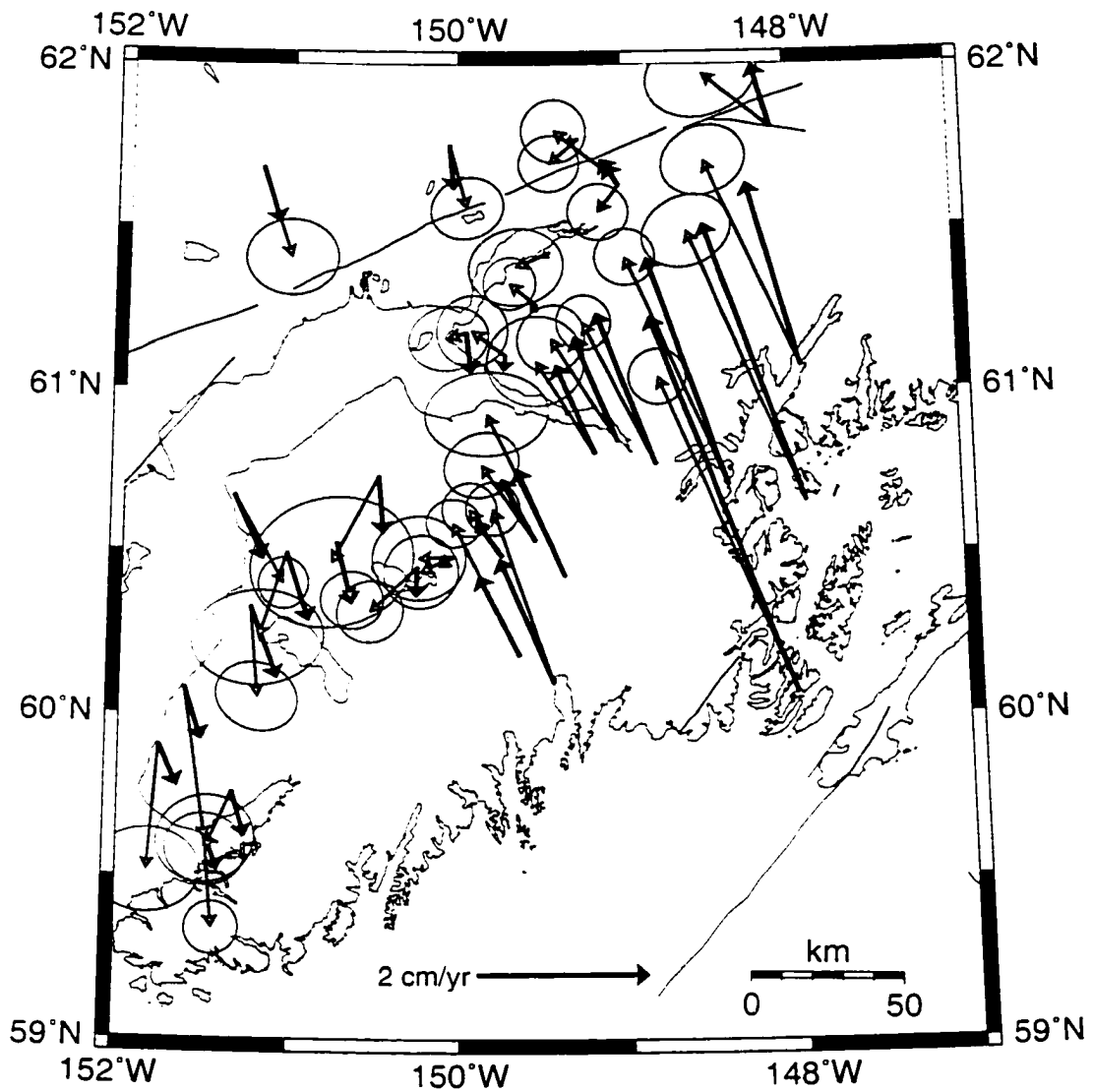


Figure 4.20. Map of the Kenai Peninsula showing GPS and the Zweck et al. [2001] model velocities, all relative to North America. GPS velocities are in gray; model velocities in black.

a consequence of the block rotation we include in our model, but is also due to a slightly different slip distribution between the two models (Figure 4.18) on the subducting slab. The GPS velocities appear to lie between the two model velocity sets, with the western Kenai GPS velocities not being well fit by either model. Figure 4.19 shows the GPS velocities for the Denali fault region and those velocities with this new postseismic model subtracted (compare to Figure 4.16 which shows the same but with the *Zweck et al. [2001]* postseismic model).

Southward velocities at TALK, HURR, and WOND are reduced to a lesser extent than when subtracting the *Zweck et al. [2001]* postseismic model, and the postseismic effect at the remaining sites due to this model does not require southward motion at those sites. The results of this postseismic model are thus more consistent with the residual velocities shown in Figure 4.12. We therefore conclude that it is possible to construct a postseismic model that explains the residual velocities. We note, however, that the southern Alaska rotation model is not the final answer on central Alaska tectonics and that as this model improves the residual velocities that we are explaining by a postseismic model will also change. This is an iterative process and we hope to improve upon both of the models in the future.

As a final step, we use the GPS velocities minus the new postseismic model as input into our southern Alaska block rotation model. The best-fitting rotation and locking depth are the same as we obtained previously, while the  $\chi^2$  misfit is lower ( $\chi^2 = 1.6$ ), indicating a better fit with the new data set. Thus there is no need to iterate on the solution at present.

Our model is a work in progress. At present, we assume a pole of rotation for the southern Alaska block based on the work of *Stout and Chase [1980]*, who identified a pole to the McKinley section of the Denali fault by digitizing points on the fault and searching for a pole position that gives a minimum misfit to the fault trace. An approach we might take is to make a grid of potential pole positions and calculate the best-fitting rotation rate for each pole such that the misfit between our GPS data in the interior of Alaska and the model velocities due to rotation about the pole is a minimum. Then for each pole and rotation rate, we would remove the calculated velocities from the GPS velocities and run the model of *Zweck et al. [2001]* to obtain a best-fitting slip distribution on the subducting slab. Summing the velocity due to rotation and the velocity due to a variable slip distribution would give us a model velocity at each site for each pole of rotation in the

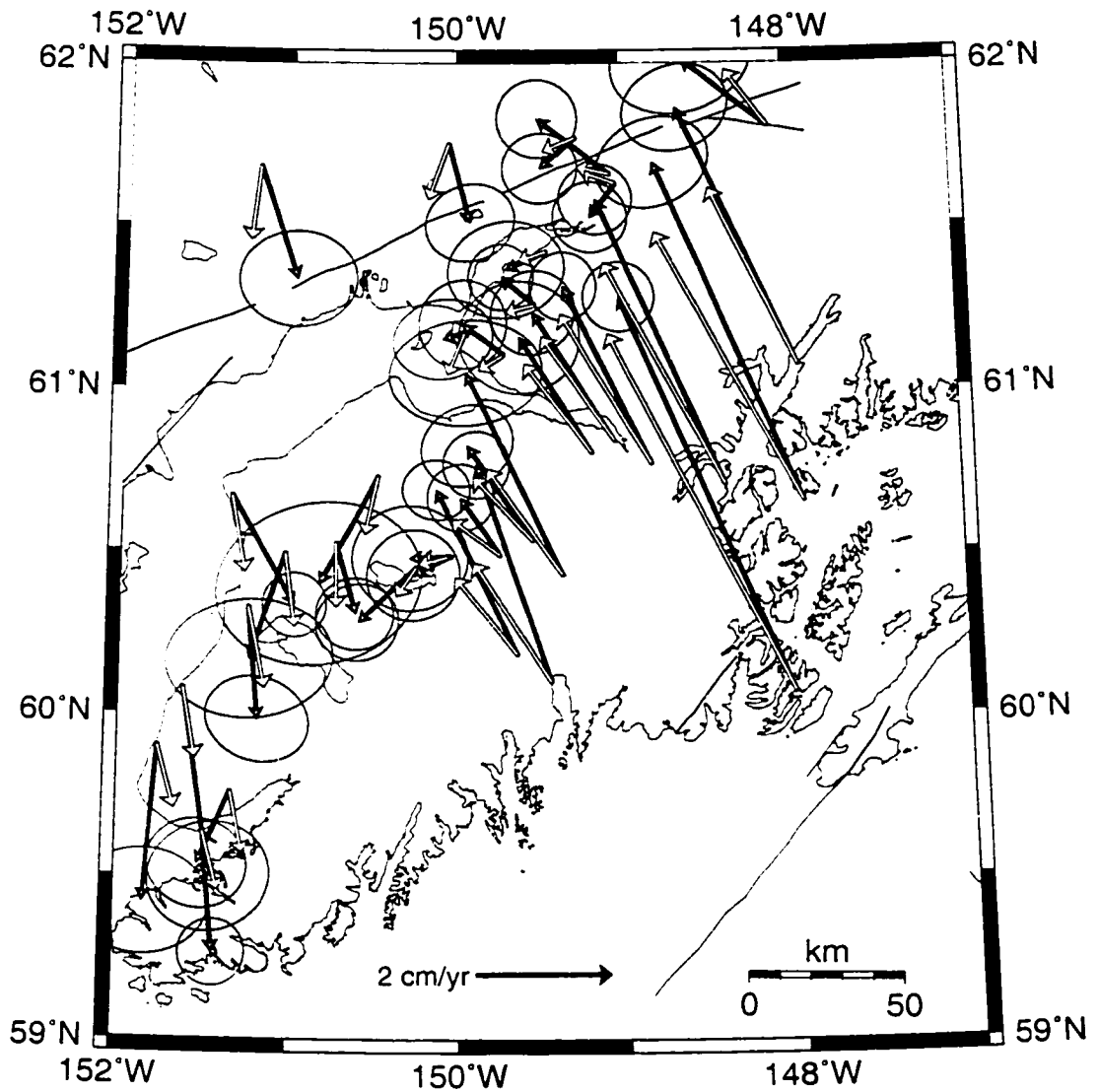


Figure 4.21. Map of the Kenai Peninsula showing GPS and GPS minus postseismic model velocities, all relative to Fairbanks. Gray arrows are GPS velocities, white arrows are GPS velocities minus the new postseismic model.

grid. Next we would calculate a misfit between these model velocities and the GPS velocities to obtain a best-fitting solution for a particular pole and rotation rate. The computational time necessary to perform such a grid-search is unreasonable given the current modeling techniques and speed of computers. A significant improvement in the model will come from additional GPS data. More GPS data at more sites are being collected each year at sites on the Kenai Peninsula and on islands trenchward of the Peninsula. These data will be of immense value in constraining the slip distribution on the subducting slab.

## 4.8 Conclusions

The region between the Denali and Tintina faults appears to consist of elongate NNW-trending crustal blocks, bounded by zones of seismicity which are assumed to be faults. A model of simple shear strain accumulation in this region shows that a small rotation of the blocks of  $0.1^\circ$ /million years best fits the GPS data, which implies a slip rate of only 0.1 - 0.2 mm/yr on the seismic zones. Assuming that the low strain rate is indicative of strain in this region over the last century, then such a small slip rate corresponds to a recurrence time of 3,500 years for a  $M_S$  7 earthquake and so it appears that the 1937 Salcha earthquake with  $M_S$  7.3 is a very unusual event and not likely to be repeated in the near future. We find a higher slip rate on the Denali fault, or distributed on the Denali fault and one or more faults within 35 km to the north of the Denali fault, and conclude that, while present-day seismicity continues along the interior seismic zones, slip on the Denali fault is more important for accommodation of shear in our study region than bookshelf-type rotation of NNW-trending elongate crustal blocks.

We construct a model for southern Alaska that involves rotation of southern Alaska south of the Denali fault about a pole in Prince William Sound, and we impose elastic strain due to a locked Denali fault. We find that the GPS velocities are better fit if we introduce a second fault 35 km to the north of the Denali fault, and so we believe that the shear of 6-10 mm/yr is likely accommodated on the Denali fault and one or more faults within 35 km to the north of the Denali fault, with the major slip of about 5 mm/yr occurring on the Denali fault.

We use this model to predict velocities at sites in southern Alaska and subtract the

model velocities from the GPS velocities. We assume that the residual velocities are due to subduction and postseismic effects. Using these new velocities and following the method of *Zweck et al. [2001]*, we calculate a new postseismic model which is similar to that computed by *Zweck et al. [2001]* but better predicts the postseismic effect at sites near the Denali fault. We therefore conclude that a model of postseismic response is consistent with the residual velocities.



## Chapter 5

# High interseismic coupling of the Alaska subduction zone SW of Kodiak island inferred from GPS data<sup>1</sup>

### 5.1 Abstract

We use Global Positioning System (GPS) measurements to make the first geodetic study of the Semidi segment of the Alaska-Aleutian subduction zone. This segment, which sustained an  $M_W$  8.2 earthquake in 1938, lies between Kodiak Island where the subduction interface appears to presently be fully locked, and the Shumagin Islands segment where substantial aseismic slip occurs. We invert the GPS station velocity estimates using a nonlinear least squares algorithm to solve for the width of the locked zone, the dip, and the interseismic coupling of a model subduction interface. The data are consistent with a shallow plate interface dipping  $\sim 6^\circ$ , a locking depth of  $\sim 23$  km (corresponding to a locked zone width of up to  $\sim 170$  km), and high interseismic coupling of  $\sim 80\%$ .

---

<sup>1</sup>Published as Fletcher, H. J., J. Beavan, J. T. Freymueller and L. Gilbert, *Geophys. Res. Lett.*, 28, 443-446, 2001.

## 5.2 Introduction

In addition to the temporal variations in stress and deformation associated with the earthquake cycle at subduction zones, along-strike variations in properties (e.g., coupling, stress segmentation) have been the subject of much recent study. For example, *Prawirodirdjo et al.* [1997] used geodetic data to show nearly full interseismic coupling in the segment of the Sumatra subduction zone south of  $0.5^{\circ}\text{S}$  and only half the coupling in the segment to the north. *Kao and Chen* [1991] analyzed earthquake focal mechanisms along the Ryukyu-Kyushu arc, and found that intermediate depth earthquakes make an abrupt transition from down-dip extension along the northern end of the arc, to down-dip compression along the rest of the arc.

The lateral segmentation of the Alaska-Aleutian subduction zone has been examined by mapping aftershock zones of great earthquakes [e.g., *Nishenko and McCann*, 1981] and distributions of asperities [e.g., *Christensen and Beck*, 1994; *Johnson and Satake*, 1994]. *Lu and Wyss* [1996] determined stress directions along the Aleutian arc from earthquake fault plane solutions, and found stress segmentation boundaries that appear to correlate with fracture zones in the Pacific Plate and may be related to the asperity and aftershock distribution of great earthquakes.

We have obtained surface velocity estimates from repeated GPS observations at a network of stations in the Semidi region of the Alaska subduction zone (Figure 5.1), and we use these velocities to invert for subduction interface parameters using dislocation modeling techniques. The stations occupy part of the segment that was ruptured by a  $M_W$  8.2 earthquake in 1938, and which lies between the rupture zone of the 1964 Great Alaska earthquake and the Shumagin segment of the arc.

The westernmost region of the 1964 Great Alaskan earthquake is accumulating strain in a manner that can be explained by a simple dislocation model of a plate interface that is fully coupled at  $\sim 5\text{-}25$  km depths during the interseismic period [*Savage et al.*, 1999]. In the Shumagin segment, the plate interface is estimated to be about 20% coupled based on geodetic data and historical earthquakes [*Zheng et al.*, 1996]. In the Sanak region further southwest, no strain is accumulating, which implies the plate interface is slipping freely at the plate convergence rate [*Frey Mueller and Beavan*, 1999].

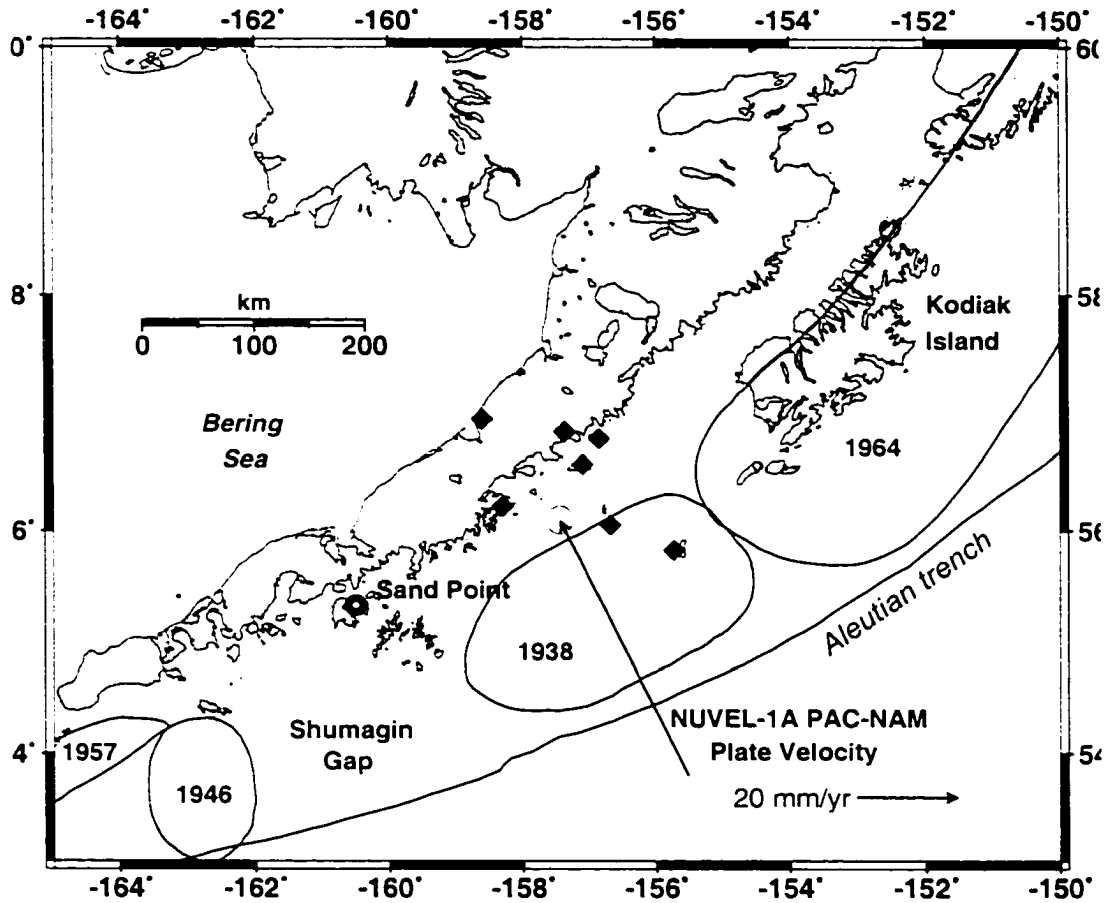


Figure 5.1. A map of the Alaska Peninsula showing the Semidi GPS stations. Outlined areas are aftershocks of great earthquakes with their dates. The arrow shows the NUVEL-1A Pacific-North America relative velocity

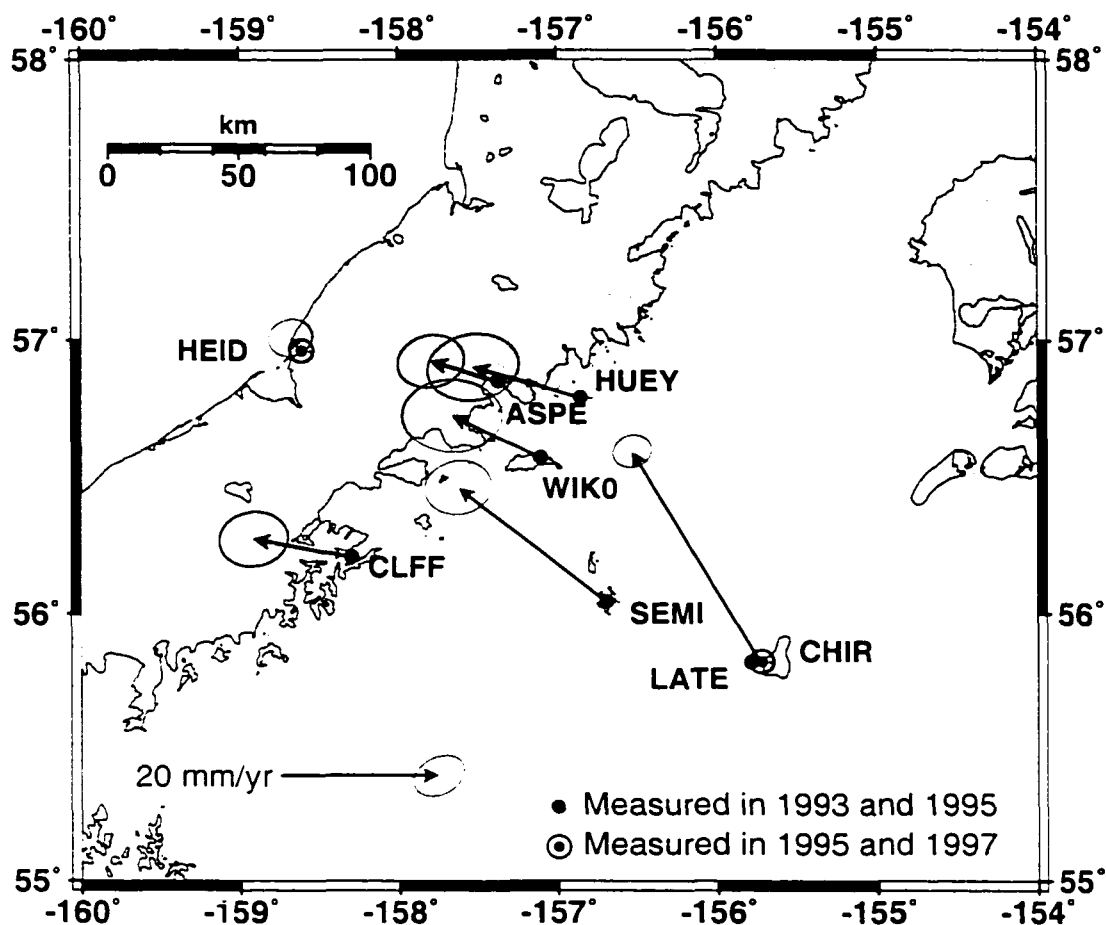


Figure 5.2. Velocities of Semidi GPS sites relative to North America. 95% confidence error ellipses are shown.

### 5.3 GPS Data

The Semidi GPS network (Figure 5.2) was established in 1993, with observations in 1993 at all stations except CHIR and HEID, in 1995 at all stations, and in 1997 at CHIR and HEID. Stations were occupied for multiple 24-hour sessions.

We use the GIPSY/OASIS II software to obtain daily coordinate and covariance estimates of our stations and globally distributed stations [e.g., Freymueller et al., 2000]. We calculate velocities in the ITRF97 reference frame [Boucher et al., 1999] (Table 1) by fitting the daily estimates to the ITRF97 coordinates and velocities of a global set of stations, retaining full covariance information. Because stations LATE and CHIR are separated by

Station	Lat	Lon	ITRF97		NAM-fixed	
			$V_{north}$	$V_{east}$	$V_{trench-}$	$V_{trench+}$
ASPE	56.85	-157.37	-18.0±1.8	-13.5±2.3	6.5±1.7	-5.9±2.0
CHIR	55.83	-155.73	8.3±0.9	-22.4±1.2	32.1±1.3	-0.0±1.4
CLFF	56.21	-158.30	-17.6±1.9	-16.9±2.3	8.2±1.8	-9.5±2.0
HEID	56.96	-158.61	-19.3±1.4	-6.2±1.7	2.2±1.4	-0.2±1.5
HUEY	56.79	-156.86	-16.3±2.4	-18.9±3.3	10.3±2.1	-6.7±2.6
SEMI	56.05	-156.69	-4.4±1.8	-24.5±2.3	22.4±1.8	-8.6±2.0
WIK0	56.58	-157.11	-14.8±2.7	-16.3±3.6	10.4±2.4	-6.7±2.6

Table 5.1. Site velocities in mm/yr

Errors are  $1\sigma$ .  $V_{trench-}$  is positive to the NNW.  $V_{trench+}$  is positive to the ENE.

only 4 km, we assume they do not move relative to each other, calculate a station tie using several overlapping days of the 1995 data, and thus estimate a velocity for CHIR over a 4-year interval. Separate estimates of the velocities of CHIR and LATE are consistent with our assumption. Finally, we obtain site velocities in a North America-fixed reference frame (Table 1, Figure 5.2) by constraining four stations (ALGO, NLIB, PENT, YELL) within the assumed stable interior of North America to zero velocity, and station FAIR to the velocity (5.0 mm/yr at N125°E) found by *Kogan* [2000]. Uncertainties in horizontal velocities are typically 2-5 mm/yr, after scaling so that the reduced  $\chi^2$  statistic of the velocity solution is 1.0.

## 5.4 Dislocation Model

Strain accumulation at a subduction boundary can be modeled using elastic dislocation theory. A simple model has the main thrust zone locked in the interseismic period while below the down-dip limit of the locked zone (the “locking depth”) rock deforms steadily and the model fault moves at the long-term slip rate. The Earth is represented by a uniform elastic half-space, the plate interface is a planar fault, and the strain accumulation rate is assumed constant through the interseismic period. The deformation is modeled by a

superposition of steady slip on the plate interface at the plate convergence rate, with virtual normal slip at the plate rate on the locked part of the interface [Savage, 1983]. This results in no slip on the locked part of the subduction zone and slip at the plate convergence rate on the remainder of the plate interface.

We use the term “locked zone” to refer to all that part of the plate interface between the steadily deforming region at depth and the steadily deforming region that may be present in the shallowest part of the interface. Interseismic coupling describes the spatial distribution of slip taking place within the locked zone [e.g., Mazzotti et al., 2000]. Here, we define interseismic coupling as the ratio of the virtual slip rate [Savage et al., 1998] estimated from geodetic data to the trench normal component of relative plate velocity given by the NUVEL-1A model [DeMets et al., 1994]. This is not the same as seismic coupling, which is the ratio of the rate of slip that occurs in earthquakes to the rate of relative plate motion [e.g., Pacheco et al., 1993]. Seismic coupling is thus averaged over decades or centuries, while interseismic coupling is generally measured over just a few years (and may change during an interseismic period if, for example, viscoelastic effects are important).

Due to the quantity and spatial distribution of our velocity estimates, a simple two-dimensional model is the best approach. Viscoelastic effects, which are not accounted for in this simple model, result in additional deformation especially in the immediate postseismic interval. However, the last major earthquake in the region was in 1938, and results from simple elastic models provide a good approximation to results from models with more realistic rheologies in the main interseismic period [e.g., Dragert et al., 1994].

We fix the strike of our model fault to  $N60^\circ E$  based on the observed orientation of the trench, and fix the depth of the up-dip end of the locked zone at the trench to 5 km (from bathymetric charts). We model only the component of velocity perpendicular to the strike of the trench, as discussed in section 5.2. We formally invert the velocity data of Figure 5.2 using a nonlinear least squares inversion [Dennis et al., 1981] to solve for the width of the locked zone, the dip, and the virtual slip rate. The full variance-covariance matrix of the velocity solution is retained in the inversion.

The inversion finds two minima. One solution is shown in Figure 5.3 and has a shallow dip of  $6^\circ \pm 1^\circ$ , a locking depth of  $23 \pm 4$  km (implying a width of  $\sim 170$  km) and a virtual slip rate of  $47 \pm 5$  mm/yr. The other solution has a slightly shallower dip ( $5^\circ$ ), larger width

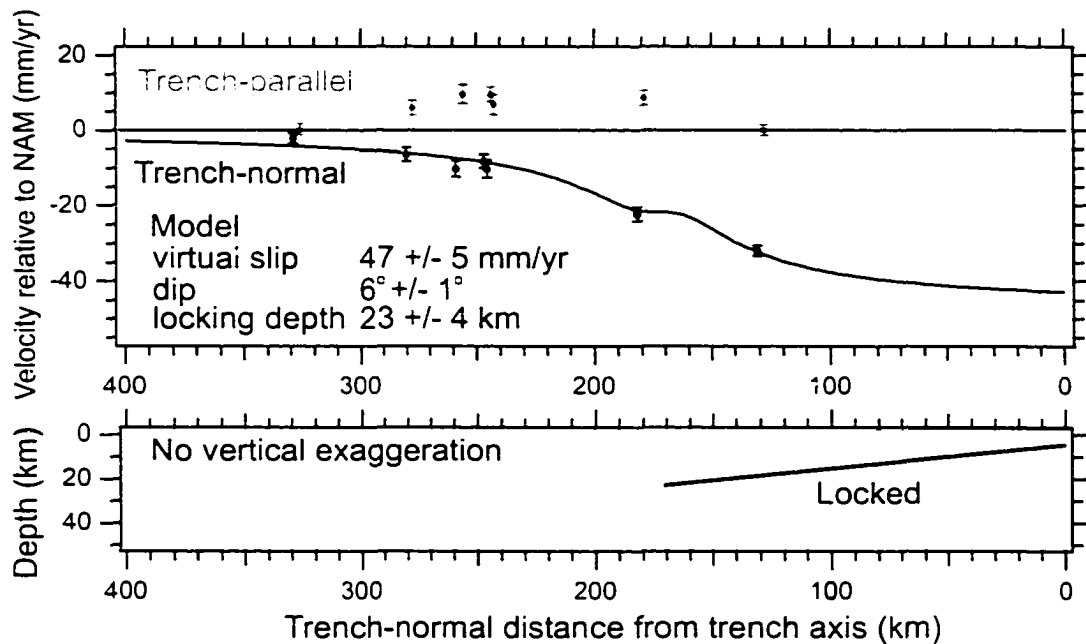


Figure 5.3. Elastic dislocation model of partial locking of plate interface. Model derived from nonlinear least squares fit to trench-normal component of observed velocities. Error estimates are  $\pm 1\sigma$ .

(200 km), and lower virtual slip rate (45 mm/yr), but is not statistically different from the first solution.

Our velocities assume that the overriding plate in the Semidi region is moving with the stable North American plate defined by sites east of the Rockies. If the overriding plate is in fact moving at a velocity closer to those of FAIR and Siberian stations [see *Kogan*, 2000], then the plate normal velocities in Figures 5.2 and 5.3 will increase by several mm/yr. The major effect on our model results is to increase the virtual slip rate by several mm/yr. The dip and locking depth are not significantly affected. The  $\sim 170$  km locked width inferred from our model may be an overestimate, since the spatial distribution of our data provide little control on any up-dip limit to the locking.

## 5.5 Discussion

### 5.5.1 Derived Parameters

The Semidi region is in an interseismic period which we assume to be typical and we propose that the estimated interseismic coupling is a good proxy for the seismic coupling in this region. The virtual slip rate in our model (Figure 5.3) is slower than the 59 mm/yr trench normal component of plate convergence from NUVEL-1A. This suggests  $\sim 80\%$  interseismic coupling, compared with coupling of up to 100% to the northeast in the vicinity of Kodiak Island [Savage et al., 1999] and  $\sim 20\%$  to the southwest in the eastern Shumagins [Zheng et al., 1996]. A coupling of lower than 100% implies either that some regions of the plate interface are slipping steadily at less than the plate convergence rate or that discrete patches on the interface are fully locked with slipping regions in between. Pacheco et al. [1993] find that almost 70% of the subduction zones they studied have a seismic coupling below 25%. We are thus seeing relatively high coupling in the Semidi network.

In their inversion of geodetic data in the Kodiak region, Savage et al. [1999] use a dip of  $5^\circ$  from results of the EDGE deep seismic reflection transect, while seismicity in the Shumagin segment of the arc indicates a dip of  $10^\circ$ - $15^\circ$  for the interplate thrust zone [Abers, 1992]. Our dip estimates of  $\sim 6^\circ$  are close to the Savage et al. [1999] values, and to the  $6^\circ$  estimated from the ALBATROSS seismic reflection transect just south of Kodiak [VonHune et al., 1987].

Tichelaar and Ruff [1993] give a maximum depth of seismic coupling in the Alaska subduction zone of 37-41 km from depth estimates of interplate events, and Oleskevich et al. [1999] suggest a depth of 40 km for the down-dip end of the seismogenic zone for southern Alaska (northeast of our region of interest) from seismic refraction studies and geodetic data. These values are deeper than our result of  $\sim 23$  km. Freymueller et al. [2000] estimate 20-25 km for the locking depth when they invert geodetic data from the eastern Kenai Peninsula, and a depth of 23.4 km from a model of the coseismic plane of the 1964  $M_W$  9.2 earthquake, based on the aftershock zone and axis of maximum coseismic subsidence. Savage et al. [1999] find that an independently-determined depth of 18 km to the base of the locked zone in the Kodiak region is consistent with their geodetic data. It is generally agreed that there is a transition zone between any strongly coupled zone



and the continuous sliding zone below, and that large earthquakes may propagate into the transition zone. The effect of the transition zone on surface displacements is subtle and we cannot model it in this case owing to the paucity of GPS sites above the down-dip end of the locked zone.

### 5.5.2 Trench-Parallel Velocities

In the Semidi segment of the arc, the NUVEL-1A plate convergence direction is towards  $335^\circ$ ,  $5^\circ$  more northerly than trench-normal. Trench-parallel velocities are thus expected to be small and to the northeast. However, Figures 5.2 and 5.3 show velocities at sites between CHIR and HEID rotated westward from trench normal, indicating that the region between these stations is being squeezed out to the southwest. The explanation of this intriguing observation is unclear, but the deformation pattern cannot be matched using a conventional Savage-type model with virtual strike-slip motion on the plate interface.

GPS-derived velocities at sites in the western Shumagin region show a similar trench-parallel component relative to North America [*Frey Mueller and Beavan, 1999*]. Very long baseline interferometry observations also indicate WSW- to SW-directed trench-parallel velocities at sites on Kodiak Island and in the Shumagin Islands, indicating that this phenomenon covers a wider region than our network. *Ma et al. [1990]* attribute this to right-lateral shear strain associated with strike slip faults in the overriding plate. This explanation is not satisfactory for our observations since we observe both right-lateral and left-lateral shear.

## 5.6 Conclusions

Interseismic coupling varies along strike of the Alaska-Aleutian subduction zone, from high coupling at Kodiak Island in the northeast to low coupling at the Shumagin and Sanak Islands in the southwest. For the Semidi region 150 km southwest of Kodiak, a nonlinear least squares inversion of geodetically-measured velocities using full covariance information estimates a model of strain accumulation with dip of the shallow plate interface of  $\sim 6^\circ$ , locking depth of  $\sim 23$  km, and relatively high interseismic coupling of  $\sim 80\%$ . It is not possible to determine whether there is a smooth or abrupt transition in coupling between

Kodiak and the Shumagin Islands.

## 5.7 Acknowledgments

We thank Ted Koczyński and Robbie Abad for helping collect the GPS data, pilots Tom Husted and Rick Farish of Alaska Helicopters who transported us safely through often-interesting weather, USGS for help with helicopter arrangements, and Stan Daily at Aleutian Dragon Fisheries for hospitality. Alaska Maritime National Wildlife Refuge, Aniakchak National Monument and Preserve, State of Alaska Dept. of Natural Resources, and Koniag Inc. allowed access to field sites, and staff at National Marine Fisheries Service helped select sites minimizing impact on marine life. JPL and UNAVCO assisted with field support; additional GPS receivers were provided by LDEO, UAF and GNS. We thank Des Darby for the dislocation inversion software, and Des Darby and Susan Ellis for their constructive comments on the manuscript. Funding from NASA Dynamics of the Solid Earth grant NAG5-1948 to LDEO, supported by New Zealand FRST contract CO5811 to GNS, LDEO contribution 6118, GNS contribution 1966.

## Chapter 6

# Implications for the Tectonics of Alaska

Using GPS as a tool to measure crustal deformation has made important contributions to our knowledge of the tectonics of Alaska. Figure 6.1 is a map of all the sites in Alaska which have been measured by GPS (white dots are sites that were measured for this thesis).

This large number of GPS sites helps us to determine how the Pacific-North American plate boundary deformation is distributed and which structures are important in accommodating the relative motion of the plates. How do the results from the different regions studied in this thesis fit together? Clearly the motion of the Pacific plate relative to Alaska is driving the deformation discussed in the chapters of this thesis, but it is not a simple tectonic picture. Figure 6.2 is a map showing all the faults mentioned in the discussion below.

Our goal is to construct a quantitative tectonic model for the region based on the results obtained in the various chapters of this thesis. Figure 6.3 shows the tectonic model of *Lahr and Plafker* [1980] for present deformation in southern Alaska. We modify their model based on the GPS velocity data and estimate fault slip rates summarized below, from work presented in Chapters 2 to 5 of this thesis. We present three models, which are variations on the *Lahr and Plafker* [1980] model. The fundamental difference between our models and theirs is that we use measured slip rates rather than assumed rates. All three of our models involve the Yakutat block, Fairweather block (a modified version of the *Lahr and Plafker*

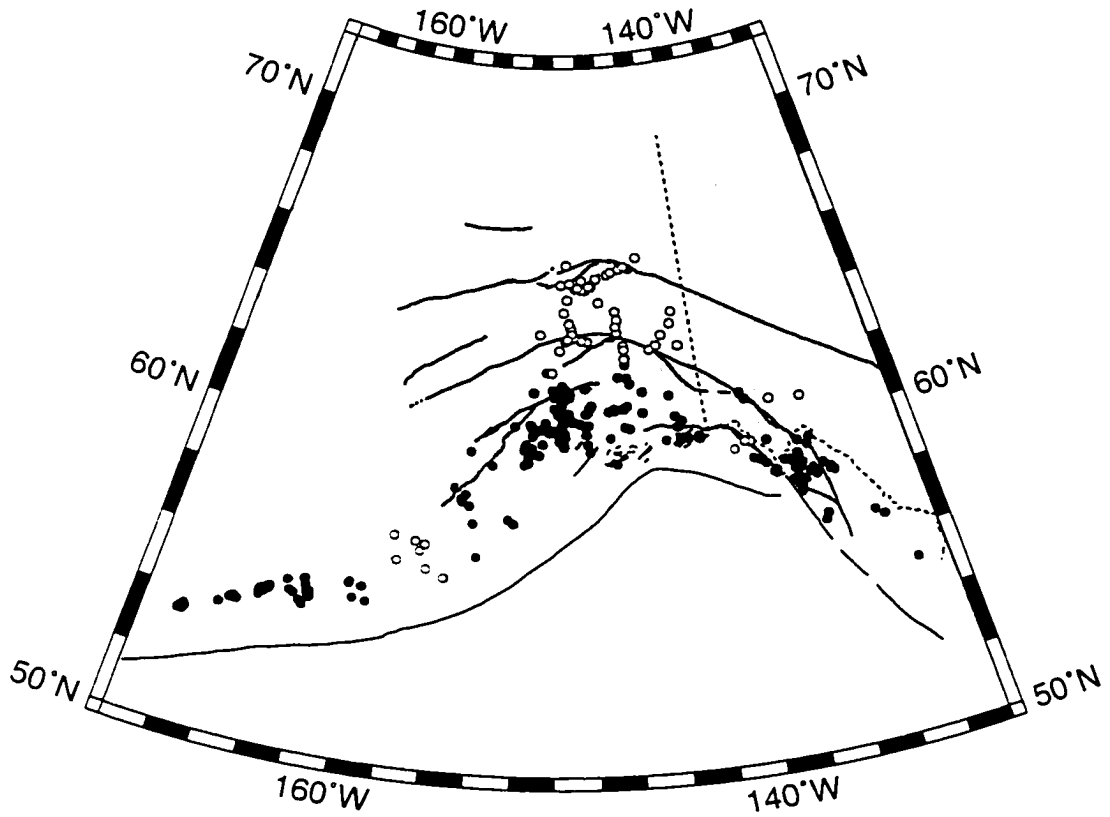


Figure 6.1. Map of Alaska showing all GPS sites. White circles are sites measured for this thesis.

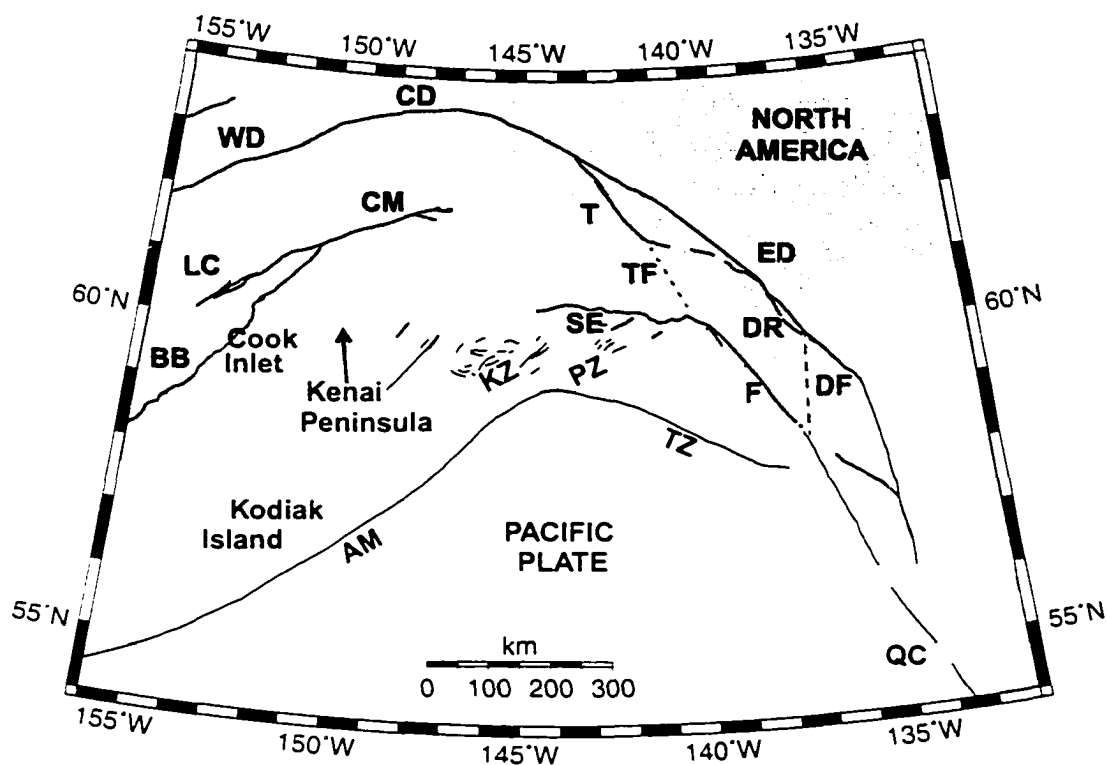


Figure 6.2. Map of Alaska showing faults relevant to tectonic model in this chapter. Faults are from *Plafker et al. [1994]*. WD = Western Denali fault; CD = Central Denali fault (or the McKinley section of the Denali fault); ED = Eastern Denali fault (or the Dalton-Chatham strait segment of the Denali fault); T = Totschunda fault; TF = Totschunda-Fairweather connecting fault; F = Fairweather fault; TZ = Transition Zone; QC = Queen Charlotte fault; PZ = Pamplona Zone; KZ = Kayak zone; DF = Denali-Fairweather connecting fault; DR = Duke River fault; LC = Lake Clark fault; SE = St. Elias fault; CM = Castle Mountain fault; BB = Bruin Bay fault; AM = Aleutian megathrust.

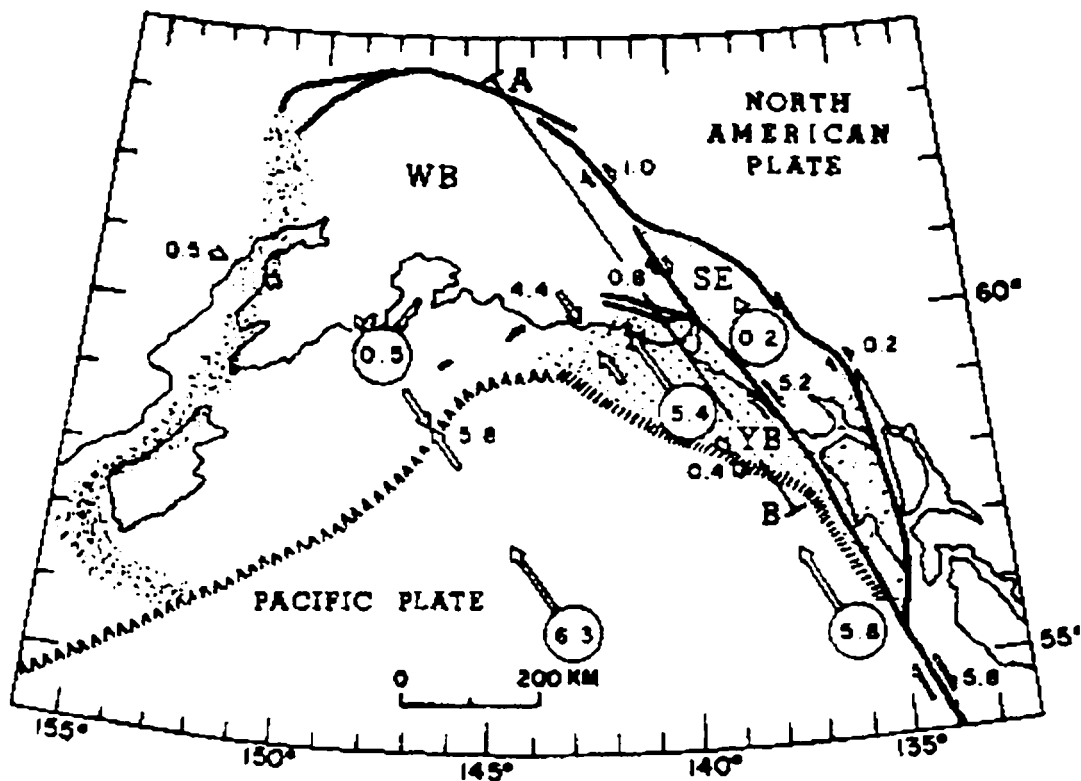


Figure 6.3. Proposed tectonic model of Alaska from *Lahr and Plafker* [1980]. Model is for present crustal deformation along the Pacific-North American plate boundary in southern Alaska. Circled numbers give rates of motion (cm/yr) of Pacific plate, Yakutat block (YB), St. Elias block (SE), and Wrangell block (WB) relative to North America. Numbers next to paired vectors give rates of motion across the indicated zone.

[1980] St. Elias block), and the southern Alaska block (called the Wrangell block by *Lahr and Plafker* [1980]). Figure 6.4 shows these crustal blocks and their sense of motion with respect to North America. The western boundary to the Southern Alaska block is the most speculative, and the nature and location of this boundary are the only differences between our three proposed models.

The first piece of the puzzle is the information from Chapter 2 about the movement of the Yakutat block. The GPS data tell us that the Yakutat block is not attached to the North American plate, nor is it moving at Pacific plate velocity. The velocity of Yakutat is parallel to the Fairweather fault, and so some other offshore structure must account for the difference in the slip rates between the Yakutat velocity and the Pacific plate velocity relative

to North America. We found that if the Transition Zone is the structure accommodating all the difference between the Pacific plate velocity and the Yakutat block velocity, then the fault must be freely slipping at  $21 \pm 3$  mm/yr in a direction  $N56^\circ E$ , perpendicular to the Fairweather fault (i.e., a combination of thrust and left-lateral strike slip motion). In all likelihood there are other structures which help to take up some of this motion such as the 250 km long north-south fault in the Pacific plate south of the Pamplona zone (see Figure 2.1), but it is not possible to determine which faults accommodate the Fairweather fault-normal slip from onshore GPS data. GPS data from sites southeast of Yakutat on the Yakutat block also show Fairweather fault-parallel motion (C. Larsen, personal communication, 2001), giving us confidence in our result.

The second piece in the tectonic puzzle comes from the work presented in Chapter 3. In this chapter, GPS data were used to study the deformation across the Fairweather fault. We found that this fault has a slip rate of  $38.2 \pm 3.1$  mm/yr which accounts for the majority of the Pacific-North American plate velocity at this part of the plate boundary. The slip rate on the Denali fault system northeast of Yakutat (henceforth called the eastern Denali fault) estimated from GPS data at sites in the Yakutat area is  $\sim 10.7 \pm 2.4$  mm/yr. The sum of these slip rates gives us the rate at which the Yakutat block is moving relative to North America, as well as the direction.

Interior Alaska was studied in Chapter 4, and we proposed a tectonic model that involves the southern part of Alaska, south of the Denali fault, rotating anticlockwise about a pole off the coast of southern Alaska. Interpreting our GPS velocities in terms of this model, we found that the Denali fault system in the vicinity of the Parks highway (henceforth called the central section of the Denali fault) has a slip rate of 8-9 mm across it and so is still important in present-day tectonics. This is similar to the slip rate estimated from Chapter 3 for the eastern section of the Denali fault system.

How does the slip transfer from the Fairweather-Queen Charlotte fault to the Denali fault? GPS sites across Chatham Strait indicate no slip on this section of the Denali fault in this area (C. Larsen, personal communication, 2001). Sites to the east and west of Chatham Strait have velocities that do not move relative to North America. This implies that as far north as at least  $58^\circ N$ , the Fairweather-Queen Charlotte fault is the main Pacific-North America plate boundary and accommodates all of the motion between the plates. *Lahr*

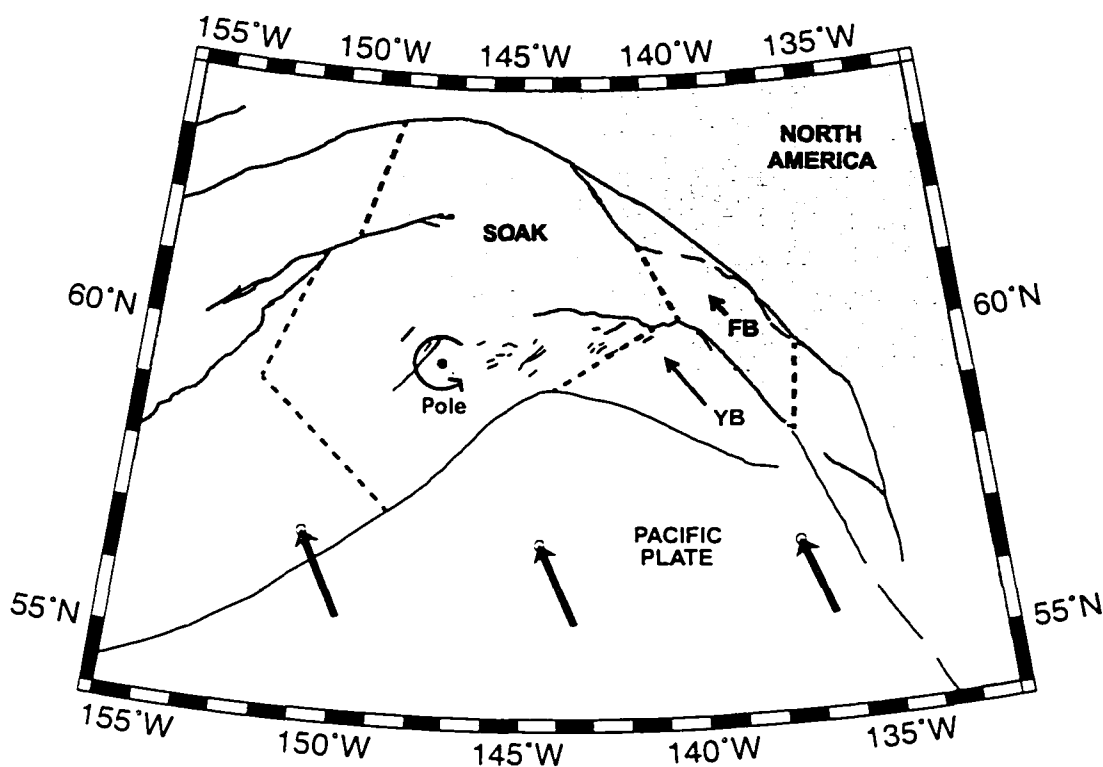


Figure 6.4. Map of crustal blocks proposed in our tectonic model of southern Alaska. Arrows indicate the sense of motion of the blocks with respect to North America. SOAK = southern Alaska block; YB = Yakutat block; FB = Fairweather block.

and *Plafker* [1980] proposed that the Fairweather fault is linked to the Totschunda fault by a connecting fault, which would provide a mechanism whereby some of the slip on the Fairweather fault could be transferred to the Denali fault. Our results show that the eastern Denali slip rate is similar to the central Denali fault, and so there must be a link between the Fairweather and Denali faults further to the east than the Fairweather-Totschunda fault proposed by *Lahr and Plafker* [1980]. *Page et al.* [1991] show plots of seismicity in this region and there appears to be a band of seismicity that trends from Lituya Bay northwards to the Denali fault. We propose that this band of seismicity outlines a fault (DF in Figure 6.2) that links the Fairweather fault to the Denali fault and thus allows some of the slip on the Fairweather fault to be transferred to the Denali fault. In reality this boundary is likely to be diffuse, with slip occurring on more than one fault.



## 6.1 Model 1

Our first model is a small modification to *Lahr and Plafker* [1980], the main differences being that the rates of the crustal blocks are based on GPS data and that the block motions are described by poles and rotation rates, not by linear velocities. In addition, the Fairweather block (FB) that we propose has a different southern boundary than the St. Elias block proposed by *Lahr and Plafker* [1980] and instead has the Denali-Fairweather connecting fault as its southeastern boundary. This block is bounded by the eastern Denali fault on the northeast, by the Fairweather-Totschunda system on the southwest and by the Denali-Fairweather connecting fault on the southeast. The Yakutat block (YB) is bounded by the Transition Zone, the Fairweather fault, the easternmost part of the St. Elias fault system, and the Pamplona zone (PZ). To the north of the Pamplona zone, the Kayak zone, most of the Chugach-St. Elias fault system, and a variety of other structures accommodate a combination of thrust and strike-slip motion. Thus, this boundary is fairly diffuse, but for the purpose of this simple model we choose the Pamplona zone as the main boundary. The slip assigned here to the Pamplona zone should be assumed to be distributed over the entire St. Elias orogen. SOAK is bounded by the central Denali fault, Totschunda fault, and Totschunda-Fairweather connecting fault (TF) on the northeast and by the Pamplona zone (PZ) and the Aleutian megathrust to the south. The western boundary of the southern Alaska block is not clear, but we discuss two possibilities. In Model 1a, the boundary is the same as that presented by *Lahr and Plafker* [1980]. Those authors admit that this boundary is purely hypothetical as it cuts across a variety of young features, but we evaluate the boundary using our results. In Model 1b the boundary is similar, but does not go around Kodiak Island (Figure 6.3).

We calculate poles and rotation rates for all of the crustal blocks in our model using the fault slip rates estimated from GPS velocities presented in the previous chapters. Using these poles and rotation rates we estimate slip rates across the boundaries where we have no GPS information and compare these estimates with seismic and geologic observations to see if the estimates are reasonable. In all of our models, the Pacific plate moves relative to the North American plate with a rotation rate of  $0.78^\circ$ /million years about a pole in eastern Canada located at  $50.5^\circ\text{N}$ ,  $75.8^\circ\text{W}$  [*DeMets and Dixon*, 1999]. The wide vectors in

Figure 6.4 show Pacific-North American relative plate motion, which varies in magnitude from about 50 mm/yr to 59 mm/yr across the region shown in the figure. The Yakutat block is not moving parallel to the Pacific plate, but instead moves parallel to the Fairweather fault. The Fairweather fault is a considered straight for all of its relatively short trace. This implies the pole of rotation of the Yakutat block is far from the fault, and we assume it is  $\sim 90^\circ$  from the fault (as opposed to say,  $75^\circ$ ) located at approximately  $16^\circ\text{S}$ ,  $161^\circ\text{E}$ , some 10,000 km away somewhere in the Pacific ocean. The velocity of the Yakutat block relative to North America along the Fairweather fault is taken to be  $48.9 \pm 4.3$  mm/yr (the sum of the Fairweather and Denali fault slip rates estimated in Chapter 3). This gives a rough estimate of  $0.44^\circ$ /million years for the angular velocity of the Yakutat block relative to North America.

*Stout and Chase* [1980] determined a pole of rotation for the eastern Denali fault at  $50.4^\circ\text{N}$ ,  $154.0^\circ\text{W}$ . In our model, the Fairweather block moves relative to North America about this pole. Given an eastern Denali fault slip rate of  $10.7 \pm 2.4$  mm/yr (Chapter 3), then the angular rotation rate about the pole is  $\sim 0.41^\circ$ /million years. The angular rotation rate of SOAK is  $\sim 1.25^\circ$ /million years about a pole located at  $59.6^\circ\text{N}$ ,  $147.4^\circ\text{W}$  (Chapter 4). Note that the rotation rates for the blocks depend on the assumed poles.

Having defined Euler poles and angular rotation rates for our proposed crustal blocks, the next step is to determine slip rates across the boundaries between the blocks. Figure 6.5 shows the calculated rates. In the Pamplona zone region, the velocity of SOAK is 6 mm/yr at  $\text{N}5^\circ\text{E}$  relative to North America and the velocity of the Yakutat block is 48 mm/yr at  $\text{N}37^\circ\text{W}$ . Thus the convergence across the Pamplona zone is 43 mm/yr towards  $\text{N}43^\circ\text{W}$ . Slip on the Totschunda fault is due to the motion of SOAK relative to the Fairweather block. Based on the pole and rotation rate of SOAK, the velocity of SOAK in the vicinity of the Totschunda fault is calculated to be 9 mm/yr parallel to the fault. The Fairweather block velocity here is 10 mm/yr oriented  $\text{N}55^\circ\text{W}$ , thus the motion of SOAK relative to the Fairweather block across the Totschunda fault is 4 mm/yr oriented  $\text{N}67^\circ\text{E}$  (i.e., mostly compression).

SOAK has a velocity of 9 mm/yr relative to North America along the proposed Totschunda-Fairweather connecting fault in a direction  $\text{N}10^\circ\text{W}$ , and the Fairweather block has a velocity of 10 mm/yr in a direction  $\text{N}45^\circ\text{W}$ . Thus the slip rate on the Totschunda-Fairweather fault

(oriented approximately N30°W) predicted by this model is 2 mm/yr of right-lateral strike slip motion and about 5 mm/yr of convergence. This proposed fault extends across the St. Elias mountains and, while it is not mapped as a single fault, it is likely that this region experiences some convergence.

The Fairweather block has a velocity of 10 mm/yr relative to North America along the proposed Denali-Totschunda connecting fault in a direction N32°W. The zone of seismicity shown in *Page et al. [1991]* is diffuse, but in general trends N-S. The 10 mm/yr Fairweather block velocity could therefore be partitioned as 8 mm/yr right-lateral slip and 5 mm/yr extension across the proposed connecting fault. *Doser and Lomas [2000]* observe no extension in this region from their studies of seismicity, and we believe that such motion is unlikely in this compressional regime. If the connecting fault had a more northwest orientation then the amount of extension across it would be reduced. We also note that the pole of the Fairweather block has a large uncertainty [*Stout and Chase, 1980*], and that if the pole were closer to the Denali fault then the extensional component of motion across the Fairweather-Denali connecting fault would also be reduced, but in either case some extension is required by the model.

Is it necessary to have a Fairweather block? If we assume that the region between the Fairweather and Denali faults is not a separate Fairweather block but instead part of SOAK, what would the slip rates be across the Denali and Fairweather faults? We calculate the velocity of SOAK relative to North America along the eastern Denali fault and the velocity of SOAK relative to the Yakutat block along the Fairweather fault and see how these velocities compare with the GPS results. The velocity of SOAK relative to North America in the vicinity of the eastern Denali fault is 12 mm/yr oriented northwards. The Denali fault is oriented N34°W in this region and this velocity could be partitioned into 10 mm/yr of right-lateral slip on the fault and 7 mm/yr of convergence across the fault. In Chapter 3 we find that the eastern Denali fault has a slip rate of 11 mm/yr, which agrees with that predicted from the rotation of SOAK. 7 mm/yr of convergence across the Denali fault is not evident from seismicity data [*Doser and Lomas, 2000*], although the Duke River fault may have accommodated convergence in Late Cretaceous and early Tertiary time [*Muller, 1967*]. The velocity of SOAK relative to the Yakutat block in the vicinity of the Fairweather fault is 41 mm/yr oriented N44°W. This is equivalent to 40 mm/yr right-lateral

slip on the Fairweather fault and 7 mm/yr extension. Such extension is highly unlikely in this compressive region.

We therefore believe it is necessary to involve a Fairweather block in our model. However, the pole location (and therefore rotation rate) of this block are somewhat unreliable. The boundaries of this block are also unclear. The southern boundary, the proposed Denali-Fairweather connecting fault is based upon a band of diffuse seismicity and we believe the slip across this boundary is not accommodated on one fault but a variety of structures. The northern boundary is proposed to be the Totschunda fault on the northwest and the Denali fault on the northeast. However, the Duke River fault connects the southern Totschunda to the Denali fault further east (Figure 6.2) and it is possible that this fault could accommodate some slip. If the Duke River were the northern boundary of the Fairweather block, then slip on the Totschunda fault would be due to the rotation of SOAK relative to North America and the right-lateral slip rate would be 9 mm/yr parallel to the fault. Holocene displacements across the Totschunda fault do show right-lateral slip [e.g., Page et al., 1991], and so it is possible that this fault has a right-lateral component of slip. In reality, the northern boundary to the Fairweather block probably consists of the Totschunda, Denali, Duke River, and even other faults.

Now we come to the western boundary of SOAK. *Lahr and Plafker* [1980] speculate that the boundary of their Wrangell block diverges southward from the Denali fault, passes through Cook Inlet, around Kodiak Island, and back to the Aleutian megathrust southwest of Kodiak Island (Figure 6.3). We use this as our boundary in Model 1a, and for Model 1b we modify the boundary so that it does not go around Kodiak Island. The path of this western boundary is speculative. There are no mapped faults that follow the boundary from the Denali fault to the Aleutian trench. However, we do not have any GPS data to the west of this proposed boundary and so we start by assuming that their proposed boundary is the western boundary of SOAK. We use our pole and rotation rate to calculate the relative motion across the boundary, assuming that west of the boundary is the North American plate. Note that *Mackey et al.* [1997] propose a Bering block that rotates about a pole in northern Chukotka and in their model western Alaska is moving westwards with respect to North America. This will be addressed in Model 3. At the northern end of the western SOAK boundary, the rotation of SOAK would produce convergence at  $\sim 9$  mm/yr.

The velocity of SOAK relative to North America is greatest at its northern boundary and becomes progressively smaller nearer the pole of rotation.

SOAK moves at about 6 mm/yr in a direction  $S50^{\circ}W$  in the vicinity of the Castle Mountain fault. This fault trends approximately  $N60^{\circ}E$  and so the slip could be partitioned as almost 6 mm/yr of right-lateral slip, with 1 mm/yr extension. Across upper Cook Inlet, just to the south of the Castle Mountain fault, the velocity of SOAK would be about 5 mm/yr in a direction  $S35^{\circ}W$ . Given that Cook Inlet trends approximately  $N30^{\circ}E$ , the right-lateral component of motion along Cook Inlet would be 5 mm/yr with a convergence of less than 1 mm/yr. In Model 1a, the proposed boundary northwest of Kodiak Island would be a normal fault, with a slip rate of 9 mm/yr towards  $S152^{\circ}E$ , and the section of the boundary connecting to the Aleutian trench would be a right-lateral strike slip fault with slip rate 12 mm/yr in a direction  $N48^{\circ}W$ . Model 1b is identical to Model 1a except that the boundary joins southern Cook Inlet to the Aleutian trench northwest of Kodiak Island, so this model does not require a normal fault along the northwest coast of Kodiak Island and the slip rate on the fault joining southern Cook Inlet to the Aleutian trench would have a slip rate of 5 mm/yr. Figure 6.5 shows the sense of motion of the faults bounding the proposed blocks for Models 1a and 1b.

Are these slip rates plausible? There are a few mapped thrust faults that diverge from the Denali fault to the south in the vicinity of the proposed western boundary (see Figure 4.1), and while there is limited evidence for young activity (probably due to difficult access and consequent lack of study), it is possible that the 9 mm/yr of convergence in this region predicted by the model could be partitioned on a variety of thrust faults in this area. *Page et al. [1991]* show a diffuse zone of seismicity that connects the Denali fault to northern Cook Inlet, and state that this band of seismicity may mark a deformational zone accommodating northwest-southeast compression between the crust south of the Denali fault and the interior of Alaska. Earthquakes as large as the 1943  $M_S$  7.4 event (located at  $61.90^{\circ}N$ ,  $150.84^{\circ}W$ ) may originate in this band. Analysis of seismic waveforms and first motions of the 1943 earthquake and composite fault-plane solutions for a few shallow microearthquakes in 1980 (*Woodward-Clyde Consultants, 1980, 1982*) suggest that reverse faulting with west to northwest oriented compressional axes may characterize this seismic belt. Given our lack of other information about this region, we propose that this boundary

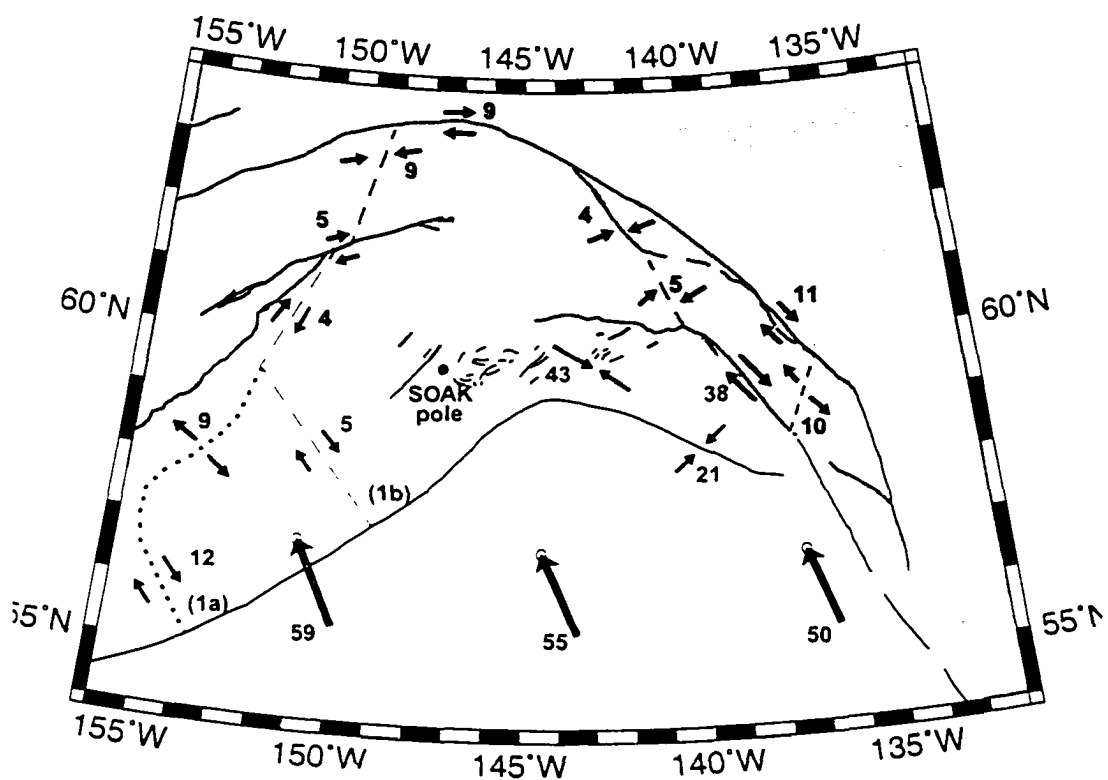


Figure 6.5. Slip rates of boundaries of proposed crustal blocks in Models 1a and 1b. The arrows show the sense of motion across the boundaries between the crustal blocks proposed in the two models. The faults are identified on Figure 6.2. The numbers are slip rates in mm/yr across the boundaries. The dotted line that goes around the northwest of Kodiak Island before rejoining the Aleutian trench is Model 1a and the dashed line between lower Cook Inlet and the Aleutian trench is the boundary for Model 1b.

consists of a network of faults that runs from the Denali fault to the north end of Cook Inlet following the path suggested by *Lahr and Plafker [1980]*.

The Castle Mountain fault, which passes 40 km north of Anchorage, also exhibits geologic evidence of Holocene offset [*Detterman et al., 1974*] and seismic evidence of current activity [*Lahr et al., 1986*]. Thus the 6 mm/yr right-lateral slip that our model predicts on the Castle Mountain fault could be possible. In our model, the eastern Castle Mountain fault is not assigned a significant slip rate, while the western part (west of northern Cook Inlet) accommodates some of the SOAK rotation by right-lateral slip. Note that this model does not yet attempt to deal with faults that have small slip rates. An  $M_b$  5.6 earthquake in 1984 is associated with right-lateral rupture of the eastern part of the Castle Mountain fault [*Lahr et al., 1986*], so perhaps the zone of deformation trending southwards from the Denali fault joins the Castle Mountain fault further eastward than suggested by our model, and it is highly likely that SOAK is subject to internal deformation.

Diffuse shallow seismicity occurs in northern Cook Inlet. Some buried folds in the upper Cook Inlet area are cored with blind reverse faults, indicating convergence across Cook Inlet [*Haeussler et al., 2000*]. Our model predicts up to 5 mm/yr of right-lateral strike slip motion across upper Cook Inlet and 1 mm/yr of convergence. Moving southwards down Cook Inlet, the velocity of SOAK relative to North America remains about the same magnitude (about 4 mm/yr in mid-Cook Inlet) but changes orientation. The velocity of SOAK in lower Cook Inlet is oriented almost due south and it is possible that this may be accommodated by right-lateral transform faulting on north-south oriented faults in the southern inlet.

Sites on the Kenai Peninsula show a southwest component of motion, part of which we believe is due to the rotation of SOAK (Figure 4.12 and Chapter 4). South of the pole of rotation, the velocity of SOAK is directed to the southeast. This implies either right-lateral slip on a fault that joins lower Cook Inlet to the Aleutian trench between Kodiak Island and the Kenai Peninsula (Model 1b, Figure 6.3), or normal faulting on a structure northwest of Kodiak Island that connects to the trench by a right-lateral fault (Model 1a, Figure 6.4). There is an absence of mapped structures oriented perpendicular to the trench both southwest of the Kenai Peninsula (as would be needed in Model 1b) and southwest of Kodiak Island (as called for in Model 1a). The SOAK velocity would be lower in the southern Kenai Peninsula region as it is closer to the pole. The velocity along a fault joining

lower Cook Inlet to the trench would be 5 mm/yr in Model 1b, compared to 12 mm/yr for a trench-normal fault southwest of Kodiak Island in Model 1a. Model 1a also requires a normal fault north of Kodiak Island with a large, 9 mm/yr, opening rate. There is no seismic evidence for large extension in the Alaska Earthquake Information Center (AEIC) catalog, nor is any geologic evidence for such extension available. The southwest boundary in Model 1b is therefore the preferred SOAK boundary, though we note that this part of the model is the least reliable. GPS velocities do in fact show a right-lateral sense of motion between sites in the southern Kenai Peninsula and sites on northern Kodiak Island [Zweck et al., 2001]. However, the GPS velocities are a combination of SOAK velocity and the much larger subduction signal and the apparent right-lateral motion is attributed to variable slip on the subducting interface due to ongoing postseismic response to the 1964 Great Alaskan earthquake as discussed in Chapter 4, based on work of Zweck et al. [2001].

No matter what structure accommodates the SOAK velocity south of the pole of rotation, it is clear that this southeastward SOAK velocity would contribute a small amount to the convergence rate across the trench. In Chapter 5, the region of study is the Semidi segment of the Alaska subduction zone, between the fully-coupled segment to the northeast and the slipping Shumagin segment to the southwest. We find that this region, which sustained a magnitude 8.2 earthquake in 1938, is highly coupled and accumulating strain, but we also find an unexplained trench-parallel component in many of the site velocities. Figure 5.2 shows that all of the sites between CHIR (nearest to the trench) and HEID (furthest from the trench) exhibit southwestward motion that cannot be explained by the simple strain accumulation model proposed in Chapter 5. Perhaps the additional compression between the southern Kenai Peninsula and the trench due to the rotation of SOAK helps to cause material to be extruded to the southwest. Mapped faults of the Kodiak Shelf fault zone south of Kodiak Island parallel the trench. These faults are seaward of Kodiak Island to the southeast [Plafker et al., 1994] and perhaps this fault zone supports left-lateral slip. This hypothesis also requires a right-lateral strike slip fault between the northwest and southeast coasts of the Alaska Peninsula. Faults and folds along the axis of the peninsula could potentially have young activity (W. Wallace, personal communication). The features are mainly compressional, but they could accommodate a strike-slip component. Sites in the western Shumagin region show a similar trench-parallel motion relative to North America



[*Frey Mueller and Beavan, 1999*], and so it appears that the southwestward component of motion continues for some distance.

## 6.2 Model 2

Model 1 does not explain the southwestward motion of GPS sites in the Semidi region presented in Chapter 5. In Models 2 and 3 we present possible scenarios to explain this motion. In Model 1 we assumed that there is no slip on the western Denali fault. Very little is known about the Denali fault system in western Alaska. *Plafker et al. [1977]* find no evidence that the Denali fault to the west of this region has been active in the Holocene, although the *Plafker et al. [1994]* neotectonic map shows one segment with Holocene activity and several sections as "suspicious". The main problem with geological estimates of activity on the western Denali fault is lack of study and a paucity of young features necessary to observe offset features. It is likely that this boundary is diffuse, with slip occurring on more than one fault. There are numerous faults both south and north of the western Denali fault that could accommodate young motion (*W. Wallace, personal communication*). Model 2 assumes that there is a small amount of slip on the fault and we look at the consequences of this. If we define the same boundary for SOAK as in Model 1b, then the region south of the Denali fault and to the west of SOAK would be a separate crustal block moving relative to North America. Very little is known about this region of western Alaska, and we have no idea where the western and southern boundaries of a western Alaska crustal block might be. We can estimate a pole for this block from the trace of the western Denali fault. The fault is fairly straight in this region and so the pole is far away from the block, we can therefore make the approximation that all points on the block move to the southwest parallel to the strike of the Denali fault at velocities similar to the slip rate on the western Denali fault.

If the Alaska Peninsula is part of the western Alaska block, then the slip rate on the western Denali fault would be limited by the trench-parallel velocity of the sites in the Semidi profile. The average trench-parallel motion of these sites (including HEID) is 5 mm/yr to the southwest. Given the assumption that these sites are on the western Alaska block and that the Euler pole is far away from the western Alaska block, then the slip rate of the western Denali fault would also be 5 mm/yr (the western Denali fault is approximately

parallel to the trench in the Semidi region). This would require opening between the Kenai Peninsula and Kodiak Island at a rate of 5 mm/yr and right-lateral slip at 5 mm/yr (7 mm/yr total slip rate). Little information is available regarding structures in this area, but there is no obvious indication of such deformation in the seismicity data from the Alaska Earthquake Information Center (AEIC) database. The deformation across Cook Inlet would be reduced to a 1 mm/yr extension rate.

If the Alaska Peninsula is not part of the western Alaska block, then there must be a southern boundary to the western Alaska block that lies to the north of the Alaska Peninsula. This would allow the Denali fault to have a slip rate that is independent of the Alaska Peninsula velocity because the difference in motion between the western Alaska block and the Alaska Peninsula could be accommodated along the boundary between the blocks. In Model 2 we choose the Lake Clark fault (the westward extension of the Castle Mountain fault), as the southern boundary of the western Alaska block. We have no information to draw on in order to estimate the slip rate on either the western Denali fault or the Lake Clark fault. Seismicity is low and there is no evidence of Holocene offset on the faults (although, as stated previously, this is perhaps due to the paucity of young features necessary to document displacements). The slip rate on the boundary between the western Alaska block and Alaska Peninsula block depends on the motion of both of these blocks. We start by assuming that the western Denali fault slip rate is low, say 2 mm/yr, and that the Alaska Peninsula block moves at 5 mm/yr to the southwest relative to North America (from the Semidi GPS data). Figure 6.6 shows the relative motions across the boundaries between SOAK, the western Alaska block, and the Alaska Peninsula block for this model.

For a Denali fault slip rate of 2 mm/yr, the convergence necessary across the deformation zone between the Denali fault and Cook Inlet would be reduced to a maximum of 7 mm/yr in the north. The slip on the Lake Clark fault would be right-lateral at a rate of 3 mm/yr. A higher Denali fault slip rate would reduce the convergence across this deformation zone and lower the slip rate on the Lake Clark fault. For a western Denali fault slip rate higher than about 6 mm/yr, there would be extension across the southern part of the deformation zone and the Lake Clark fault would need to accommodate left-lateral motion.

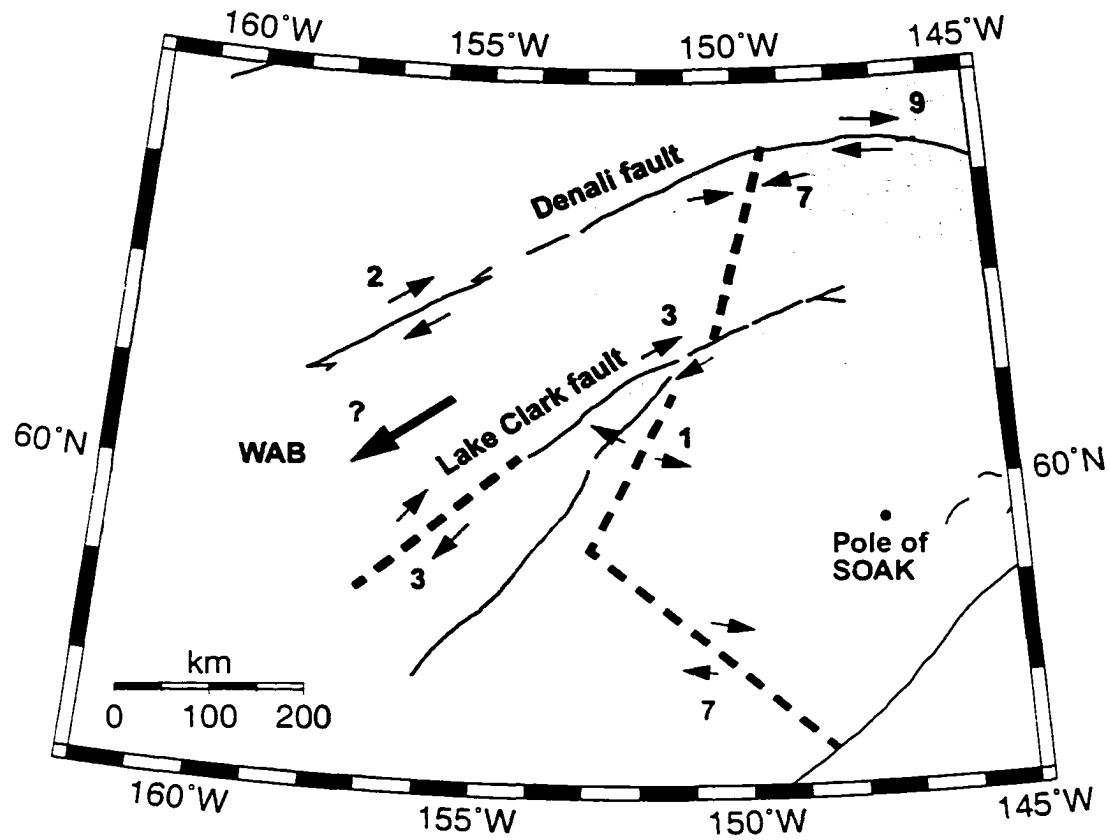


Figure 6.6. Slip rates associated with boundary between SOAK, WAB, and APB. The arrows show the sense of motion across the boundaries between SOAK, the western Alaska crustal block (WAB), and the Alaska Peninsula block (APB) proposed in Model 2. The numbers are slip rates in mm/yr relative to North America.

### 6.3 Model 3

Model 1 assumed that western Alaska is stable with respect to North America, and Model 2 assumed that a small amount of slip occurs on the western Denali fault. The seismicity in western Alaska is apparently low, but this could be due in part to the low seismic station density. We have no GPS data or quantitative fault slip rates from this region to provide further information. *Mackey et al. [1997]* proposed the existence of a Bering block that rotates clockwise about a pole in northern Chukotka (Figure 6.7). They based their model on observed seismicity and focal mechanisms. The eastern boundary of their proposed Bering block follows the western boundary of the Wrangell block as proposed by *Lahr and Plafker [1980]*, thus western Alaska is moving westward with respect to North America.

*Mackey et al. [1997]* give no rate of rotation for the Bering block in their model, but it is believed to be low. Given a pole in northern Chukotka, the velocity of the Bering block relative to North America should be highest along the Aleutian Arc. In general terms, a rotating Bering block would reduce the convergence necessary across the deformation zone that trends south from the Denali fault to Cook Inlet in our model and would add a component of extension across the boundary that connects southern Cook Inlet to the Aleutian trench. The sense of rotation of the Bering block predicts a southwestward trench-parallel component of velocity at sites along the eastern Aleutian arc, consistent with that observed in the data presented in Chapter 4. We take the location of the Bering block pole to be about  $68^{\circ}\text{N}$ ,  $176^{\circ}\text{E}$  from Figure 3 in *Mackey et al. [1997]*. The average trench-parallel velocity of the sites in the Semidi region (including HEID) is 5 mm/yr, which gives a rotation rate of  $0.16^{\circ}$ /million years (again, this rate depends on the exact location of the pole).

Given this pole and rotation, we can now calculate the slip rate across the Bering block-SOAK boundary. The calculated slip rates and directions are shown in Figure 6.7. Along the Kaltag fault, this model predicts 3 mm/yr of northeast directed slip, which could be partitioned as 2 mm/yr right-lateral slip on the Kaltag fault and 1mm/yr extension across it. The Kaltag fault has 140 km of right-lateral displacement across it since the Late Cretaceous [*Patton and Hoare, 1968*], is currently seismically active [*Estabrook et al., 1988*] and has visibly offset stream beds. The magnitude and direction of model slip on the Kaltag

fault thus seems to be not unreasonable. Between the Tintina and Denali faults (e.g., across the seismic zones of interior Alaska), the model predicts 5 mm/yr left-lateral slip, oriented N28°E, which is close to the N33°E oriented seismic zones (Chapter 4). The sense of motion is the same as that found in Chapter 4 for slip on the seismic zones, but the magnitude of the slip rate predicted by this model is much larger than the total rate of slip on the seismic zones estimated in Chapter 4 from GPS data. Between the Denali fault and upper Cook Inlet, this model predicts 3 mm/yr right-lateral slip on the deformation zone, which is certainly possible. Finally, this model predicts 7 mm/yr extension at N80°W along the boundary joining lower Cook Inlet to the trench.

## 6.4 Summary

Whilst none of the three models discussed above provide a fully satisfactory explanation for western Alaska tectonics, the models provide a first step towards a coherent framework for understanding the tectonics of a large part of Alaska. With no GPS data, low seismicity and little geological information on western Alaska, it is hard to put constraints on this region of the model. The three models proposed are certainly simplifications of reality, but armed with these quantitative models we have a starting point for further investigations. Reality probably includes some aspects of each of the three models.

The main problems with the models are summarized below. Model 1a requires 9 mm/yr of extension on a fault along the northwest side of Kodiak Island, and 12 mm/yr of right-lateral slip on the section of the boundary that joins the Aleutian trench, both of which are hard to explain given current geologic and seismic observations. Model 1b requires 5 mm/yr along a boundary joining southern Cook Inlet to the trench, and again there is no obvious indication of such motion. Model 2 requires 5 mm/yr extension along the boundary joining lower Cook Inlet to the trench, and model 3 requires 7 mm/yr extension along this boundary. It is likely that SOAK is not a rigid block as proposed in the models, but deforms internally by slip on faults that are not addressed in our models. This might help to eliminate some of the problems with the western boundary of SOAK.

The slip rates we calculated for the Denali and Fairweather faults provide good constraints to the models and the slip rates estimated for the remaining boundaries can be

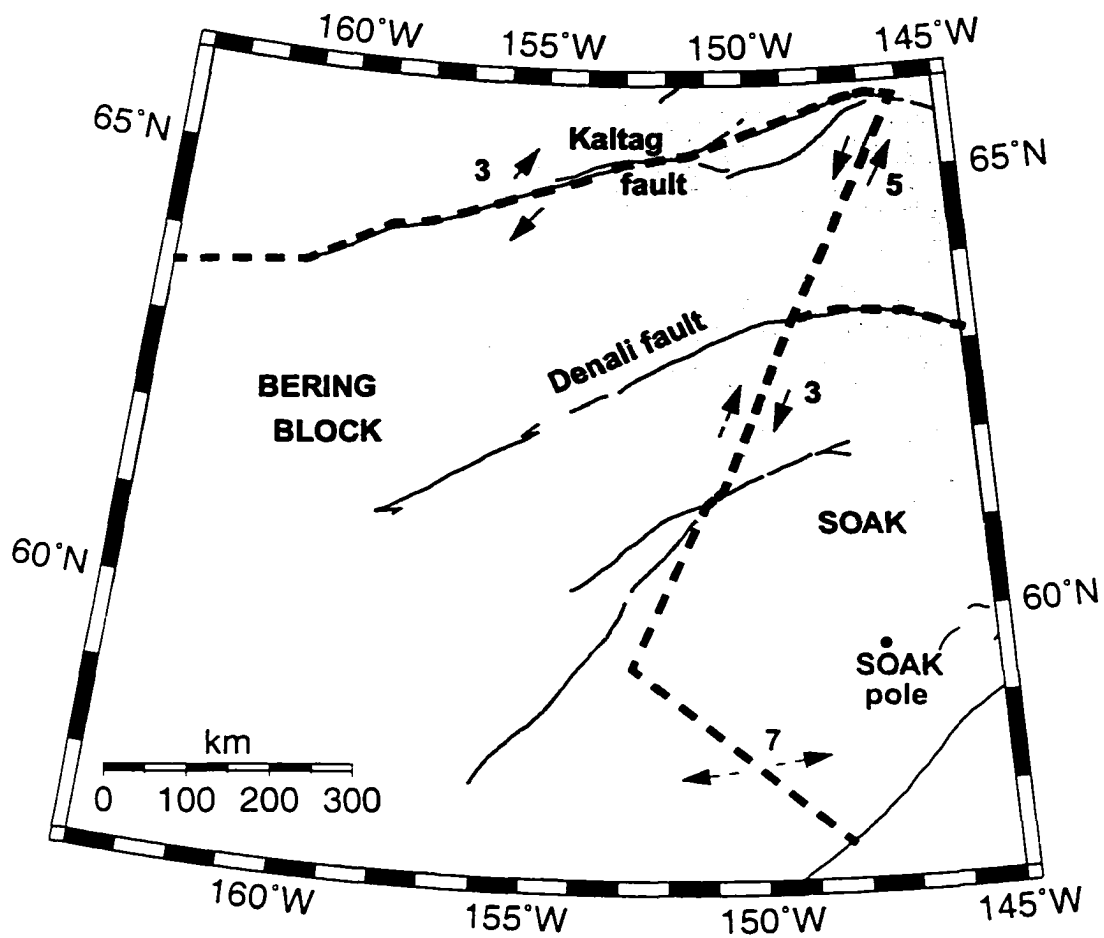


Figure 6.7. Slip rates associated with boundary between SOAK and the Bering block. The arrows show the sense of motion across the boundaries between SOAK and the Bering block crustal block (WAB) proposed in Model 3. The numbers are slip rates in mm/yr relative to North America.

tested by further GPS studies. The questions we need to answer are: 1) Is there any slip on the Fairweather-Denali connecting fault? If so, how much? This measurement, plus a reliable estimate of slip rate on the western Denali fault would greatly help our understanding of southern Alaska tectonics. 2) Is there any motion across the proposed boundary between the Denali fault and northern Cook Inlet, and if so is it convergence as predicted by Model 2, or is it right-lateral slip as predicted by Models 1 and 3? 3) Is there any slip on the Castle Mountain and Lake Clark faults? 4) What is the slip rate across Cook Inlet? Is there convergence, as predicted by Model 2, right-lateral slip as predicted by Models 1 and 3, or some other motion? 5) Is there any slip across the proposed boundary between lower Cook Inlet and the Aleutian trench? Models 1 and 2 predict right-lateral slip and Model 3 predicts extension. 6) Is there any slip on the western Denali fault, and if so what is the slip rate? An estimate of slip rate would help to constrain our estimates of slip on the Lake Clark fault in Model 2. 7) Does the Bering block exist? We observe trench-parallel slip at sites in the Semidi region. Model 3 partially explains this observation by proposing that these sites lie on the Bering block.

As with all tectonic studies, the work is never truly completed. Data from more sites will help to determine more accurately the spatial distribution of crustal deformation in Alaska, and data over longer time periods will be invaluable in studying the deformation associated with an entire earthquake cycle.

This thesis has presented the results of a direct study of surface deformation in a variety of places in Alaska using GPS observations. The measured surface velocities were used to estimate slip rates and locking depths on the Denali fault, Fairweather fault and the Semidi segment of the Aleutian subduction zone. The velocity field was also used to constrain the Yakutat block motion and the proposed southern Alaska block motion. To tie together all the observations reported in this thesis, three quantitative tectonic models were presented in this chapter. In reality, some combination of all three models is likely. The work presented in this thesis has made important steps forwards in our understanding of the tectonic framework of Alaska.

# Appendix A

## How GPS works

GPS is funded by and controlled by the U. S. Department of Defense (DOD). While there are many millions of civil users of GPS world-wide, the system was designed for and is operated by the U. S. military. The Space Segment of the system consists of the GPS satellites which send radio signals from space. The nominal GPS constellation consists of 24 satellites at an altitude of 20,000 km that orbit the earth in 12 hours. There are often more than 24 operational satellites as new ones are launched to replace older satellites. The orbit altitude is such that the satellites repeat the same track and configuration over any point approximately each 24 hours (4 minutes earlier each day). There are six orbital planes (with nominally four SVs in each), equally spaced (60 degrees apart), and inclined at about fifty-five degrees with respect to the equatorial plane. This constellation provides the user with up to twelve SVs visible from any point on the earth.

GPS satellites transmit two carrier frequencies, L1 at 1.57542 GHz and L2 at 1.22760 GHz (with wavelengths of 19cm and 24.4 cm, respectively). Each carrier is modulated by lower frequency signals. Each carrier is modulated by the Precise (P) code and in addition carrier L1 is modulated by a lower frequency Coarse Acquisition (C/A) code. A receiver with knowledge of the code structure and an internal clock can recover an estimate of signal transit time by cogenerating the code sequence and performing a cross-correlation between the received signal and its internal code, determining the time delay necessary to match the two sequences. The receivers used for the work in this thesis can recover the phase of the carrier as a by-product of the correlation process, with knowledge of the signal transit time



(difference between transmit time,  $t_s$  and receive time,  $t_r$ ), the range,  $\rho$  between satellite and receiver is simply  $c(t_r - t_s)$ , where  $c$  is the speed of light. However, the satellite and receiver clocks are not perfectly synchronized and so the pseudorange (so called because of the satellite and clock errors in the range estimate), is more accurately defined as:

$$R = \rho + c(\Delta t_r - \Delta t_s + \Delta t_p) \quad (\text{A.1})$$

where  $\Delta t_r$  is the receiver clock offset from true GPS system time,  $\Delta t_s$  is the satellite clock offset and  $\Delta t_p$  is the delay associated with all other error sources.

A higher precision GPS measurement is achieved using the carrier phase information on L1 and L2 and it is this observable that allows us to obtain GPS measurements at the precision needed to observe crustal deformation. Once the receiver has begun to track a satellite, it precisely measures the fractional part of the phase, after which it continually tracks the phase. Assuming perfect clocks and ignoring propagation effects,

$$\rho = n\lambda + \phi\lambda = \left(\frac{v_\phi}{f}\right)(n + \phi) \quad (\text{A.2})$$

where  $n$  is the number of integer carrier wavelengths at signal acquisition (initially unknown),  $\phi$  is the phase in cycles,  $\lambda$  is the wavelength,  $f$  is the frequency and  $v_\phi$  is the phase velocity. Since the wavelength of the carrier is considerably shorter than that of the lower frequency code modulations, the resulting length measurement, though ambiguous by the initial number of wavelengths, is considerably more precise than a pseudorange measurement. Determining the correct initial integer number of wavelengths is called ambiguity resolution and several techniques are available. In general, by observing several satellites over long periods of time (a few hours) and by knowing the approximate position of the GPS antenna (often through use of the P code), it is possible to estimate the range bias to better than half a carrier wavelength and then fix the bias to the nearest integer value.

Sources of error in GPS positioning include clock errors, the atmosphere, including the frequency-dispersive ionosphere and the nondispersive troposphere, tropopause, and mesosphere, all of which affect signal velocity and thus our estimate of satellite-receiver distance, uncertainties in the satellite position at the time of signal transmission, and, as

discussed above) carrier phase cycle ambiguities. For a single satellite-receiver pair, the phase can be defined as:

$$\phi = \omega \left( \frac{\rho}{c} = t_s + t_r + t_{trop} \right) + \phi_{ion} \quad (\text{A.3})$$

where  $\omega$  is frequency,  $t_s$  and  $t_r$ , the satellite and clock errors, and  $t_{trop}$ , the sum of the delays due to the troposphere, tropopause, and mesosphere, are non-dispersive. The ionospheric delay,  $\phi_{ion}$ , is frequency-dispersive and with dual frequency receivers, this ionospheric term can be eliminated.

Relative positioning involves simultaneous observation of a group of satellites by a network of receivers and this enables many of the aforementioned errors to be reduced or eliminated, resulting in the few millimeter-level precision required for the work in this thesis.

By simultaneously tracking a single satellite with two receivers, one can form a "single difference". This linear combination of observables is simply the difference between the phase observable at stations 1 and 2,  $\phi_1$  and  $\phi_2$ , which yields:

$$\Delta\phi = \phi_1 - \phi_2 = \omega \left[ \frac{\Delta\rho}{c} + \Delta t_{trop} + \Delta t_r \right] \quad (\text{A.4})$$

The satellite clock error is removed. By tracking two satellites with two receivers the double difference observable is formed:

$$\Delta\phi(\text{sat1}) - \Delta\phi(\text{sat2}) = \omega \left[ \frac{(\Delta\rho(\text{sat1}) - \Delta\rho(\text{sat2}))}{c} + \Delta t_{trop}(\text{sat1}) - \Delta t_{trop}(\text{sat2}) \right] \quad (\text{A.5})$$

which eliminates the receiver clock errors. The software used to process the GPS data used in this thesis does not perform this differencing technique but instead estimates the receiver and clock errors as part of the solution.

The nondispersive atmospheric delay is modeled in order to remove or greatly reduce the effect. Roughly three-quarters of the delay and most of the variability is associated with the troposphere. All components of the atmosphere contribute to the delay, but it is convenient to separately consider the "dry" delay, associated with molecular constituents

of the atmosphere in hydrostatic equilibrium, and the "wet" delay, associated with water vapor not in hydrostatic equilibrium. The dry delay is typically about 2 m equivalent path length (delay time multiplied by the speed of light) at zenith at altitudes near sea level, while the zenith wet delay is an order of magnitude lower. The delay at other elevation angles is larger and so an elevation dependence must be included in any model.

The orbital error is now the largest remaining error to be reduced. For millimeter-level accuracy on baselines longer than 100 km, meter-level precision in satellite orbit estimates is required. Tracking stations (stations for which we have an accurate position) define an Earth-fixed reference frame. These stations simultaneously track many satellites and instead of solving for the receiver position we solve for satellite position relative to the known position of the tracking sites. Once the satellite positions are known, it is possible to determine the positions of the GPS sites that do not form part of the tracking network.

## Appendix B

# Fieldwork procedures

Appendix I describes the steps necessary to enable millimeter-level precision in the estimation of the phase center of the GPS antenna. These steps are invalidated if the antenna is set up incorrectly over the site mark, or if the height of the antenna is measured incorrectly or if the mark is unstable with respect to the ground. Here I describe the fieldwork procedures undertaken while collecting data for this thesis.

### B.1 Site selection

A good GPS site is one that is solidly embedded in bedrock and has a good unobstructed view of the sky. For my work it was also beneficial to use sites that were easily accessible but not within view from roads and footpaths. I used several sites that were already in place, most often U. S. Coast and Geodetic Survey bench marks but I was careful to ensure that the sites were stable. In many places I could not use previously existing marks and so I installed my own bench marks. All the marks I installed were in bedrock or large boulders. A rock drill was used to drill a hole in the rock and a monument mark was fixed in the hole using epoxy.

### B.2 Antenna set up

A tripod or spike mount is used to hold the antenna directly above a marked point on the monument. With both types of set up it is absolutely essential to have the antenna

completely levelled and oriented towards North. The phase center of the antenna, the point of the antenna at which the position is determined, is not exactly at the center of the antenna and so we correct for this later, but the programs assume a level antenna oriented correctly. The antenna is screwed directly on to the spike mount, which has a known height, while an optical plumbing device called a tribrach is necessary to attach the antenna to the tripod. The slant height of the antenna on a tripod is measured by placing one end of a measuring rod on the marked point on the monument and reading the length at the point where the rod touches the rim of the antenna. This is measured at 3 different places around the antenna rim and the average is noted. Typically these values are within 1 mm of each other. The antenna dimensions are known and so we can convert the slant height to a vertical height. Assuming no blunders in the set up and assuming a well-calibrated tribrach, errors in the set up should be no larger than 1 mm.

## Appendix C

# Position and velocity data for all sites used in this thesis

Table C.1. Site velocities in mm/yr

Station	Lat	Lon	ITRF97		NOAM-fixed	
			$V_{north}$	$V_{east}$	$V_{north}$	$V_{east}$
CENA	65.4982	-144.6776	-0.84±0.05	-2.49±0.04	0.03±0.14	-0.47±0.14
CLGO	64.8738	-147.8605	-0.72±0.01	-2.40±0.01	0.04±0.13	-0.34±0.13
FAIR	64.9780	-147.4992	-0.73±0.01	-2.27±0.01	0.05±0.13	-0.22±0.13
GRNR	63.8358	-148.9783	-0.72±0.02	-2.37±0.02	-0.00±0.13	-0.29±0.13
WHIT	60.7505	-135.2221	-1.15±0.01	-1.56±0.01	-0.03±0.13	0.28±0.13
0999	63.6650	-142.2748	-1.11±0.55	-2.49±0.41	-0.18±0.57	-0.52±0.43
2999	64.0287	-142.0761	-1.24±0.68	-3.65±0.50	-0.30±0.69	-1.68±0.52
7297	62.6880	-145.4261	-1.25±0.04	-1.90±0.03	-0.42±0.14	0.12±0.13
ASPE	56.8538	-157.3721	-1.22±0.22	-1.64±0.17	-0.79±0.25	0.52±0.21
ATT	63.5025	-145.8472	-0.83±0.61	-2.68±0.45	-0.01±0.62	-0.66±0.47
BRWN	64.1707	-149.2951	-1.09±0.21	-2.36±0.12	-0.38±0.25	-0.28±0.17
BSB4	63.9065	-145.7891	-0.65±0.21	-1.99±0.16	0.17±0.25	0.04±0.20
CARL	63.5515	-148.8089	-1.05±0.29	-2.35±0.20	-0.33±0.32	-0.28±0.24
CGLO	63.3883	-148.9496	-0.60±0.18	-2.02±0.14	0.12±0.22	0.06±0.19
CHIR	55.8259	-155.7285	-2.27±0.07	1.00±0.06	-1.79±0.15	3.15±0.14
CLFF	56.2115	-158.2992	-1.55±0.22	-1.65±0.17	-1.16±0.25	0.53±0.21
COGH	61.0704	-147.9471	-2.25±0.23	1.11±0.16	-1.51±0.27	3.17±0.21
COMB	59.6699	-138.6393	-2.17±0.10	-0.17±0.08	-1.16±0.16	1.73±0.15
DFLY	63.7936	-148.9198	-0.87±0.10	-2.32±0.08	-0.15±0.17	-0.24±0.15
DH97	63.2652	-147.8551	-1.54±0.13	-2.34±0.11	-0.79±0.18	-0.27±0.17
DONLY	63.6951	-145.8876	-1.05±0.15	-2.41±0.11	-0.23±0.20	-0.38±0.17
EGL2	65.4909	-145.3876	-1.11±0.18	-2.24±0.13	-0.26±0.22	-0.22±0.19

Station	Lat	Lon	ITRF97		NOAM-fixed	
			$V_{north}$	$V_{east}$	$V_{north}$	$V_{east}$
EST1	64.8793	-148.0549	-1.04±0.11	-2.39±0.09	-0.29±0.17	-0.33±0.16
FAIT	65.3471	-146.2610	-1.20±0.19	-2.43±0.14	-0.38±0.23	-0.39±0.19
FCRK	63.0907	-145.4753	-1.27±0.06	-2.02±0.04	-0.44±0.14	0.01±0.14
GRIZ	63.6524	-148.8330	-1.17±0.12	-2.28±0.11	-0.44±0.18	-0.21±0.17
HEID	56.9639	-158.6123	-1.04±0.07	-1.96±0.05	-0.66±0.15	0.21±0.14
HIDD	59.7055	-138.9455	-3.06±0.08	0.93±0.06	-2.06±0.15	2.84±0.14
HIWA	63.4588	-148.7787	-0.86±0.11	-2.42±0.10	-0.14±0.17	-0.35±0.16
HUEY	56.7944	-156.8554	-1.77±0.31	-1.47±0.23	-1.33±0.34	0.70±0.27
HURR	62.9993	-149.6089	-0.81±0.06	-2.76±0.05	-0.11±0.14	-0.67±0.14
L2C6	63.3828	-148.8662	-0.99±0.12	-2.49±0.10	-0.26±0.18	-0.42±0.17
LOG	63.0226	-143.3455	-1.24±1.65	-2.59±1.03	-0.34±1.66	-0.59±1.04
LUKY	64.9267	-148.5157	-0.61±0.08	-2.43±0.06	0.14±0.15	-0.36±0.14
M110	63.3055	-148.1870	-1.51±0.23	-2.42±0.15	-0.76±0.26	-0.36±0.20
MAC	65.8262	-144.0624	-0.70±0.21	-2.12±0.16	0.19±0.25	-0.12±0.21
MDPK	64.9529	-148.3553	-0.79±0.05	-2.30±0.04	-0.04±0.14	-0.24±0.14
MEN	62.9095	-143.7954	-1.05±0.72	-1.94±0.52	-0.16±0.73	0.06±0.54
MINT	65.1006	-148.9009	-0.72±0.09	-2.43±0.07	0.01±0.16	-0.36±0.15
NENA	64.5794	-149.0798	-0.89±0.11	-2.63±0.09	-0.17±0.17	-0.56±0.16
ORTT	62.9610	-141.9364	-0.59±0.21	-2.08±0.13	0.35±0.25	-0.11±0.18
PANA	63.4838	-148.8204	-1.25±0.16	-2.53±0.11	-0.53±0.21	-0.45±0.17
PAXS	62.9673	-145.4517	-1.14±0.06	-1.97±0.05	-0.31±0.15	0.06±0.14
PEDR	65.0434	-147.4147	-0.60±0.11	-2.27±0.09	0.18±0.17	-0.21±0.16



Station	Lat	Lon	ITRF97		NOAM-fixed	
			$V_{north}$	$V_{east}$	$V_{north}$	$V_{east}$
PISA	63.2847	-149.2105	-1.24±0.14	-2.48±0.12	-0.53±0.19	-0.40±0.18
PPLN	64.1549	-145.8461	-0.80±0.08	-2.38±0.06	0.03±0.15	-0.35±0.14
R109	63.3953	-148.6468	-1.23±0.15	-2.54±0.12	-0.50±0.20	-0.47±0.18
REFL	64.9864	-147.5988	-0.85±0.15	-2.37±0.12	-0.08±0.20	-0.31±0.17
SEMI	56.0481	-156.6921	-2.16±0.22	-0.37±0.17	-1.72±0.25	1.79±0.21
SLCH	64.4768	-146.9764	-0.90±0.07	-2.37±0.05	-0.11±0.15	-0.33±0.14
SLIM	63.5120	-148.8041	-1.05±0.15	-2.59±0.12	-0.33±0.20	-0.51±0.18
SSWB	63.3413	-149.0902	-1.31±0.14	-2.39±0.11	-0.59±0.19	-0.31±0.17
STRI	63.3334	-142.9531	-0.89±0.15	-2.18±0.11	0.03±0.20	-0.19±0.17
SWB4	65.5622	-145.0266	-0.75±0.26	-2.82±0.17	0.11±0.29	-0.80±0.21
TALK	62.2986	-150.1057	-0.43±0.05	-3.19±0.04	0.25±0.14	-1.10±0.14
TOLO	65.0543	-149.5041	-0.48±0.18	-2.49±0.14	0.23±0.22	-0.41±0.19
TWLV	65.4090	-145.9845	-0.75±0.17	-2.48±0.13	0.08±0.22	-0.45±0.18
WICK	65.1827	-148.0662	-0.40±0.20	-2.49±0.15	0.36±0.24	-0.43±0.20
WIK	56.5765	-157.1086	-1.53±0.34	-1.28±0.25	-1.10±0.37	0.88±0.28
WOND	63.4912	-150.8737	-0.55±0.18	-3.04±0.14	0.11±0.22	-0.94±0.19
X7	60.8592	-137.0629	-1.03±0.11	-1.48±0.07	0.04±0.17	0.39±0.15
YKTT	59.5107	-139.6488	-3.24±0.03	2.23±0.02	-2.26±0.13	4.15±0.13
YUKO	65.6762	-149.0930	-0.47±0.51	-2.56±0.38	0.26±0.52	-0.48±0.40

# Bibliography

- Abers, G. A., Relationship between shallow- and intermediate-depth seismicity in the Eastern Aleutian subduction zone. *Geophys. Res. Lett.*, *19*, 2019-2022. 1992.
- Biswas, N. N. and G. Tytgat, Intraplate seismicity in Alaska. *Seismol. Res. Lett.*, *59*, 227-233. 1988.
- Boucher, C., Z. Altamimi, and P. Sillard, The 1997 International Terrestrial Reference Frame (ITRF97), in *IERS Technical Note 27*, Observatoire de Paris, France. 1999.
- Brocher, T. M., G. S. Fuis, M. A. Fisher, G. Plafker, M. J. Moses, J. J. Taber, and N. I. Christensen, Mapping the megathrusts beneath the northern Gulf of Alaska using wide-angle seismic data. *J. Geophys. Res.*, *99*, 11663-11686. 1994.
- Bruno, T. R., Model for the origin of the Yakutat block, an accreting terrane in the northern Gulf of Alaska. *Geology*, *11*, 717-721. 1983.
- Castillo, D. A. and W. L. Ellsworth, Seismotectonics of the San Andreas fault system between Point Arena and Cape Mendocino in Northern California: implications for the development and evolution of a young transform. *J. Geophys. Res.*, *98*, 6543-6560. 1993.
- Christensen, D. H. and S. L. Beck, The rupture process and tectonic implications of the Great 1964 Prince William Sound earthquake. *Pure Appl. Geophys.*, *142*, 9-53. 1994.
- Cohen, S. C. and J. T. Freymueller, Crustal uplift in the south central Alaska subduction zone: New analysis and interpretation of tide gauge observations. *J. Geophys. Res.*, *106*, 11259-11270. 2001.

- DeMets, C. and T. H. Dixon. New kinematic models for Pacific-North American motion from 3Ma to present. I: Evidence for steady state motion and biases in the NUVEL-1A model. *Geophys. Res. Lett.*, 26, 1921-1924, 1999.
- DeMets, C., R. Gordon, D. Argus, and S. Stein. Effect of recent revisions to the geomagnetic reversal time scale on estimates of current plate motions. *J. Geophys. Res.*, 21, 2191-2194, 1994.
- Dennis, J. E., D. M. Gay, and R. E. Welsch. Algorithm 573 NL2SOL - an adaptive non-linear least-squares algorithm [E4]. *ACM Trans. Math. Software*, 7, 369-383, 1981.
- Detterman, R. L., G. Plafker, T. Hudson, R. G. Tysdal, and N. Pavoni. Surface geology and Holocene breaks along the Susitna segment of the Castle Mountain fault, Alaska. *USGS Misc. Field Studies Map MF-618*, 1 sheet, scale 1:24,000, 1974.
- Dmowska, R. and L. C. Lovison. Influence of asperities along subduction interfaces on the stressing and seismicity of adjacent areas. *Tectonophysics*, 211, 23-43, 1992.
- Doser, D. I. and R. Lomas. Transition from strike-slip to oblique subduction in southeastern Alaska. *Tectonophysics*, 316, 45-65, 2000.
- Dragert, H., R. D. Hyndman, G. C. Rogers, and K. Wang. Current deformation and the width of the seismogenic zone of the northern Cascadia subduction thrust. *J. Geophys. Res.*, 99, 653-668, 1994.
- Estabrook, C. H., D. B. Stone, and J. N. Davies. Seismotectonics of Northern Alaska. *J. Geophys. Res.*, 93, 12,026-12,040, 1988.
- Estabrook, C. H., J. L. Nabelek, and A. L. Lerner-Lam. Tectonic model of the Pacific-North American plate boundary in the Gulf of Alaska from broadband analysis of the 1979 St. Elias, Alaska, earthquake and its aftershocks. *J. Geophys. Res.*, 97, 6587-6612, 1992.
- Fletcher, H. J. and D. H. Christensen. A determination of the source properties of large intraplate earthquakes in Alaska. *PAGEOPH*, 146, 21-41, 1996.
- Fletcher, H. J. and J. T. Freymueller. GPS constraints on the motion of the Yakutat Block. *Geophys. Res. Lett.*, 26, 3029-3032, 1999.

- Forbes, R. B., D. L. Turner, T. E. Smith, J. H. Stout, and F. R. Weber. The Denali fault offset problem. *U. S. Geol. Surv. Alaska Program, U. S. Geol. Surv. Circ.*, 683, 46. 1973.
- Frey Mueller, J. T. and J. Beavan. Absence of strain accumulation in the Western Shumagin segment of the Alaska subduction zone. *Geophys. Res. Lett.*, 26, 3233-3236. 1999.
- Frey Mueller, J. T., M. H. Murray, P. Segall, and D. Castillo. Kinematics of the Pacific-North American plate boundary zone, northern California. *J. Geophys. Res.*, 104, 7419-7441. 1999.
- Frey Mueller, J. T., S. Cohen, and H. Fletcher. Spatial variations in present-day deformation, Kenai Peninsula, Alaska, and their implications. *J. Geophys. Res.*, 105, 8097-8101. 2000.
- Gabrielse, H.. Major dextral transparent displacements along the northern Rocky Mountain Trench and related lineaments in northcentral British Columbia. *Geol. Soc. Am. Bull.*, 96, 1-14. 1985.
- Garfunkel, Z. and H. Ron. Block rotation and deformation by strike-slip faults 2. The properties of a type of macroscopic discontinuous deformation. *J. Geophys. Res.*, 90, 8589-8602. 1985.
- Haeussler, P., R. L. Bruhn, and T. L. Pratt. Potential seismic hazards and tectonics of the upper Cook Inlet basin, Alaska, based on analysis of Pliocene and younger deformation. *Geological Society of America Bull.*, 112, 1414-1429. 2000.
- Hickman, R. G., C. Craddock, and K. W. Sherwood. Structural geology of the Nenana River segment of the Denali fault system, central Alaska Range. *Geol. Soc. Am. Bull.*, 88, 1217-1230. 1977.
- Hreinsdottir, S., P. Einarsson, and F. Sigmundsson. Crustal deformation at the oblique spreading Reykjanes Peninsula, SW Iceland: GPS measurements from 1993 to 1998. *J. Geophys. Res.*, 106, 13,803-13,816. 2001.
- Johnson, H. O. and F. K. Wyatt. Geodetic network design for fault-mechanics studies. *Manu. Geod.*, 19, 309-323. 1994.

- Johnson, J. M. and K. Satake. Rupture extent of the 1938 Alaskan earthquake as inferred from tsunami waveforms. *Geophys. Res. Lett.*, 21, 733-736. 1994.
- Kao, H. and W. Chen. Earthquakes along the Ryukyu-Kyushu Arc: strain segmentation, lateral compression, and the thermomechanical state of the plate interface. *J. Geophys. Res.*, 96, 21,443-21,485. 1991.
- Kawasaki, I., Y. Asai, and Y. Tamura. Space-time distribution of interplate moment release including slow earthquakes and the seismic-geodetic coupling in the Sanriku-oki region along the Japan trench. *Tectonophysics*, 330, 267-283. 2001.
- Kogan, M. G.. Geodetic constraints on the rigidity and relative motion of Eurasia and North America. *Geophys. Res. Lett.*, 27, 2041-2044. 2000.
- Lahr, J. C. and G. Plafker. Holocene Pacific-North American Plate interaction in southern Alaska: Implications for the Yakataga seismic gap. *Geology*, 8, 483-486. 1980.
- Lahr, J. C., R. A. Page, C. D. Stephens, and K. A. Fogelman, Sutton. Alaska, earthquake of 1984: Evidence for activity on the Talkeetna segment of the Castle Mountain fault system. *Bull. Seis. Soc. Am.*, pp. 967-983. 1986.
- Lahr, J. C., R. A. Page, C. D. Stephens, and D. H. Christensen. Unusual earthquakes in the Gulf of Alaska and fragmentation of the Pacific plate. *Geophys. Res. Lett.*, 15, 1483-1486. 1988.
- Lanphere, M.. Displacement history of the Denali fault system, Alaska and Canada. *Can. J. Earth Sci.*, 15, 817-822. 1978.
- Larson, K. L., J. T. Freymueller, and S. Piliplisen. Global plate velocities from the Global Positioning System. *J. Geophys. Res.*, 102, 9961-9981. 1997.
- Lisowski, M., J. C. Savage, and R. O. Burford. Strain accumulation across the Fairweather and Totschunda faults, Alaska. *J. Geophys. Res.*, 92, 11,552-11,560. 1987.
- Lisowski, M., J. C. Savage, and W. H. Prescott. The velocity field along the San Andreas fault in central and southern California. *J. Geophys. Res.*, 96, 8369-8389. 1991.

- Lowey, G. W., A new estimate of the amount of displacement on the Denali Fault system based on the occurrence of carbonate megaboulders in the Dezadeash Formation (Jura-Cretaceous), Yukon, and the Nutzotin Mountains sequence (Jura-Cretaceous), Alaska. *Bull. Can. Petr. Geol.*, 46, 379-386, 1998.
- Lu, Z. and M. Wyss, Segmentation of the Aleutian plate boundary derived from stress direction estimates based on fault plane solutions. *J. Geophys. Res.*, pp. 803-816, 1996.
- Lundgren, P., F. Saucier, R. Palmer, and M. Langon, Alaska crustal deformation: Finite element modeling constrained by geologic and very long baseline interferometry data. *J. Geophys. Res.*, 100, 22,033-22,046, 1995.
- Ma, C., J. M. Sauber, L. J. Bell, T. A. Clark, D. Gordon, W. E. Himwich, and J. W. Ryan, Measurement of horizontal motions in Alaska using very long baseline interferometry. *J. Geophys. Res.*, 95, 21,991-22,011, 1990.
- Mackey, K. G., K. Fujita, L. V. Gunbina, V. N. Kovalev, V. S. Imaev, B. M. Kozmin, and L. P. Imaeva, Seismicity of the Bering Strait region: Evidence for a rotating Bering block. *Geology*, 25, 979-982, 1997.
- Mao, A., C. G. A. Harrison, and T. H. Dixon, Noise in GPS coordinate time series. *J. Geophys. Res.*, 104, 2797-2816, 1999.
- Mazzotti, S., X. L. Pichon, P. Henry, and S.-I. Miyazaki, Full interseismic locking of the Nankai and Japan-west Kurile subduction zones: An analysis of uniform elastic strain accumulation in Japan constrained by permanent GPS. *J. Geophys. Res.*, 105, 13,159-13,177, 2000.
- Menke, W., *Geophysical Data Analysis: Discrete Inverse Theory*. Academic Press, San Diego, CA, 1984.
- Minster, J. B. and T. H. Jordan, Present-day plate motions. *J. Geophys. Res.*, 83, 5331-5354, 1978.
- Muller, J. E., Kluane Lake map-area, Yukon Territory, in *Geological Survey of Canada. Memoir*, volume 340, 1967.

- Nishenko, S. P. and W. R. McCann. Seismic potential for the worlds major plate boundaries, in D. W. Simpson and P. G. Richards (eds.), *Earthquake Prediction: An International Review, Maurice Ewing Series, vol. 4*, pp. 20-28. AGU, Washington, D. C. 1981.
- Nokleberg, W. J., D. L. Jones, and N. J. Siberling. Origin and tectonic evolution of the Maclaren and Wrangellia terranes, eastern Alaska Range, Alaska. *Geol. Soc. Am. Bull.*, 96, 1251-1270, 1985.
- Okada, Y., Surface deformation due to shear and tensile faults in a halfspace. *Bull. Seis. Soc. Am.*, 75, 1135-1154, 1985.
- Oleskevich, D. A., R. D. Hyndman, and K. Wang. The up and downdip limits to great subduction earthquakes: Thermal and structural models of Cascadia, South Alaska, S.W. Japan, and Chile. *J. Geophys. Res.*, 104, 14,695-14,991, 1999.
- Pacheco, J. F., L. R. Sykes, and C. H. Scholz. Nature of seismic coupling along simple plate boundaries of the subduction type. *J. Geophys. Res.*, 98, 14,133-14,159, 1993.
- Page, R. and J. Lahr. Measurements for fault slip on the Denali, Fairweather, and Castle Mountain Faults. *J. Geophys. Res.*, 76, 8534-8543, 1971.
- Page, R. A., N. N. Biswas, J. C. Lahr, and H. Pulpan. Seismicity of continental Alaska, in D. B. Slemmons, E. R. Engdahl, M. D. Zoback, and D. D. Blackwell (eds.), *Neotectonics of North America*, volume Decade Map Volume 1, Boulder, Colorado, Geol. Soc. Am., 1991.
- Page, R. A., G. Plafker, and H. Pulpan. Block rotation in east-central Alaska: A framework for evaluating earthquake potential?. *Geology*, 23, 629-632, 1995.
- Patton, W. and J. M. Hoare. The Kaltag fault, west central Alaska. *U. S. Geol. Surv. Prof. Pap.*, 600-D, 1968.
- Perez, O. J. and K. H. Jacob. Tectonic model and seismic potential of the eastern Gulf of Alaska and Yakataga seismic gap. *J. Geophys. Res.*, 85, 7132-7150, 1980.

- Pewe, T. L., C. Wahrhaftig, and F. Weber. Geologic map of the Fairbanks Quadrangle, Alaska, in *Miscellaneous Geologic Investigations Map*. Reston, VA, U. S. Geological Survey, United States, 1966.
- Plafker, G.. Regional geology and petroleum potential of the northern Gulf of Alaska continental margin, in D. W. Scholl, A. Grantz, and J. G. Vedder (eds.), *A workshop on evaluation of regional and urban earthquake hazards and risk in Alaska*, U.S. Geological Survey Open-File Report 86-79, pp. 76-82, 1987.
- Plafker, G., T. Hudson, and D. H. Richter. Preliminary observations on late Cenozoic displacements along the Totschunda and Denali fault systems, in K. M. Blean (ed.), *The United States Geological Survey Circular 751-B*, pp. B67-B69, 1977.
- Plafker, G., T. Hudson, T. Bruns, and M. Rubin. Late Quaternary offsets along the Fairweather fault and crustal plate interactions, *Can. J. Earth Sci.*, 15, 805-816, 1978.
- Plafker, G., L. M. Gilpin, and J. C. Lahr. Neotectonic map of Alaska, in G. Plafker and H. C. Berg (eds.), *The geology of North America*, pp. v.G1, plate 12, scale 1:2,500,000, Geol. Soc. Am., Boulder, Colorado, 1994.
- Prawirodirdjo, L., Y. Bock, R. McCaffrey, J. Genrich, E. Calais, C. Stevens, S. S. O. Puntodewo, C. Subarya, J. Rais, P. Zwick, and Fauzi. Geodetic observations of interseismic strain segmentation at the Sumatra subduction zone, *Geophys. Res. Lett.*, 21, 2601-2604, 1997.
- Prescott, W. H., J. C. Savage, and W. T. Kinoshita. Strain accumulation rates in the western United States between 1970 and 1978, *J. Geophys. Res.*, 84, 5423-5435, 1979.
- Ratchkovski, N. A. and R. Hansen. New constraints on tectonics of interior Alaska: Earthquake locations, source mechanisms and stress regime, *Bull. Seis. Soc. Am.*, in press, 2002.
- Savage, J. C.. A dislocation model of strain accumulation and release at a subduction zone, *J. Geophys. Res.*, 88, 4984-4996, 1983.



- Savage, J. C. and R. O. Burford. Geodetic determination of relative plate motion in California. *J. Geophys. Res.*, 78, 832-845, 1973.
- Savage, J. C. and M. Lisowski. Strain accumulation along the Denali fault at the Nenana river and Delta river crossings. *J. Geophys. Res.*, 96, 14,481-14,492, 1991.
- Savage, J. C., J. L. Svarc, W. Prescott, and W. K. Gross. Deformation across the rupture zone of the 1964 Alaska earthquake, 1993-1997. *J. Geophys. Res.*, 103, 21,275-21,283, 1998.
- Savage, J. C., J. L. Svarc, and W. H. Prescott. Deformation across the Alaska-Aleutian Subduction Zone near Kodiak. *Geophys. Res. Lett.*, 26, 2117-2120, 1999.
- Sella, G., T. H. Dixon, and A. Mao. REVEL: a model for recent plate velocities from space geodesy. *J. Geophys. Res.*, in press, 2002.
- Stauder, W.. The Alaska earthquake of July 10, 1958: Seismic studies. *Bull. Seis. Soc. Am.*, 50, 293-322, 1960.
- Stein, S. and R. G. Gordon. Statistical tests of additional plate boundaries from plate motion inversions. *Earth Planet. Sci. Lett.*, 69, 401-412, 1984.
- Stephens, C. D., J. C. Lahr, K. A. Fogelman, and R. B. Horner. The St. Elias, Alaska, earthquake of February 28, 1979: Regional recording of aftershocks and short-term, pre-earthquake seismicity. *Bull. Seis. Soc. Am.*, 70, 1607-1633, 1980.
- Stout, J. H. and C. G. Chase. Plate kinematics of the Denali fault system. *Can. J. Earth Sci.*, 17, 1527-1537, 1980.
- Stout, J. H., J. B. Brady, F. Weber, and R. B. Page. Evidence for Quaternary movement on the McKinley strand of the Denali fault in the Delta River area, Alaska. *Geol. Soc. Am. Bull.*, 84, 939-948, 1973.
- Tarr, R. S. and L. Martin. Earthquakes at Yakutat Bay, Alaska, in September, 1899. *U. S. Geological Survey Professional Paper*, 69, 135, 1912.
- Thatcher, W. and G. Plafker. The 1899 Yakutat Bay, Alaska earthquake. *IASPEI and IAVCEI Assembly Abstracts with Programs*, p. 54, 1977.

- Tichelaar, B. W. and L. J. Ruff. Depth of seismic coupling along subduction zones. *J. Geophys. Res.*, *98*, 2017-2037, 1993.
- Turner, D. L., T. E. Smith, and R. B. Forbes. Geochronology of offset along the Denali fault system in Alaska. *Geol. Soc. Am. Abstracts with Programs*, *6*, 268-269, 1974.
- VonHuene, R., M. A. Fisher, and T. R. Bruns. Geology and evolution of the Kodiak margin, Gulf of Alaska, in D. W. Scholl and J. G. V. A. Grantz (eds.), *Geology and Resource Potential of the Continental Margin of Western North America and Adjacent Ocean Basins - Beaufort Sea to Baja California*, pp. 191-212, Circum-Pacific Council for Energy and Mineral Resources, Houston, Texas, 1987.
- Wahrhaftig, C., D. L. Turner, F. R. Weber, and T. E. Smith. Nature and timing of movement on the Hines Creek strand of the Denali fault system. *Geology*, *3*, 463-466, 1975.
- Zheng, G., R. Dmowska, and J. R. Rice. Modeling earthquake cycles in the Shumagin subduction segment, Alaska, with seismic and geodetic constraints. *J. Geophys. Res.*, *101*, 8383-8392, 1996.
- Zweck, C., J. T. Freymueller, and S. C. Cohen. Three dimensional elastic dislocation modeling of the postseismic response to the 1964 Alaska earthquake. *J. Geophys. Res.*, submitted 2001.